CoA Report No.109
October 1956.

THE COLLEGE OF AERONAUTICS

CRANFIELD

A Theoretical and Experimental Study of the Boundary Layer Flow on a 45° Swept Back Wing

by

F. M. Burrows, D.C.Ae.

SUMMARY

In this paper an account is presented of a theoretical and experimental study made in relation to the boundary layer flow on a 45° swept back wing. Particular attention is given to the onset of boundary layer instability and its association with critical values of secondary flow Reynolds numbers as defined by Owen and Randall (Ref.17).

Several aspects of the problem are considered, each in some detail, and some interesting results both theoretical and experimental are presented.

To satisfy the need for tests at Reynolds numbers compatible with full scale, the experiments were performed, in flight, on a large untapered, untwisted, 45° swept back half wing mounted as a dorsal fin upon the mid upper fuselage of an Avro Lancaster (P.A.474), the Reynolds number range thus achieved being $0.88 \times 10^{6} - 1.92 \times 10^{6}$ per foot.

Curves are presented giving details of the measured distributions of static pressure, chordwise loadings, and the boundary layer flow, the latter in extensive detail, for wing geometric incidences in the range $0^{0} - 10^{0}$, upper and lower surfaces, and for test Reynolds numbersin the range defined above.

No laminar flow was found to exist on either the upper or lower surface of the wing for Reynolds numbers at, and in excess of 1.55×10^{6} per foot thus showing the need for some form of boundary layer control to suppress the effects of sweep instability.

CONTENTS

4

CoA Report No.109
October 1956.

THE COLLEGE OF AERONAUTICS

CRANFIELD

A Theoretical and Experimental Study of the Boundary Layer Flow on a 45° Swept Back Wing

by

F. M. Burrows, D.C.Ae.

SUMMARY

In this paper an account is presented of a theoretical and experimental study made in relation to the boundary layer flow on a 45° swept back wing. Particular attention is given to the onset of boundary layer instability and its association with critical values of secondary flow Reynolds numbers as defined by Owen and Randall (Ref.17).

Several aspects of the problem are considered, each in some detail, and some interesting results both theoretical and experimental are presented.

To satisfy the need for tests at Reynolds numbers compatible with full scale, the experiments were performed, in flight, on a large untapered, untwisted, 45° swept back half wing mounted as a dorsal fin upon the mid upper fuselage of an Avro Lancaster (P.A.474), the Reynolds number range thus achieved being 0.38 x 10^6 - 1.92 x 10^6 per foot.

Curves are presented giving details of the measured distributions of static pressure, chordwise loadings, and the boundary layer flow, the latter in extensive detail, for wing geometric incidences in the range 0° - 10°, upper and lower surfaces, and for test Reynolds numbersin the range defined above.

No laminar flow was found to exist on either the upper or lower surface of the wing for Reynolds numbers at, and in excess of 1.55 x 10^6 per foot thus showing the need for some form of boundary layer control to suppress the effects of sweep instability.

CONTENTS

Page

PREFACE

The experimental programme of work discussed in this report was made possible by a Ministry of Supply Contract (M.o.S. 6/Aircraft/9807/CB/6a).

The experiments were performed during the early summer of 1956, following the design construction and installation of the required model and equipment into the aircraft used as test vehicle (Lancaster P.A. 474,) this work being almost entirely carried out at the College of Aeronautics.

To some extent the programme has been one of a previously untried nature, but the quality of the experimental results obtained would appear to suggest that the particular methods of test adopted might be more fully exploited in the future in order to facilitate aerodynamic investigations and explorations at Reynolds numbers compatible with full scale.

The author is however aware of the existence of some minor shortcomings in the details of the techniques employed for the boundary layer explorations, but suggests that these are by no means as serious as might at first be supposed. Refinements to these techniques, if considered necessary, might follow as logical developments.

The experimental programme was completed in a comparatively short length of time, this being made possible by the enthusiasm and close support of a number of persons, all of whom the author would gratefully thank. Space considerations do not permit the presentation of a complete list of separately detailed references to all those directly and indirectly involved, and in making mention of but a few names the author implies references to all associates.

The piloting of the aircraft was performed in the main by Mr. B.F. Russell and to a lesser extent by Wing Commander C.G.B. McClure, A.F.C. The exacting skill exhibited by both pilots (assisted by G. Longland, Flight Engineer) in consistently and accurately reproducing the required experimental flight conditions, at all times left nothing to be desired, whilst the ready availability of the aircraft and its equipment is to be attributed to Mr. H.W. Gover, Chief Aircraft Engineer, Mr. W. Abbott, Chief aircraft Inspector, and their staff.

The experiments were supervised by Mr.M.C. Wilson, A.F.C., Senior Lecturer in the Department of Flight, on whose experience in the field of flight testing the author was allowed at all times freely to draw, whilst the laborious task of reduction of the experimental results to the required form was to a large extent performed by Mr. J. Walton, who also flew with the author as an observer.

The design of the experimental wing and its installation was performed by Mr. A. MacDonald, working under the direction of Mr. A.F. Newell, Deputy Head of the Department of Aircraft Design. These designs received pre-flight approval from the Resident Technical Officer of

Messrs. A.V.Roe Ltd., Manchester.

Helpful discussions with members of the staff of the Department of Aerodynamics are also gratefully acknowledged, as is the assistance of Mr. S.W.Ingham in performing numerical computations.

By close cooperation between all concerned it has been possible to perform the experiments as reported and it is hoped that these will form the basis for future but more elaborate work of this kind at the College of Aeronautics, Cranfield.

LIST OF SYMBOLS USED

Only the principal symbols used are listed, other symbols being defined as and where they occur in the text.

$x, y, z,$	orthogonal cartesian coordinate system (see para. 2.2 and fig. 14)
$x_1, y_1, z_1,$	orthogonal cartesian coordinate system
$x_2, y_2, z_2,$	orthogonal curvilinear coordinate system
$u, v, w,$	velocity components in the boundary layer referred to x, y, z
$u_1, v_1, w_1,$	velocity components in the boundary layer referred to x_1, y_1, z_1
$u_2, v_2, w_2,$	velocity components in the boundary layer referred to x_2, y_2, z_2
$q(x,y)$	potential flow velocity at the wing surface in the plane x,y
$q_1(x_1 y_1)$	potential flow velocity at the wing surface in the plane $x_1 y_1$
$U, V, W,$ etc.	velocity components just outside the boundary layer along $x, y, z,$ etc. (suffices denote axes of reference)
q_s	total local velocity along streamline just outside the boundary layer
ξ_1, ζ_1 -,	streamline coordinate system (see fig. 16)
$Q_2 = \dfrac{U_2(x_2)}{U_2 \cos \Lambda}$	
U_0	velocity of the undisturbed stream
Λ	angle of sweepback (or shear)
$W_0 = U_0 \sin \Lambda$	velocity component parallel to wing leading edge
p	local static pressure
p_0	free stream static pressure
$C_p = \dfrac{P - P_0}{\frac{1}{2}\rho U_0^2}$	static pressure coefficient
$\Delta C_p = C_{p_L} - C_{p_U}$	(L denotes lower surface of wing, U denotes upper surface of wing
R	Reynolds number (particular cases are separately denoted)
χ	Secondary flow Reynolds number

$\bar{\rho}$	streamline curvature in the plane $x_2 z_2$ $(y_2 = 0)$
ϕ	angle between the streamline and the axis x_2
ρ	air density
ν	kinematic viscosity
$c_,$	wing chord measured parallel to the undisturbed stream
c'_σ	wing chord measured normal to wing leading edge
α	geometric incidence of wing
δ	boundary layer thickness (absolute physical value)

$$\delta_1 = \int_0^\delta \left(1 - \frac{u}{U}\right) dy$$ boundary layer displacement thickness

$$\delta_2 = \int_0^\delta \frac{u}{U}\left(1 - \frac{u}{U}\right) dy$$ Boundary layer momentum thickness

$$\delta_3 = \frac{\delta_1}{\delta_2}$$ shape parameter

1. INTRODUCTION

1.1 Purpose of this work

The reason for and purpose of this work was to further the study of the swept wing boundary layer, begun by W.E. Gray (ref 28) with particular reference to the onset of boundary layer instability, and subsequent transition, and its association with "critical" values of the Reynolds number ascribed to the secondary flow as defined by Owen and Randall (ref. 17)

Since the scale effect is of prime importance in such a study, the idea of constructing the equipment and conducting an experiment at something approaching full scale Reynolds numbers was exploited, resulting in the testing of a large model swept back half wing mounted as a dorsal fin upon the mid upper fuselage of an Avro Lancaster Mk.VII, the aircraft being suitably adapted and modified to accommodate the necessary equipment.

By a suitable choice of both experimental equipment and techniques, it has been possible to make an extensive yet rapid exploratory survey of the boundary layer in this way for a number of conditions of Reynolds numbers and incidences, and a number of interesting results so obtained are to be discussed.

1.2. Range and Extent of the Investigations

The experiments were performed on an untapered, untwisted, 45° Swept back half wing of general dimensions as given in figs. 3 & 4. It will be noted from fig.4. that the wing was of unconventional section, and the reasons for this choice of section are discussed in para. 2.1.

The range of the tests was to include measurement of the static pressure distribution over the model from the position of maximum thickness to the leading edge for a Reynolds number range of from 0.88×10^6 per foot to 1.92×10^6 per foot, and for a geometric incidence range of from $\alpha = 0^\circ$ to $\alpha = 10^\circ$, both upper and lower surfaces being considered.

Boundary layer velocity profiles were measured at three spanwise stations, together with the distributions of total head at, and near to, the wing surface at four spanwise stations, at suitably spaced intervals along the chord extending from near to the leading edge to the position of maximum thickness, and for selected values of Reynolds number and geometric incidence in the ranges 0.88 to 1.92×10^6 per foot and $\alpha = 0^\circ - 10^\circ$ respectively for both upper and lower surfaces.

Theoretical consideration is given to the boundary layer flow near to the leading edge of the infinite sheared wing at zero incidence, the steady boundary layer flow being calculated using the method of Prandtl (ref.19.) and Sears (ref. 20) for the spanwise flow and the Blasius series for the chordwise (normal to the leading edge) flow, the calculations being performed on the basis of both the theoretically and experimentally derived velocity distribution for the section. Consideration is also given to the secondary flow occurring in the boundary layer of a wedge shaped profile using the methods of Hartree (ref.31) and Cooke (ref.32).

The experimental results quoted give details of the general nature of the boundary layer flow found to exist on the wing, and summarising quite generally, show to the further support of already existing evidence (refs. 6, 26, 29) that without the application of some form of boundary layer control the possibility of maintaining regions of laminar flow of any appreciable magnitude on either the upper or lower surface of a swept back wing at full scale Reynolds numbers, is remote.

1.3. Limitations of Present Work

The investigation of the flow in the boundary layer on a swept back wing by the methods of test with which we are to be concerned, leads to a number of problems which would not arise in the case of similar experiments conduct in a wind tunnel. The main difficulties arise from the fact that the bound layer is essentially three dimensional in character and strictly speaking does not permit the use of techniques established for two dimensional flows for its measurement. For a detailed and precise exploration a traversing mechanism with at least four degrees of freedom is required, and this need together with the problem of pilot fatigue which is very closely related to the satisfactory use of such gear in flight (see para. 3.2.) leads to the adoption of more simple methods for measurement.

Now the number and degree of the simplifications made to the experimental techniques will depend upon the general nature of the flow to be investigat and upon the information so required. Hence if we can distinguish two types of flow, the one in which three dimensional effects are known to be o first order importance and which definitely requires a three dimensional technique for its measurement, and the other in which three dimensional effects are of lesser significance and which can be measured to a good first approximation using simplified techniques, then if we concern ourselv with the latter we are in a position to make a number of useful measurement by methods which can be easily simply and rapidly applied in flight experim

For the work to be discussed it was observed from wool tuft observations th for certain regions on the wing a fairly wide range of wing incidence ~ sp configurations existed in which three dimensional effects could be consider as being small, such an observation being made understanding the limits to which the flow directions as indicated by wool tufts could be interpreted (ref.9). Consequently it was assumed that techniques for measurement of the boundary layer, strictly correct for the two dimensional case only, cou be applied in the above regions on the wing and which could be expected to yield results accurate to a very good first order approximation. (see para 3.2. for further details).

Such an assumption does however constitute a limitation which must be impos upon the interpretation and validity of the experimental results quoted and the reader should quite clearly understand that taken all in all these resu give only a general picture of the boundary layer on the swept back wing.

It is possible that there were cases in which the effects of transverse flow assumed greater significance than has here been assigned, but until such time as a great deal of effort has been expended in making more detailed and accurate measurements, then experimental results such as those quoted will be of value with regard to the assessment of the swept wing boundary layer.

As far as the theoretical work is concerned so little is known of the behaviour of the swept wing boundary layer that for its calculation we may only apply existing theories with some reservation. By means of the Independence Principle however (ref.4.), calculations of the steady boundary layer flow over sufficiently short distances of the wing surface can be made using existing methods (e.g. ref. 20), and since the effects of secondary flow in which we are interested occur in the neighbourhood of the leading edge we may accordingly take steps leading to results of interest. Such a procedure does lead to approximations, and hence, we must endeavour to make sure that these are both reasonably accurate and valid.

Thus with regard to the interpretation of both the theoretical and experimental results quoted the reader should quite clearly understand the limitations and assumptions which it has been found necessary to impose and make in this treatment of the problem. They will accordingly be detailed as and when they occur in the text.

1.4. Outline of the General Problem.

Although it is some time now since the swept back wing was introduced in aircraft design, there is little known as yet relating to the characteristics of the strictly three dimensional boundary layer associated with this type of wing. We can generalise by saying that although the compressibility drag rise accompanying the attainment of the critical Mach number can be successfully delayed by using a wing of swept planform, other phenomena are known to occur which affect the boundary layer flow over the wing to such an extent that the skin friction and hence profile drag become increased to the detriment of the low speed characteristics. By low speed characteristics we do of course make reference to speeds below that range in which compressibility effects must be taken into account, speeds which might readily be associated with the problems of, for example, the long range cruise of civil transport aircraft. If from the results of both experiment and theory a sound understanding and appreciation of the nature and mechanics of the flow in the boundary layer on the swept back wing at low speed may be obtained then it becomes possible to give consideration to further associated problems such as the possibility of using devices incorporating distributed or discreetly applied boundary layer suction, for its improvement.

It was the observations of W.E. Gray (ref. 28) that first brought to light the presence of swept wing boundary layer phenomena of a special nature and his investigations at full scale Reynolds number suggested that for most flight conditions the possibility of maintaining any appreciable areas of laminar flow upon the upper surface of a swept back wing might be more than somewhat remote. Gray's observations (ref.33) of the striations occurring in the laminar boundary layer above certain values of Reynolds number (subsequently to become termed critical Reynolds numbers) were to provide in subsequent years an experimentally determined basis for more elaborate studies of the flow problems of the three dimensional boundary layer with special reference to its stability. The trend in this direction was towards a theoretical investigation of the effect of small perturbations of the type $u(x, y, z)\ e^{i\lambda}$. ,(where λ is in general complex and dependent on time) upon the equations of motion for steady flow in the three dimensional boundary layer. These investigations performed by Owen and Randall and by Stuart (refs. 16, 17.) have quite clearly shown that under certain conditions of the flow just outside the boundary layer we can expect the development of systems of vortices, (of a type similar to that considered by Gortler in a study of the boundary layer flow over a concave surface), within the boundary layer itself, which, for certain external flow conditions tend to result in a drastic change over from laminar to turbulent flow occurring. The vortex formation to be expected differs from the usual Gortler formation in that the rotation of the flow about each vortex axis is in the same sense (ref. 17) as compared with the opposite rotation of adjacent vortices which occur in the flow over concave surfaces.

The alignment of the axes of the vortices is such that they are very nearly parallel to the stream lines at the outer edge of the boundary layer and trail downstream as shown in fig.16a. It is due to the presence of such a system of vortices that striations may be observed in the surface pattern on a swept wing when making liquid film studies of the boundary layer flow, the spacing of the striations corresponding to the spacing of the vortices or more particularly to one disturbance wavelength (ref. 17.).

The theoretical studies of Stuart and Owen and Randall showed that whilst for steady boundary layer flow in three dimensions the independence principle may be applied, in the case of the disturbed flow there is no longer an independence of the main and spanwise flows and the study of the disturbances resolves itself into an eigen value problem for the compounded motion.

Following the initiation of these preliminary ideas on the cause and effect of swept wing boundary layer instability a number of experiments have been performed to provide further data (ref's. 6, 29). These experiments have in general provided information of great value but perhaps the most noticeable feature of all was the surprising result, obtained from both theoretical and experimental consideration, (e.g. ref. 29) that an increase of incidence or Reynolds number, the latter to beyond values $R_{crit.}$ is accompanied by boundary layer instability of considerable intensity giving rise to rapid forward movements of the transition fronts on the lower surface of a swept back wing. Similar results in flight experiments were also observed by Allen and Burrows (ref. 26.).

With regard to the flow conditions on the lower surface, the forward movement of the transition fronts occurring with increase of incidence is of course contrary to what would normally be expected for wings of zero sweep on which favourable pressure gradients existed, and it is here that the true significance of the possible consequences of a three dimensional boundary layer flow is illustrated. That such a phenomenon can occur in the presence of favourable pressure gradients also gives some idea of the magnitude of the destabilising influence.

The root of the problem may be found in the flow conditions over the nose of the wing as it is in this region that for both upper and lower surfaces the curvature of the stream lines just outside the boundary layer is large. If we resolve the steady boundary layer flow into components along and normal to this streamline, we find that whilst the component distribution of velocity along the streamline is well ordered, the component distribution normal to the streamline contains a point of inflexion (see fig.16.) the velocity of this secondary flow reaching a maximum at some fraction (i.e. $z/\delta < 1$) of the boundary layer thickness from the wing surface. Owen and Randall have put forward sound physical arguments for the existence of this type of flow which have been strongly substantiated by calculation.

Thus given the existence of such flow conditions we are further led to suppose (e.g. ref. 34) that since this secondary flow profile contains a point of inflexion then for values of secondary flow Reynolds Number x above the critical it is inherently unstable to the effect of small disturbances, such a supposition following on naturally from a study of the flow in laminar wakes.

We can therefore argue to show that since the secondary flow profile depends upon the local streamline curvature, (just outside the boundary layer) and the magnitude of the local velocity, it in turn depends upon the distribution of velocity along the span and along the chord (normal to the leading edge) which again and in themselves depend upon the nose radius of curvature and upon the angle of sweep.

Since due to the magnitude of the secondary flow Reynolds number required for instability to occur, the general effect on the swept wing boundary layer is one of full scale then it is only by systematic tests at something approaching or even at full scale (e.g. Gray's experiments) that we can hope to obtain further experimental information to make for a better understanding of the behaviour of the swept wing boundary layer, and it was thus to this end that the experiment to be discussed was directed.

1.5. Final Introductory note.

The work presented is essentially divided into two sections: one devoted to a theoretical discussion of the problem, the other to experimental considerations etc. In general, only results are quoted in the text, the details of their derivation being relegated to appendices to which attention is drawn as and where necessary.

2. Theoretical Considerations.

2.1. Choice of Wing Section.

The three dimensional boundary layer instability phenomena in which we are interested requires a study of the flow over and near to the leading edge of the wing at something in the region of full scale Reynolds numbers for an understanding of its essential details. Consequently if we suppose that we can simulate the flow conditions in this region by using a representative or effective wing section having a foreshortened trailing edge without so incurring any undesirable effects in the general flow over the wing, then ideally we need only concern ourselves with the flow over the forward portion of such a representative wing (i.e. from the position of maximum thickness to the leading edge) in making our study of the boundary layer. Moreover, when considered in the absence of sweep instability, the boundary layer flow characteristics depend upon the Reynolds number referred to the distance from the stagnation point (two dimensional case) or line (three dimensional case) to the plane considered, and so in attempting to reduce the effects of scale to a minimum we endeavour to construct our test model with the largest possibl dimensions consistent with the experimental facilities available.

The aerofoil section chosen for this experimental work is shown in fig.4. and was intended to form a compromise between the above two factors. It was made up of two semi ellipses, one of which constituted a faired or foreshortened trailing edge, the other corresponding to the leading edge portion of a 10% thickness to chord ratio aerofoil of some 130" chord (measured in the free stream direction). This 10% thickness to chord ratio, 130" chord aerofoil we shall subsequently refer to as the "effective" section since it was towards this section that the representation, by double ellipse and partial chord, was directed. The wing section used we shall refer to as the "actual" section.

By the use of a foreshortened or faired trailing edge the maximum test Reynolds Number, based on the length between the leading edge and the positior of maximum thickness (which for wings of conventional section corresponds to the distance to maximum suction at zero incidence) may be obtained for a wing of relatively small area and which when at incidence and thus providing lift would provide acceptable conditions with regard to the aircraft fuselage design load limitations and also from the point of view of aircraft handling in flight.

It might be argued that in using what really amounts to a "bluff" trailing edge some difficulties might be encountered due to wake instability, but as we shall see later, experimental evidence has shown (para.7.4) that for this particular wing no trace of such a flow condition could be detected.

It is evident both from the present series of tests and from previous work of a more qualitative nature (ref. 26.) on a sweptback wing of similar section, that this supposed representation of an effective section constitute an erroneous argument as far as the simulation of flow conditions is concerne This we shall show later by recourse to both theory and experiment.

At the same time however, it does not mean that the experimental results obtained are invalidated. It simply means that the results quoted may be compared, with reservation as dictated by circumstance, to those for wings on which similar distributions of pressure may be found to exist in the regions considered.

2.2. The Co-ordinate Systems Used.

For both the theoretical and experimental work it is convenient to use three orthogonal co-ordinate systems of reference, these being as shown in fig.14. The system x, y, z, has its origin at a point along the chord line corresponding to the position of maximum thickness of the wing and the axis x is along the direction of the undisturbed stream. The axis z is normal to x and lies in the plane of symmetry of the wing section, and y is orthogonal with x and z.

The second system of axes, x_1, y_1, z_1, has the axis x_1 along the direction of the wing chord normal to the leading edge and its origin coincident with that for x, y, z : z_1 and y_1 are orthogonal with x_1 as before.

To describe the boundary layer flow we shall require an orthogonal curvilinear system of axes x_2, y_2, z_2; the axis x_2 having its origin on the stagnation line at the leading edge of the wing and following the contour of the wing surface in a plane normal to the leading edge. The axis z_2 will be taken parallel to the leading edge and lies in the plane of the wing surface whilst y_2 is orthogonal with x_2 and z_2.

Components of velocity etc. referred to in one or other of the above systems of axes will unless otherwise defined bear the same suffix as the axes to which they may be referred.

The physical visualisation of these systems of axes in relation to the wing is simplified by reference to two planes (plane x y and plane Λ) these being as shown in fig.14.

2.3. Theoretical Distributions of Velocity and Pressure for the Swept Back Wing.

To facilitate the study of the boundary layer flow and to make comparison between the results of theory and experiment we require to know the distributions of velocity and static pressure over the swept back half wing. If this requirement is restricted to the zero incidence and hence zero circulation (symmetrical section) case then it is possible to make the necessary calculations to a sufficiently high degree of accuracy by considering the wing to be of infinite span and representing the section thickness by a system of sources distributed along the chord line. In this way the perturbation potential takes the form:-

$$\bar{w} = -\frac{1}{2\pi} \int_{\text{L.E.}}^{\text{T.E.}} \sigma'(\xi) \ln(\bar{z} - \xi)\, d\xi \qquad (2.3.1)$$

- in which the total source strength along an elementary length dx is given by $\sigma'(x)\,dx$. For the wing of infinite span sheared by an angle Λ and having the "actual" section of fig.15. it can be shown (see appendix II.) that the velocity distribution is given by an equation of the form:-

$$q\,\frac{(x,y)}{U_0} = \sqrt{\left(\frac{q_1}{U_0}\right)^2 + \sin^2\Lambda} \qquad (2.3.2)$$

where

$$\frac{q_1}{U_0}(x_1, y_1) = \frac{1}{B_{x_1}}\left\{\cos\Lambda + \frac{b}{\pi}\sum_{n=1}^{2}(-1)^{2-n}\,\frac{1}{a_n}\left(\frac{\pi}{2} + \frac{(-1)^n \frac{x}{a_n}}{\sqrt{1 - \frac{x^2}{a_n^2}}}\,\operatorname{sech}^{-1}\frac{x}{a_n}\right)\right\} \qquad (2.3.3)$$

and the pressure coefficient by:

$$C_p(x,y) = 1 - \left\{\frac{q(x,y)}{U_0}\right\}^2 \qquad (2.3.4)$$

- in which expressions the co-ordinates are as defined in para. 2.2 and shown in figs. 14 and 15.

An adequate account relating to the derivation of the above expressions is given in appendix II. where both the two dimensional and the infinite sheared cases are discussed. The "effective" section (fig.15) referred to in para.2.1. is also considered in appendix II

The pressure distribution calculated from (2.3.4.) is shown in fig.17. where it is compared with that calculated for the "effective" section the marked differences in the two distributions being very evident.

We may at once deduce that provided good agreement is to be obtained between the calculated (e.g. 2.3.4.) and measured distributions of static pressure for the actual wing section then we should no longer concern ourselves with the idea of an effective section as discussed in para. 2.1. As we shall see, this is subsequently confirmed.

2.4 The Potential Flow Streamline Over the Infinite Sheared Wing.

For the sheared wing at incidence the components of the free stream velocity U parallel to and normal to the leading edge are respectively (ref. 5):-

$$\left.\begin{aligned} & U_o \cos\alpha \sin\Lambda \\ \text{and} \quad & U_o \sqrt{\cos^2\alpha\cos^2\Lambda + \sin^2\alpha} \end{aligned}\right\} \tag{2.4.1}$$

where the true wing incidence is given by:

$$\beta = \tan^{-1}(\tan\alpha \sec\Lambda). \tag{2.4.2}$$

For sufficiently small values of incidence α, (2.4.1) and (2.4.2) reduce to

$$\begin{aligned} & U_o \sin\Lambda = W_o, \\ & U_o \cos\Lambda, \\ & \beta = \alpha\sec\Lambda, \end{aligned} \tag{2.4.3}$$

Now the effect of the wing thickness distribution is to cause the flow velocity along the wing surface in a direction normal to the leading edge to vary with chordwise position, whilst the spanwise component remains constant since the wing surface in this case is a stream surface. Hence, using the orthogonal curvilinear co-ordinate system $x_2\ y_2\ z_2$ (fig.14.) as a frame of reference, for any streamline in potential flow we have

$$\frac{dz_2}{dx_2} = \frac{W_o}{U_2(x_2)} \tag{2.4.4}$$

- since the streamline lies wholly in the plane $x_2 z_2$ (i.e. the wing surface). Thus any streamline is given by

$$z_2 = \int \frac{W_o}{U_2(x_2)}\, dx_2 + c \tag{2.4.5}$$

- where c is an arbitrary constant of integration depending on the spanwise position of the streamline.

If we now define the non dimensional velocity Q_2 as

$$Q_2 \triangleq \frac{U_2(x_2)}{U_o\cos\Lambda} \tag{2.4.6}$$

then (2.4.4.) takes the form:-

$$\frac{dz_2}{dx_2} = \frac{\tan \Lambda}{Q_2}$$

together with
$$\frac{d^2 z_2}{dx_2^2} = \frac{-\tan \Lambda}{Q_2^2} \cdot \frac{dQ_2}{dx_2} \qquad (2.4.7.)$$

- so that for the curvature of the streamline we obtain -

$$\frac{1}{\rho} = \frac{-Q_2 \tan \Lambda}{\left\{ Q_2^2 + \tan^2 \Lambda \right\}^{3/2}} \cdot \frac{dQ_2}{dx_2} \qquad (2.4.8.)$$

It can be seen from (2.4.8) that, since the velocity gradient $\frac{dQ_2}{dx_2}$ is relatively large for regions close to the stagnation line at the leading edge, the streamline curvature will also be large in that region (ref.17.). That this is true for the swept back wing under consideration may be seen from an inspection of figs. 20 and 28b., the curve shown in fig.20 being derived by noting that if ϕ is the angle between any streamline and the axis x_2, then from (2.4.4.)

$$\phi = \tan^{-1} \frac{W_0}{U_2(x_2)} \qquad (2.4.9)$$

The significance of this streamline curvature * in relation to the boundary layer flow is one of major importance for it gives rise to the secondary flow with which we have learned (refs. 16 and 17) to associate the phenomena of sweep instability.

2.5. The Boundary Layer in Relation to the External Stream Line.

The streamline just outside the boundary layer we choose to regard as a datum to which the flow in the boundary layer may be referred. It is, to a very close approximation, curved according to the relationship (2.4.8.) and it is convenient to set up a right angled planar co-ordinate system ξ_1, ζ_1, with its origin at any arbitrarily chosen position on the streamline as shown in Fig.16. If the total local velocity along the streamline is q_S then together

---

* Note here that we may with sufficient accuracy associate the potential flow streamline with the streamline in viscous flow just external to the boundary layer.

with the angle ϕ calculated from (2.4.9), we may write

$$\left.\begin{aligned} \bar{u}_{\xi_1} &= \frac{u_{\xi_1}}{q_s} = \frac{w_2}{q_s} \sin\phi + \frac{u_2}{q_s}\cos\phi \\ \bar{w}_{\zeta_1} &= \frac{w_{\zeta_1}}{q_s} = \frac{w_2}{q_s}\cos\phi - \frac{u_2}{q_s}\sin\phi \end{aligned}\right\} \tag{2.5.1}$$

in which u_{ξ_1} and w_{ζ_1} are the components of the steady boundary layer flow resolved along and normal to the streamline respectively, and u_2 and w_2 are the components of the steady boundary layer flow referred respectively to the axes x_2, z_2, and which may be calculated from equation (4.3.7.)

Now Stuart (Ref. 23) and Owen and Randall (Ref. 17) have independently shown that the boundary layer velocity distribution characterised by $\bar{u}_{\xi_1}$ yields a profile of the usual form, whilst that given by $\bar{w}_{\zeta_1}$ (secondary flow) contains a point of inflexion, the two profile forms being illustrated in Fig.16. An association of the form of the $\bar{w}_{\zeta_1}$ profile with that developed in a laminar wake together with its inherent inflexional instability formed the basis for theoretical studies of a three dimensional boundary layer flow of this kind by the above authors (Refs. 23 and 17). It appears that we can conveniently relate the onset of the inflexional instability of the secondary flow to the external flow conditions by an expression of the form -

$$\frac{\chi \text{ crit.}}{R^{\frac{1}{2}}} = \frac{N}{R^{\frac{1}{2}}_{\text{crit}}}, \quad R = \frac{U_0 c_0}{\nu} \tag{2.5.2}$$

in which χ is the Reynolds Number referred to the secondary flow and which takes the form -

$$\chi = \left| \frac{w_{\zeta_1 \max}\delta}{\nu} \right| \tag{2.5.3}$$

the modulus being taken since w_{ζ_1} is in general negative with respect to the co-ordinates ξ_1, ζ_1, of Fig.16.

With the onset of this type of instability, a system of vortices is formed, in the outer region of the boundary layer, which trail approximately downstream from the disturbance origin and the effect of their growth is to lead to an ultimate breakdown of the flow into turbulence. The axes have discreet spacing corresponding approximately to one disturbance wave length (ref.17) and are so aligned as to be very nearly parallel to the external stream lines.

Experimental observations of the initial formation of striations in the laminar boundary layer using the liquid film ~ china clay technique, (e.g. ref. 6) and the association of these striations with the vortex formations referred to above have led to the possibility of fixing a value for N in equation (2.5.3) (see ref. 34). On the supposition that the initial appearance of the striations coincides approximately with the initial formation of the vortices, it has been suggested that N lies somewhere in the region of 100 - 150 which is of the same order of magnitude as that found in the case of a laminar wake. Thus from a knowledge of the distribution of x over the surface of the wing under consideration, it would appear possible to estimate the Reynolds number R_{crit} referred to the external flow above which laminar flow may be expected to break down.

The restriction imposed at present on the use of such an empirically derived relationship is the lack of evidence available with regard to its generality. Furthermore, the evidence obtained from the present experiments does not permit an attempt to give confirmation to the above chosen value for N since the techniques required to illustrate the presence of the striations were not and could not readily be employed. From a knowledge of the extent of laminar flow observed, together with the external flow Reynolds number, we are, however, in a position to infer both an upper and lower bound to the value of N as we shall see later, (para 7.6)

2.6. The Calculation of the Three Dimensional Boundary Layer in Steady Flow

2.6.1 General Notes

The difficulties to be encountered in attempting a calculation of three dimensional boundary layers cannot readily be surmounted because, since so little is accurately known of their behaviour, any approximations made must inevitably be associated with some degree of uncertainty. As far as the yawed cylinder and the sheared wing of infinite span is concerned, it has been suggested (ref.4) that since the equations of motion for the boundary layer flow show no interdependence between the chordwise and spanwise component expressions, then we may calculate the boundary layer giving separate consideration to each component flow. As to how the actual calculations are performed is a question of choice in relation to the degree of accuracy required together with the methods available, but it is nevertheless usual to encounter severe restrictions in applying more exact methods to the problem.*

Prandtl, Sears and Cooke (refs. 19, 20 and 32) have given consideration to the equations for three dimensional laminar boundary layer flow and the calculations due to Sears (which were later extended by Gortler, Ref. 10) have facilitated the application of a solution by method of series. This latter method received a thorough treatment by Howarth (ref. 7) for the two dimensional case and the extension to three dimensional flow is for convenience summarised in Appendix III.

In practice we find that to apply this method to the calculation of the three dimensional swept wing boundary layer, the problem reduces to one of expressing the velocity normal to the leading edge as a power series in the arc length from the stagnation line, the form being

$$U_2\ (x_2) = \sum_{n=0}^{m} A_{2n+1}\ x_2^{\,2n+1}; \quad n = 0,1,2,\dots m$$

- the upper bound in the summation occurring by virtue of the at present restricted range of tabulated functions $f(\eta)$ and $g(\eta)$ (see Appendix III) necessary for the calculation of the required flow components.

Although a number of flow configurations exist which can be accurately described by putting $0 \leqslant m \leqslant 4$, the type of velocity distribution $U_2(x_2)$ in which we are interested (i.e. swept wing, low incidence case) does not in general lend itself to expression in the above series form with m limited, (for the sake of argument, to 4, say,) if we are to proceed for any appreciable distance from the stagnation line, and the difficulties (both analytical and numerical)

---

* The supposition that the principle of independence is true can only be asserted for the steady flow case as is shown by Stuart (ref.16) who has studied the equations of motion for disturbed flow.

become more serious as the thickness to chord ratio is decreased. However, if we restrict ourselves to a consideration of relatively short distances from the stagnation line, then the calculations not only become possible but can in fact be made quite simple. In passing we may note that the extension of the Von Karman-Pohlhausen approximate two dimensional solution to the three dimensional case has been performed by Wild (ref. 35) and Rott and Crabtree (Ref.36) have shown that the calculation of the laminar boundary layer to an adequate degree of accuracy may be accordingly simplified. We shall not however concern ourselves with a discussion of these methods here.

For the present work two methods of calculating the laminar boundary layer over the leading edge of the swept wing were tried which we shall now discuss.

2.6.2. The Boundary Layer at the leading edge of the Swept Back Wing.

For an enquiry into the nature of the secondary flow occurring near to the leading edge of the swept back wing at zero incidence used in the present experiments we refer first to the measured and calculated distributions of velocity, between which there is excellent agreement (see Fig.19). Ideally we require to calculate the boundary layer over an extensive region of the wing, but the shape of the velocity distribution (Fig.19) does not lend itself to expression as a series of the required form (see A.3.5.) having small number of terms. We can however, represent the distribution over the leading edge very accurately by an expression of the form

$$\sum_{n=0}^{m} A_{2n+1} \, x_2^{2n+1} = \frac{\pi x_2}{5} - \frac{1}{6}\left(\frac{\pi}{5}\right)^3 x_2^3 + \frac{1}{120}\left(\frac{\pi}{5}\right)^5 x_2^5$$

(see A.3.12) for $o \leqslant x_2 < 2.5$ (where x_2 is in dimensional form (inches) since we are considering a particular case) and hence proceed to a calculation of the boundary layer by the method of series. The chosen procedure is given adequate discussion in Appendix III.

Resolution of the calculated chordwise and spanwise boundary layer velocity components on to the co-ordinate system ξ_1, ζ_1 of the external streamline (Fig.16) yields the primary and secondary distributions shown (Fig.21) and in this case the secondary flow Reynolds number is given by:

$$\frac{\chi}{R^{\frac{1}{2}}} = \left| \bar{w}_{\zeta_1 \max} \right| \; \bar{q}_s \; \eta_\delta \; \sqrt{\frac{5}{\pi c_0 \cos \Lambda}} \qquad (2.6.1)$$

in which $\bar{q}_s = \frac{q_s}{U_0}$, and where η_δ is the value of η chosen to represent the boundary layer thickness. In this case it is convenient to take the value of η corresponding to $\bar{u}_{\xi_1} = 0.99$ thus referring the secondary flow Reynolds number to a "physical profile width". It would no doubt prove more suitable to choose values for η corresponding to the boundary layer displacement or momentum thickness along the streamline since these quantities are more readily defined precisely. However, as stated above, the choice was made for convenience, and the resulting distribution of $\chi / R^{\frac{1}{2}}$ is shown in fig.24.

2.6.3. The Boundary Layer Flow for a "Wedge" Profile

Referring again to fig.19. it can be seen that to the exclusion of regions in the immediate vicinity of the leading edge an approxi-mately similar velocity distribution to that existing over the forward part of the wing is represented by an expression of the form :

$$Q_2 = A_1 \, x_2^m$$

for which the boundary layer may be readily calculated following the methods of Hartree (ref.31.) and Cooke (ref.32), (see Appendix $\overline{\text{IV}}$ for details). More particularly a velocity distribution of this kind describes the flow in the neighbourhood of the leading edge of a wedge shaped profile (for which in the plane A, the wedge angle β is given by $\beta \; \frac{2m}{m+1}$, and the nose radius is vanishingly small) and hence does not strictly bear any relation to the present work as far as the experiments are concerned but is nevertheless an interesting example worthy of some consideration from a theoretical point of view. We use it here together with the results of para. 2.6.2. to illustrate (para. 2.7.) the effects of nose radius upon the secondary flow for regions very close to the leading edge.

The calculations (performed as outlined in Appendix $\overline{\text{IV}}$ yield the velocity distributions shown in fig.22., whilst the Reynolds numbers for the secondary flow (fig.24) are given by:

$$\frac{x_1}{R^{\frac{1}{2}}} = \left| \bar{w}_{\zeta_1} \max \right| \bar{q}_s \frac{\eta_\delta}{\sqrt{\frac{m+1}{2}}} \sqrt{\frac{x_a}{c_o}} \cdot \sqrt{\frac{U_o}{U_2(x_2)}} \qquad (2.6.2)$$

2.7. Secondary Flow Velocity and Associated Reynolds Numbers.

The calculated distributions of the maximum values of the secondary flow velocities associated with the two types of external stream considered, exhibit very different properties in the neighbourhood of the leading edge, as was expected. The results clearly show the important influence of the absolute magnitude of the leading edge nose radius upon the maximum velocity attained in the secondary flow and its corresponding influence upon the profile Reynold's Numbers. Illustration of this effect in relation to the velocity along the external streamline is facilitated by reference to the curves shown in fig.24.

From the calculations made for the boundary layer flow over the wing leading edge (according to the method of para.2.6.2) it may be seen that the secondary flow Reynolds Number reaches a peak value $\left(\frac{x}{R^{\frac{1}{2}}} = 0.0485\right)$ at a short distance from the stagnation line, this trend agreeing qualitatively with that given by the calculations of Owen and Randall (ref.17.).

The calculations do not unfortunately give any definite indication of the behaviour of $\frac{x}{R^{\frac{1}{2}}}$ for regions further downstream than those considered. To obtain such information using the more exact methods of boundary layer theory would involve a step by step integration starting from some chosen calculated velocity profile, from thence proceeding the requisite distance downstream. However, on the assumption that the peak shown (fig.24) represents the maximum value attained by $x/R^{\frac{1}{2}}$, then following Owen and Randall (ref.17) the condition for instability to occur in the secondary flow may be written as:-

$$\frac{x_{max}}{R^{\frac{1}{2}}} = \frac{N}{R^{\frac{1}{2}}_{crit.}} \qquad (2.7.1)$$

with $\frac{x_{max}}{R^{\frac{1}{2}}} = 0.0485$ from the calculations.

Thus by experimentally determining the Reynolds number $\left(R_{crit} = \frac{U_{o\,crit.}\, c_o}{\nu}\right)$ at which the first indication of secondary flow instability is apparent, N can be fixed.

2.8. Secondary Flow: General Notes

The calculation of the boundary layer by the method of para.2.6.2. yields an accurate representation of the flow conditions occurring over a short distance from the stagnation line. It has shown the principal effects of the secondary flow to be confined well within the region considered, thus rendering them readily calculable. Furthermore, since the distribution of $x/R^{\frac{1}{2}}$ is accurately known with regard to distance along the wing surface then the regions in which some form of boundary layer control should be applied to suppress the secondary flow instability are correspondingly well defined.

The calculations for the wedge profile suggest that, since for the case considered $\frac{x}{R^{\frac{1}{2}}}$ increases continuously with increase in x_2 then a detailed study of secondary flow instability together with the subsequent vortex formation in its relation to the Reynolds number of the external stream, is possible.

3. EXPERIMENTAL CONSIDERATIONS.

3.1. Suitable Test Methods

In para.1.4. we have made reference to the fact that the study of the three dimensional boundary layer occurring on a swept back wing is one in which the effects of scale are of great significance and it was pointed out that the needs were, therefore, for experiments enquiring into the nature of this flow to be conducted at something approaching full scale Reynolds Numbers. To achieve this object we can proceed in one of two ways; we can choose either to perform our tests using a very large wind tunnel or by mounting the test wing on to a suitable aircraft as test vehicle, in the manner described. The problem was reviewed by Britland (Ref.15.) and the various problems associated with either technique briefly outlined.

As far as wind tunnel tests are concerned, in the case of a swept wing of finite span we are very much more restricted than would be the case with the two dimensional wing. Briefly, this is mainly due to the compounded effect of sidewash and wind tunnel constraint, the result being that a relatively large working section is required for the satisfactory testing of a model of relatively small span. There is also the added effect of wind tunnel turbulence which is necessarily related to and has an effect upon the behaviour of boundary layer transition. On the other hand, if we mount our test wing in the manner to be described and in fact make free flight tests, we have firstly the added advantage of an easily obtained high value of Reynolds number and secondly the further advantage of a presumably small degree of free air turbulence. Arguments will inevitably arise that the effects of propeller noise on the stability of the boundary layer might lead to premature movement of the transition fronts, but in reality little is known of the precise significance of such an effect. However, in some previous experimental test work performed in flight on the boundary layer characteristics of a swept back wing (Ref.26.) it was found possible to achieve appreciable areas of laminar flow and we may conclude that the effects of propeller noise and the disturbance effects of the slip stream tubes did not influence the behaviour of boundary layer transition to any apparent extent. In tests on the 'King Cobra' wing, Gray observed also that there appeared to be no apparent effects of any significance, arising from propeller noise and slip stream disturbance, in relation to the boundary layer flow.

Consideration of both the advantages and disadvantages inherent in either method of test led to the choice of testing in free flight (using an Avro Lancaster MK VII as test vehicle), the experimental wing being mounted as a dorsal fin upon the mid upper fuselage. Tested in this way the wing may be considered free from any constraint whatsoever on its induced side wash. Such a procedure however necessitated the derivation of a simplified test technique for the measurement of the boundary layer so that the experiments could easily, simply and rapidly be accomplished with the minimum of flying time and whilst, in view of these simplifications, we are necessarily restricted to some degree in our interpretation of the experimental results so obtained, it has nevertheless been found that the chosen test method was most satisfactory in its application.

3.2. Choice of Experimental Plan, Techniques and Procedure

In the initial stages of the conception of this experimental work it was hoped that pressure transducers could be used for the required aerodynamic measurements, but lack of experience with this type of equipment resulted in reverting to the usual liquid manometer methods for the recording of pressures. In view of the relatively high test Reynolds Numbers to be encountered and the liquids available as manometric fluids, together with the degree of accuracy required in measurement, it was necessary to use a very large vertical manometer installed in the aircraft. Although at first this presented a problem of some difficulty it was eventually overcome and as described in Ref.25 a 50 tube manometer, some 7 ft. in height, was installed in the rear fuselage of the aircraft together with camera observation unit. This latter is a necessity for experiments of this kind when conducted in flight for although the required experimental conditions can be set with a high degree of accuracy and stability by the pilot, such conditions can only be set and maintained for a relatively short space of time due to the combined effects of pilot fatigue and natural disturbances to the steady flight of the aeroplane. Thus the requirement is for measuring apparatus in which pressures can be displayed and recorded with an absolute minimum of time delay so as to eliminate as nearly as possible the inevitable discrepancies which would occur in measurements of this kind made over relatively long periods of time. Experience had previously shown that a maximum time delay of 10 seconds was all that could be allowed between the initial establishment of the required experimental conditions and the recording of the displayed pressures if the degree of accuracy aimed at was to be achieved. To this end, therefore, the design and construction of the experimental equipment was directed from the outset.

The measurement of the static pressure distribution over the swept wing model presented no difficulty at all, the pressures being measured in the usual way and displayed on the manometer. However, for the measurements in the boundary layer, the choice of a suitable experimental technique was at first one of some difficulty because of the very nature of the boundary layer flow to be expected on a wing of this kind. Nevertheless as was stated in Paragraph 1.3. it was thought possible for the wing under consideration to greatly simplify the boundary layer measurements by applying techniques strictly correct for the two dimensional case only, to certain regions of the wing. The actual techniques chosen were similar to those used in the flight experiment of Stevens and Haslam, (Ref.11) the type of boundary layer combs used in this case being as shown in Figs.12 and 13. The method of experiment was to study first the boundary layer at the maximum thickness of the wing by attaching a number of the boundary layer combs to the wing surface by means of Sellotape at various positions along the span, from thence proceeding in stages of chosen length towards the leading edge of the wing. In this way it was possible to conduct the experiment with the best possible surface finish always existing in regions ahead of the plane of measurement. With the combs in position at any one chordwise station, on one surface of the wing a flight was made and the boundary layer measured for a number of configurations of speed and wing incidence. The measurements were referred to both upper and lower surfaces of the wing;

this being possible because the wing was of symmetrical section and the installation in the aircraft permitted its rotation in either direction about the axis of the main spar extension to an extent of $\pm$ 10°. Thus since the measurements were made using one side of the wing only, the effects of any contour irregularities would thus be common to the results obtained for both upper and lower surfaces. With a view to pilot and crew fatigue, a boundary layer exploration of this kind was found to constitute sufficient experimental work for one flight, these occupying on the average about $1\frac{1}{2}$ hours flying from take-off to landing and roughly involving measurements in some 230 boundary layers. Provided the limitations imposed upon the results so obtained by the nature of the technique used are understood, it can be seen that the method does nevertheless constitute a very rapidly determined assessment of the boundary layer flow.

By way of comparison we refer to a number of other swept wing boundary layer tests which have been conducted at the College using a traversing gear as described in Ref.26, the measurement of all components of the boundary layer flow in curvilinear planes adjacent to the wing surface being possible with this gear. It was found that, to explore the boundary layer at one chordwise station for one value of wing incidence and test Reynolds Number, a flight of approximately 30 minutes duration was required (inclusive of take off and landing).

4. EXPERIMENTAL EQUIPMENT

4.1. The Aircraft

The aircraft used as vehicle for the series of tests under consideration was an Avro Lancaster Mk 7 P.A. 474. This aircraft was subjected to a number of structural modifications in order that the wing could be mounted above the mid upper fuselage. The position chosen for the mounting of the wing on the mid upper fuselage was a compromise between fuselage structural design considerations and the results of preliminary exploratory tests relating to the nature of the flow field over the fuselage. We shall not concern ourselves with a discussion of the various design features in this report, the reader's attention being drawn to Ref.23 for a detailed discussion of the work involved.

4.2. The Pressure Plotting Mast

Consideration of the nature of the flow field over the mid upper fuselage of the aircraft into which the wing was to be immersed has been the subject of discussion in Ref.24 in which the equipment methods and techniques employed for calibrating this field were treated. Since a full description of the pressure plotting mast is therein contained, further consideration in this work is unnecessary.

4.3. The Wing and Installation

The swept back half wing constructed for the tests under discussion was of general dimensions as shown in Figs.3 and 4. It was of 45° sweep, untapered and untwisted and its streamwise section was intended to effectively represent a 10% thickness to chord ratio aerofoil of 130 inches chord (as discussed in paragraph 2.1.), the representation being attempted by geometrically constructing the wing section of two semi ellipses each of minor axis 13 inches and of major axes 104 inches and 68 inches for the forward and rear portions respectively. Although the leading edge itself was detachable so that different nose radii could be fitted if so desired, only one value of leading edge nose radius has been considered in the present series of tests, this value being 0.822 inches.

Consideration of the structural design and surface finish requirements together with the constructional problems involved led to the choice of a composite wood metal structure for the wing. Basically it consists of a conventional metal spar, having birch ply bonded to each face of the wing, and leading and trailing edge beams of spruce. The wooden ribs were closely spaced (at 6inches centre line to centre line), and the skin was 16 S.W.G. Light Alloy Sheet bonded to birch ply. The skin was attached to the ribs using the normal glueing technique and during assembly an internal humidity seal was effected by spraying the wooden members with phenoglaze G.300 as and where necessary. The leading and trailing edge members themselves were of laminated mahogany construction, these also being coated with phenoglaze.

For attachment of the wing to the aircraft, two heavy steel joint plates are used to carry the spar boom end loads into both the root end rib and the wing spar extension, the latter of which is attached to internal members of the aircraft fuselage (see Ref.23) and is suitably hinged to permit rotation of the wing about the axis of the spar extension so that the axis of symmetry of the wing section may be moved to any desired angular position relative to the plane of symmetry of the aircraft within the range $\pm 10^\circ$ (see Fig.6b). The angular position of the wing in relation to the plane of symmetry of the aircraft (i.e. wing geometric incidence) could be fixed as desired by means of two simple spigot clamps as shown in Fig.6c. Between the forward spigot clamp and a suitably chosen fuselage member a heavy incidence actuating jack was attached, and the arrangement of the whole assembly was such that the wing geometric incidence (i.e. angular position relative to aircraft plane of symmetry) could be conveniently adjusted to any desired position in the range $\pm 10^\circ$, indexing being achieved by reference to the incidence sector plate and pointer as shown in Fig.6c.

To reduce the interference effects of the aircraft fuselage boundary layer upon the flow over the wing, a wide boundary layer fence was fitted as shown in Fig.6c. This fence was not large enough however to consitute a reflection plate.

For pressure distribution measurement chordwise rows of static pressure tappings were built into the wing at three spanwise stations. There were thirteen tappings in each row and their positions along both the span and chord of the wing are given in Table I and Fig.3. The leads from the static pressure tappings were of 5/32" diameter copper tubing and passed through the interior of the wing adjacent to the main spar and from thence into the interior of the aircraft fuselage and so on to the manometer. Provision for a number of additional static pressure tappings positioned around the nose of the wing was made by means of neoprene tubing let into the leading edge as shown in Fig.6a. In this way a number of closely spaced static pressure tappings could be obtained by simply drilling into the neoprene tubes at chosen chordwise positions, each hole so formed being sealed with beeswax upon becoming redundant.

The wing surface was finished using Titanine lacquers (colour, black) and to meet the requirements for surface waviness in relation to laminar flow a number of measurements were made during the preparation of the surface for the purpose of locating "high spots" etc., so to direct the course of the "rubbing down" and filling processes. Initial measurements were made to this end by means of a curvature gauge of the usual type, but difficulties encoutered with the interpretation of such measurements together with the times required to so inspect the surface led to the choice of an oblique lighting technique not unlike that devised by Gray (Ref.27). In this case a fluorescent strip light was suitably mounted alongside the wing in the painting room and by observing an oblique reflection of this light in the wing surface local high spots and surface waviness could be simply and rapidly detected. Using this technique the spraying, rubbing down and filling processes became one of continuity, and by much careful work the desired results were eventually achieved.

For the convenience of surface position reference on the wing, a white "grid" was sprayed onto the surface (see Fig.10.) this being made possible by suitably masking the wing and proceeding in the usual way. Only an extremely thin coat of paint was required to achieve this object and so whilst in fact each line of the "grid" does constitute a discontinuity of surface contour, the magnitude of this discontinuity was considered small enough to be neglected. As a final measure the wing surface was finished to very high gloss using wax polish.

The wing structure and assembly weighs approximately 500 lbs. and was constructed by and under the direction of Mr.Martin in the workshops of the Department of Flight at the College of Aeronautics.

4.4. Instrumentation: The Manometer and Recording Apparatus

A fifty tube manometer, some 7 feet in height and 30 inches wide, complete with camera observer unit, was installed in the rear fuselage of the aircraft as indicated in Fig.2. A detailed description of the design, construction, and installation of this large instrument in the relatively confined interior of the aircraft fuselage may be found in Ref.25 and we shall not therefore concern ourselves with the various design features of the unit here. Suffice it to say that static and dynamic pressures supplied from connections made in the usual way to the chosen pressure sources, were displayed as required on the instrument, the free stream dynamic head (uncorrected for S.P.E.C.) being directly indicated on a separate 'U' tube unit incorporated in the manometer and connected to the aircraft pitot static system. Two further tubes, one at each side of the manometer face were connected to the aircraft static system for the purpose of providing under test conditions a datum to which all measurements could be referred. By this means allowance could be made for the effect of small angles of bank occurring during tests and the corresponding settling of the fluid to its gravitational level. Depending upon the range of pressures to be measured two different manometric fluids were used as required. These were:-

Carbon Tetrachloride S.G. = 1.599
Distilled Water (using fluorescene for colouration)

Observations of the manometer were facilitated by means of an F.24 camera in a form slightly modified for improved film economy, illumination of the manometer being accomplished in a most satisfactory manner by means of a system of back lighting (see Ref.25 for full details) supplied from one of the 24 V. power circuits available on the aircraft.

4.5. Directional Yawmeter

Since one of the basic requirements of the tests performed was for steady, straight and level flight at predetermined angles of sideslip a vane type yawmeter was fitted to the starboard wing tip of the aircraft as shown in Fig.2. This yawmeter was connected to a Desynn type indicator mounted on the pilot's instrument panel, and following a suitable calibration provided an accurate means of consistently reproducing the required angles of sideslip (to approximately $\pm \frac{1}{4}^{\circ}$) in steady flight.

4.6 The Boundary Layer Combs and Transition Indicators

For an exploration of the boundary layer on the wing, two types of comb were used, these being as shown in Figs.12 and 13, the one for the purpose of determining the boundary layer velocity profile (Fig.13 and the other (Fig.12) for the purpose of measuring the distribution of total head, at, near to, and along the wing surface respectively. They were designed to give satisfactory operation for a fairly wide range of experimental conditions and were conveniently and simply attached as and where required to the wing surface by means of Sellotape, the brass strap and moveable brass stirrup (see Fig.13) of the boundary layer comb serving not only as a brace but also as a datum fixing for the tube assembly. A full description of both types of comb together with details of some simple wind tunnel tests performed to assess their usefulness may be found in Ref.25.

4.7. Pressure Leads and Piping

The pressure leads from the boundary layer combs etc., positioned on the wing surface to the manometer inside the aircraft were for convenience split into two stages as shown in Fig.9, each stage being united via the thoroughfare tube assembly units positioned at the trailing edge of the wing at a number of spanwise stations. The leads from the boundary layer combs to the trailing edge of the wing were of 3 mm.O.D. neoprene tubing (which by virtue of its resistance to kinking was found to be very suitable) and were initially made of sufficient length to enable the traverse to the leading edge to be completed without further attention being given to the lead length, the excess tube length during intermediate tests being coiled and "stored" at the trailing edge.

For the pipe work from the thoroughfare tube assembly units to the manometer a number of 'tapes' of tubes were used. These tube 'tapes' were approximately 3" wide and each consisted of ten plastic (P.V.C.) tubes of 3/16" O.D. They were rigidly fixed to the trailing edge of the wing by means of a number of 18 S.W.G. brass fixing straps screwed in place and the whole of this pressure lead assembly was completed by an entire covering of Sellotape which proved very satisfactory under test conditions.

5. DETAILS OF EXPERIMENTS PERFORMED

5.1. Choice of Test Altitudes and Airspeeds

From previous experience of experiments of this kind together with a consideration of the aircraft operating conditions and the requirements of the test led to the selection of a basic test altitude of 10,000 feet (I.C.A.N.) with provision for testing at either 5,000 feet or 7,000 feet the final choice depending upon the suitability of weather conditions. (no corrections for non standard temperature conditions were made.) The test airspeeds were chosen to give the maximum attainable range of Reynolds numbers consistent with both ease of operation and with design limitations imposed by the speed - incidence boundary curve for the aircraft (see Fig.8).

The actual Reynolds number range achieved was from 0.88×10^6 to 1.92×10^6 per foot and for Lancaster P.A. 474 this corresponds to a speed range of from 90 - 195 knots (I.A.S.) at a test altitude of 10,000 feet (I.C.A.N.) the altimeter pressure error correction being neglected in all cases. It is of interest to note that although flaps were not used for these experiments it was found possible to increase the workable speed range of the aircraft down to a minimum safe comfortable flying speed of 90 knots (I.A.S.10,000 feet I.C.A.N.) against the value of 100 knots (I.A.S. 5,000 feet I.C.A.N.) quoted in Ref.24.

Although for such a variation in aircraft forward speed the directional characteristics of the flow over the fuselage in the pitching plane might possibly attain considerable proportions, initial tests performed to determine these changes showed that in the worst case the directional change did not in fact become one of significance (the maximum observed variation being one of $\pm 2^{\circ}$ for the entire speed range) and hence the angle of sweep of the half wing was treated as being sensibly constant at 45° (see Ref.24).

5.2. Measurement of S.P.E.C. and Calibration of the Fuselage Flow Field

Full details of the tests performed to determine both the S.P.E.C. curve and the nature of the flow field above the mid upper fuselage into which field the wing was immersed, have been reported elsewhere (ref.24) and hence will not receive further attention here.

5.3. Incidence Zero Datum Setting of the Half Wing

Although as pointed out in paragraph 4.3. the geometric incidence of the wing could be accurately set by rotation about the axis of the spar extension and reference to the incidence sector plate, such a setting does not of course necessarily correspond to an equivalent incidence setting in flight due to the small but almost inevitable conditions of assymetry which arise. To make allowance for these conditions and to make for ease of repetition of the required test configurations the following method of setting the wing geometric incidence was adopted.

It was decided to refer the wing geometric incidence at all times to an exact reading on the incidence sector plate and by suitably fixing the angle of sideslip of the aircraft (at a value corresponding to that giving zero aerodynamic incidence with the wing geometric incidence at zero according to the sector plate reading) it was possible to achieve experimental conditions which could be accurately and consistently reproduced.

The angle of sideslip required for a zero aerodynamic incidence setting of the half wing was determined by observing the static pressure differential across six static tubes paired off on opposite surfaces of the wing and connected to the manometer. With the wing set at zero geometric incidence, the pressure differential across each pair of tubes was balanced in flight by sideslipping the aircraft the requisite amount, and the corresponding reading on the pilot's sideslip Desynn indicator (see paragraph 4.5) noted. At chosen speeds throughout the range required for experiment this reading was found to be constant and correspond very nearly to zero sideslip as was hoped for.

This particular test provided occasion to observe the manometer fluid columns very closely indeed, and this subsequently gave an indication of the accuracy which might be achieved in future experiments. It was found that experimental conditions could be set and maintained such that the fluctuation of the fluid columns in the instrument did not exceed 1/32" given favourable atmospheric conditions, and it was thus to achieve a similar standard of accuracy that the aims of subsequent experimental operations were directed.

5.4. Measurements of the Static Pressure Distribution over the Swept Back Half Wing

With the static pressure tappings in the swept back half wing connected to the manometer and using carbon tetrachloride as the manometric fluid a flight was made to determine the distributions of static pressure over the half wing for incidences of 0°, 2°, 4°, 6°, 8° and 10°, and for Reynolds numbers in the range $0.88 \times 10^{6} - 1.92 \times 10^{6}$ per foot, for both upper and lower wing surfaces. Manometer readings were recorded photographically using the F.24 observer camera, and from these records the required readings were obtained, corrected for S.P.E.C. and reduced to yield the non dimensional pressure coefficients.

5.5. Flow Visualisation on using the Tuft Technique

The nature of the flow at and near to the surface of the swept back wing together with its relation to the boundary layer and the techniques employed for measurements has received some consideration in paragraph 1.3. To assess the nature of the flow over the particular wing under consideration, one surface of the wing was extensively tufted using white 3 ply wool tufts.

Although it was possible to observe part of the wing surface from the aircraft cockpit, a satisfactory arrangement for making the required flow studies such as the fitting of a remotely controlled observer camera or camera periscope combination could not conveniently be contrived and consequently the wool tuft observations of the flow over the wing were performed from a second aircraft (D.H.Dove G-ALVF) flying in close formation with Lancaster P.A.474. The observations were of course made photographically using both a 35 mm. camera fitted with a long focus lens and a 16 mm. cine camera. By working to a systematic schedule and by close co-operation between the pilots (in radio communication) and observers in both aircraft this part of the experimental programme was successfully completed and the necessary results obtained.

Since there was some difference between the operating speed ranges of both aircraft the tests were in fact only performed at one nominal air-speed (approximately 120 knots I.A.S. at a test altitude of approximately 7,000 ft.) this being chosen as the most suitable compromise for flying the two aircraft in close formation.

5.6. Explorations of the Boundary Layer

The boundary layer on the swept back half wing was explored extensively using the two types of comb discussed in paragraph 4.6, measurements in the boundary layer being made at a number of stations along the chord commencing at the position of maximum thickness to regions close to the leading edge and at spanwise stations as indicated in Fig.3. For each flight undertaken the measurements were made at one chosen chordwise station for incidence values of 0°, 2°, 4°, 6°, 8°, 10°, upper and lower surfaces, and for Reynolds numbers of $1.08 - 1.92 \times 10^{6}$ per foot with additional tests at a Reynolds number of 0.88×10^{6} per foot for incidence of 0°, 2° and 4°.

The restriction of the wing incidence to 4° at the Reynolds number of 0.88×10^{6} per foot was by reason of problems encountered in the handling of the aircraft at the forward flight speed (90 knots I.A.S.) required to give this Reynolds number, for whilst flight at this low speed was under normal circumstances quite easily achieved, the effect of the wing itself, when at the higher values of incidence (i.e. $\alpha = 6^{\circ}$ approximately) upon the handling of the aircraft was quite noticeable to the extent that it was considered inadvisable to attempt to consistently and accurately reproduce experimental conditions in which the wing incidence exceeded values of $\alpha = 4^{\circ}$.

To determine whether or not flow separation was occuring at the leading edge of the boundary layer fence and consequently disturbing the flow near the wing root, two transition indicators (Fig.12) were attached to the upper and lower surfaces respectively. They were positioned approximately 3 inches from the leading edge and "piped" to adjacent tubes on the manometer. By observing the difference between the readings given by the total head tubes the presence of any serious flow separation could, if it occurred, be detected. No such conditions were however observed for the flight test configurations.

Throughout the tests, observations of the manometer were recorded photographically and from the film records so obtained the required readings were taken, corrected as and where necessary for S.P.E.C., and reduced to yield the boundary layer velocity profiles together with the distributions of total head at, near to and along the wing surface for the various chosen test configurations.

During two of the initial flights in which the boundary layer was being measured an attempt was made to obtain some idea of the extent of laminar flow to be expected at the lower Reynolds numbers an at an incidence $\alpha = 0^{\circ}$ by making use of the chemical sublimation technique. Prior to flight the forward portion of the wing was sprayed with a 3% solution of acenapthene in petroleum ether and observations of the wing were made during the climb to, and for a flight of some fifteen minutes duration at, test altitude. On neither of the two occasions could any discernible patterns be observed from the aircraft flight deck blister and hence the method was not subsequently tried. It is true to say that perhaps more extensive and elaborate tests could have been performed using this technique, but the idea was abandoned in favour of the boundary layer explorations detailed above. The actual chemical sublimation tests performed do therefore constitute little more than a 'by the way' experiment conducted in addition to the main boundary layer exploration.

6. PRESENTATION OF EXPERIMENTAL RESULTS

The above experiments (paragraph 5) have yielded a fairly comprehensive range of results of which a large selection is presented in Figs. 25 - 35. Many of these have been left in dimensional form for convenience.

The measured distributions of static pressure and the corresponding chordwise loadings are presented in both tabular (Tables II and III) and graphical (Figs.25 and 26) form : the boundary layer measurments only graphically, these being grouped according to the test Reynolds number ($R = U_o c_o / \nu$) and chordwise position(x/c_o) of investigation. Reference to the various figures is made as and when they receive discussion.

7. DISCUSSION OF THE EXPERIMENTAL RESULTS

7.1. Behaviour of the Aircraft and Equipment under Experimental Conditions

The behaviour of Lancaster P.A.474 together with its ancillary equipment during the series of tests described was at all times very good, and the simplicity of the techniques employed permitted the completion of the experimental programme in a generally trouble free manner.

By working to a systematic schedule in the air a large amount of experimental work could be completed in a short flying time, but to achieve this a great deal of time was however required for 'ground work' to ensure as nearly as possible a faultless behaviour of the equipment whilst airborne.

Now that this method of test has satisfactorily proceeded through the initial stages it is hoped that future more elaborate experiments of a similar kind will be performed at the College.

7.2. Accuracy of Results

In assessing the accuracy of the results obtained the principal factors to be considered are:

1. the limitations of the methods employed for measurement
2. the attainable stability of experimental conditions
3. the accuracy involved in the reading of the observer camera film records

1. and 2. are discussed in paragraphs 1.3 and 5.3 whilst 3. receives consideration in Ref.25.

The only serious influence is likely to arise from 1. in relation to the boundary layer measurements. However, a careful scrutiny of the various experimentally derived curves shows that the degree of point scatter is, almost without exception very small, each curve being well represented by the experimental points to which it is fitted. Moreover, no immediate effects indicating the unsuitability of the apparatus to fulfil the purpose were apparent, and hence there is reason to suppose that the quoted results represent a good deal more than just a generalised qualitative assessment of the boundary layer flow.

The accuracy of particular sets of results will be mentioned as they receive discussion.

7.3. Distributions of Static Pressure

The distributions of static pressure as measured for the swept back half wing may be seen in Fig.25.

When plotted out as individual curves (at constant incidence) for each of the test Reynolds numbers considered, small differences were found to exist between them. This was not due to point scatter, as each curve was too well defined, but to a generalised displacement of the curve as a whole away from its neighbour. This displacement was as stated above quite small and since it did not show any particular trend with change in Reynolds number could not definitely be attributed to any apparent cause. Moreover it was found that the measured chordwise loadings $\Delta C_p = \left(C_{p_L} - C_{p_U}\right)$ yielded identical (within acceptably small limits) curves for different Reynolds numbers. It was therefore assumed quite in order to represent the measured distributions of static pressure as mean values for the Reynolds number range considered. In this way the curves shown in Fig.25 together with the pressure coefficients quoted in Table II were obtained.

It can be seen that the curves (Fig.25) are very well defined and it is of particular interest to note the distribution of the experimental points in the neighbourhood of the leading edge, where both the suction peaks (upper surface) and the stagnation lines (lower surface, $C_p \approx + 0.5$) are clearly indicated. It is appreciated that the curves for the lower surface as depicted in Fig.25 appear somewhat congested near to the leading edge and are therefore not readily interpreted but the trends under discussion were observed from plots to approximately four times the scale shown. With regard to the suction peaks, the very fact that these are defined so well is a direct indication of the accuracy and stability to which the experimental conditions could be set and maintained whilst measurements were being made. This is realised by considering a small momentary disturbance to the test aircraft resulting in sideslip and the accompanying change in incidence of the swept back wing. For regions near to the leading edge such a condition results in the development of oscillations of considerable amplitude in the fluid columns at the manometer and the required measurements cannot thus be made.

The distribution of static pressure calculated on the basis of the infinite sheared wing at zero incidence (see paragraph 2.3 and eq. 2.3.4) is compared with the measured distributions in Fig.27. The agreement between theory and measurements at the mid semi span station is good and the tip and root station measurements show the type of departure to be expected when making such a comparison, e.g. greater concentration of suction near the nose with increasing distance outboard along the span. This latter effect is also illustrated by the measured chordwise loadings which are shown in Fig.26.

The transition to turbulence of the flow in the boundary layer on the upper durface of a swept back wing is influenced both by the onset of sweep instability (also common to the lower surface) and by the development of nose suction peaks. For the wing under consideration the nose suction peak is well developed at each of the chosen spanwise stations when the wing incidence reaches $a = 6^{\circ}$. Accordingly, at this ($a = 6^{\circ}$) and higher values of incidence little, if any, laminar flow may be expected. This is subsequently shown to be the case.

7.4. The Flow over the Wing: Tuft Observations

The flow over the wing as indicated by wool tufts may be studied on referring to Fig.28b where a selection of results are presented. Here it is necessary to distinguish between an actual change in flow (indicated by an orientation of the tuft about its point of attachment to the wing surface) and an apparent change due to unequal spacing of the tufts upon the wing surface in the spanwise direction.

The remarks which are to be made concerning these observations are founded not only upon results of the type shown in Fig.28b but also upon existing cine film records.

At zero incidence the flow over the wing appeared to be perfectly steady with no indication whatever of the formation of an unstable wake at the trailing edge. The tufts attached to the trailing edge were long (about 12 inches) and their general behaviour suggested a flow of the type shown in Fig.28c. As far as could be determined, separation occurred quite close to the trailing edge.

For the forward portion of the wing the streamline curvature is most serious in the neighbourhood of the stagnation line and this is well illustrated in the case for $a = 10^{\circ}$ lower surface. The presence of the tip vortex is also clearly indicated in general.

Some idea of the sensitivity of the tufts to changes in flow direction may be obtained from careful scrutiny of the flow at the wing root (below the boundary layer fence, bottom row of tufts) for $a = 8^{\circ}$ upper surface. Here the flow appears to separate from the vertical supporting member for the boundary layer fence which is positioned at the leading edge of the wing, and to subsequently result in a very disturbed flow formation in the region of the trailing edge.

The tufts did not indicate the presence of any disturbance in the flow over the wing which might be associated with a leading edge separation off the boundary layer fence. This is in agreement with the explorations made using transition indicators positioned near to the leading edge of the fence and mentioned in paragraph 5.6.

The tuft observations show that for a substantial portion of the wing surface (in particular for a region extending approximately from the 5 per cent chord position to the position of maximum thickness) there are no substantial departures in flow deviation from that of the undisturbed stream which is a necessary condition for the successful application of the techniques chosen for the boundary layer measurements.

7.5. Boundary Layer Measurements

7.5.1. Velocity profiles

A selection of the boundary layer velocity profiles as measured using the combs (Fig.13) is presented in Figs.29 to 31. It can be seen that, although the number of experimental points obtained for each profile is small in comparison with the number usually taken during normal boundary layer explorations in which traversing gear is employed, the curves as shown are nevertheless very well defined in general.

In some simple tests performed to assess the usefulness of the boundary layer combs (see Ref.25) the effect of yawing the comb in relation to the stream direction was discussed. It was found that under such conditions the measured profile was seriously affected with the angle of yaw fixed for example at 10°. No such effects could be detected in the results obtained from the present series of experiments thus indicating that the method employed for measurement was adequate. It is true that in some cases the odd experimental point has been ignored in the fitting of the curves, but the discrepancies in such cases have been attributed to the occurence of experimental error. It is useful here to point out the great difficulty of checking the experimental observations with regard to individual points as they are made in flight. Such a task becomes impossible when a large number of readings is being simultaneously recorded for each test configuration as was the case during the series of experiments described. Moreover the inevitable delay associated with the interpretation of the observer camera film records usually means that the experiment has meanwhile progressed through many further stages so that the checking of occasional results of doubtful accuracy becomes prohibitive for economical reasons. By careful work however, both in the preparation of the experimental equipment and in performing the actual experiment, such occasions seldom arise as may be seen from an overall and general inspection of the results quoted in this paper.

The measured velocity profiles show quite generally that very little laminar flow existed on the wing for the test configurations considered. In particular the occurrence of transition very close to the leading edge is indicated for all values of wing incidence, both upper and lower surfaces, with the test Reynolds number at, and above 1.55×10^6 per foot. The latter result appears to be quite definitely linked with the phenomena of sweep instability. At the same time however, it appears evident, that whilst following the onset of sweep instability at low incidence the boundary layer thickness δ rapidly increases with distance along the chord, this increase is not nearly so great as that accompanying the presence of an unfavourable pressure gradient. More detailed measurements may therefore show the corresponding increase of friction at the wall in the destabilised layer to be similarly affected.

No attempt has been made at this stage to give detailed consideration to the measured velocity profiles as a whole since it has been considered of greater importance to illustrate trends rather than to direct the course of the work along the lines of detailed analysis.

7.5.2. Boundary layer transition

From the measured distributions of total head at, near to, and along the wing surface (of which specimen results are shown in Fig. 34) together with the boundary layer velocity profiles of Fig. 29 to 31, it was possible to obtain a general picture of the position and behaviour of boundary layer transition as it occurred on the wing. The curves so obtained, and shown in Fig. 35, strictly correspond to the end of the transition region for they are defined by the positions at which the total head rise occurring in passing from the laminar to the turbulent boundary layer was completed. Consequently on making a comparison between the curves showing the positions of transition with the boundary layer velocity profiles, semi turbulent or 'transitional' profiles will be found corresponding to given transition front positions.

As stated in paragraph 7.5.1. very little laminar flow was found to exist on the wing, and for Reynolds numbers of 1.55×10^6 per foot and above, transition was observed to be very close to the leading edge for all incidence configurations and for both upper and lower surfaces. This behaviour of the transition front illustrates well the physical consequences of sweep instability.

7.5.3. Displacement thickness, momentum thickness, and shape parameter variation

A selection of curves showing the variation of the boundary layer displacement thickness δ_1, momentum thickness δ_2, and shape parameter δ_3, with wing incidence and test Reynolds number at different chordwise stations is presented in Figs.32 and 33. These curves were derived from the velocity profiles as measured at the mid semi span station and are thus approximately independent of tip and root effects. The usual distinctions for the laminar and turbulent boundary layer are in general quite clearly shown but in particular it may be noted that at the maximum test Reynolds number considered (1.916×10^6 per foot) at which the boundary layer was everywhere turbulent, the shape parameter appears to be very nearly independent of incidence.

7.6. The Critical Reynolds Number for the Secondary Flow

From the test results it is not possible to make a precise evaluation of the number N (eq. 2.7.1.) since we cannot determine the flow conditions for which the secondary flow instability is initiated. We can however infer both an upper and lower bound by noting that since virtually no laminar flow existed for a test Reynolds number of 1.552×10^6 per foot, then referring conditions to the wing chord along the stream (i.e. c_0 = 86 inches) we have on taking

$\frac{\dot{x}_{max}}{R^{\frac{1}{2}}} = 0.0485$ and substituting in eq. 2.7.1. that

$$N \simeq 160$$

Now the critical Reynolds number for the secondary flow strictly relates to the onset of the instability and subsequent vortex formation - it does not correspond to and accompany, but precedes boundary layer transition, so that firstly we conclude that

N cannot exceed 160

Secondly since laminar flow existed (i.e. to $\frac{x}{c_0} = 30\%$) at the lowest test Reynolds number considered (i.e. 0.884×10^6 per foot) we derive the second although somewhat less definite condition that (again with $\frac{x_{max}}{R^{\frac{1}{2}}}$ = 0.0485 and eq.2.7.1.)

$$N \nless 120$$

Thus the conditions for sweep instability are given by an equation of the type

$$\frac{x_{max}}{R^{\frac{1}{2}}} = \frac{N}{R^{\frac{1}{2}}_{crit}} , \quad 120 < N < 160$$

which is in very good agreement with the original work due to Owen and Randall (Ref.17)

8. CONCLUSIONS

I. A series of experiments relating to the boundary layer flow on a swept back wing mounted as a dorsal fin upon the mid-upper fuselage of Lancaster P.A.474 have been successfully completed by flight test methods.

At all times the behaviour of the aircraft used as test vehicle, together with its equipment etc. was found to be perfectly satisfactory.

II. Calculations for the boundary layer flow over the leading edge of the wing using the method of Series have shown the effects of secondary flow in relation to the instability of the laminar boundary layer to be confined within a very short distance from the stagnation line, as also found by Owen and Randall (Ref.17). Reference to the experimental results has shown the conditions for instability of the secondary flow to be given by an equation of the type

$$\frac{x_{max}}{R^{\frac{1}{2}}} = \frac{N}{R^{\frac{1}{2}}_{crit}} , \quad 120 < N < 160$$

III. Pressure distribution measurements have been made on the swept back wing for a geometric incidence range of 0° - 10° and Reynolds number range 0.88×10^{6} - 1.92×10^{6} per foot upper and lower surfaces being considered.

The measured distributions are in close agreement with calculations based on the infinite sheared wing and an equivalent source distribution for the zero incidence case (symmetrical section).

IV. Tuft explorations giving details of the flow over the wing on both upper and lower surfaces have shown that for incidences in the range $0^\circ - 10^\circ$ three dimensional effects do not achieve first order importance, thus permitting the use of strictly two dimensional techniques for boundary layer measurements.

V. A large number of boundary layer explorations have been successfully made showing that for both upper and lower surfaces virtually no laminar flow existed for Reynolds numbers (based on the wing chord in the free stream direction) at and in excess of 1.55×10^6 per foot.

For all incidence configurations, this is due to the occurence of instability in the secondary flow at the leading edge, and to a combination of secondary flow instability and the adverse pressure gradient following the development of (upper surface) suction peaks at an incidence of 6° and above.

The experiments have shown to the further support of already existing evidence (Refs.6, 26 and 29) that without the application of some form of boundary layer control, the possibility of maintaining regions of laminar flow of any appreciable magnitude on either the upper or lower surface of a swept back wing at full scale Reynolds numbers, is remote.

List of References and Bibliography of Works Consulted

1.	Goldstein, S. (Editor)	Modern Developments in Fluid Dynamics Vols. I & II Oxford 1952.
2.		Boundary Layer Effects in Aerodynamics N.P.L. Symposium Proceedings 1955 H.M.S.O.
3.	Keuthe, A.M. McKie, P.B. Curry, W.H.	Measurements in the Boundary Layer of a Yawed Wing. N.A.C.A. Tech. Note 1946. 1949.
4.	Jones, R.T.	Effects of Sweepback on Boundary Layer and Separation. N.A.C.A. Tech. Note 1402.
5.	McKoen, C.H.	Resolution of Velocity for the Swept Back Wing at Incidence. R.Ae.S. Journal, 1953.
6.	Anscombe, A. Illingworth, L.N.	Boundary Layer transition on a Wing at various angles of sweepback. R.A.E.Tech.Note Aero.2170. 1952.
7.	Howarth, L.	On the calculation of Steady Flow in the Boundary Layer near the surface of a cylinder in a Stream. A.R.C. R & M. 1632. 1935.
8.	Kuchemann, D.	Boundary Layers on Swept Wings. R.A.E.Tech.Note Aero.2370. 1955.
9.	Kuchemann, D.	Types of Flow on Swept Wings. R.A.E.Tech.Note Aero.2234. 1953.
10.	Gortler, H.	Zur laminaren Grenzschicht am schiebenden Zylinder. I. Arch. Math.3, 216-231, (1952).
11.	Stevens, A.V. Haslam, J.A.G.	Flight Experiments on Boundary Layer Transition in Relation to Profile Drag. A.R.C. R & M. 1800. 1938.
12.	Head, M.R. Johnson, D. Coxon, M.	Flight Experiments on Boundary Layer Control for Low Drag. R.A.E. Report Aero 2541. 1955.

13. Emslie, K., Hosking, L., Marshall, W.S.D. — Some Experiments on the Flow in the Boundary Layer of a 45° Sweptback Wing of Aspect Ratio 4. College of Aeronautics Report No.69. 1953.

14. Gray, W.E. — A Laminar Flow Experiment in Flight on a Swept Wing. R.A.E. Tech.Note Aero 2240. 1953.

15. Britland, C.M. — Techniques for laminar flow Research at high Reynolds Number. R.A.E. Tech Memo Aero 101.

16. Stuart, J.T. — An Interim Note on the Stability of the Boundary Layer on a Swept Wing. A.R.C. Report 14,991. 1952.

17. Owen P.R., Randall, D.G. — Boundary Layer Transition on a Sweptback Wing: A Further Investigation. R.A.E. Tech Memo Aero.330. 1953.

18. Byrd P.F., Freidman, M.D. — Handbook of Elliptic Integrals for Engineers and Physicists. Springer-Verlag. Berlin 1954.

19. Prandtl, L. — On boundary layers in three dimensional flow. M.A.P. Volkenrode Reports and Translations No.64. 1946.

20. Sears, W.R. — The Boundary Layer of Yawed Cylinders Journal of Aero Sciences 15, 49 1948.

21. Weber, J. — A simple Method for Calculating the Chordwise Pressure Distribution on Two Dimensional and Swept Wings. R.A.E. Report Aero. 2391. 1950.

22. Schlichting, H. — Boundary Layer Theory. Pergammon Press. London. 1955.

23. Addendum to Type Record. Avro Lancaster P.A.4.74. Dept. of Aircraft Design. College of Aeronautics, Cranfield 1956.

24.	Burrows, F.M.	Characteristics of the Flow Field over the mid upper Fuselage of Lancaster P.A.4.74. College of Aeronautics Note No.36. 1956.
25.	Burrows, F.M.	Equipment Used for Boundary Layer Measurements in Flight. College of Aeronautics Note No.49. 1956.
26.	Allen, L.D. Burrows, F.M.	Flight Experiments on the boundary layer characteristics of a swept back wing. College of Aeronautics Report No. 104. 1956.
27.	Gray, W.E.	A Quick Method of reducing the surface waviness of laminar flow wings. R.A.E. Tech.Note Aero.2078. 1950.
28.	Gray, W.E.	The effects of wing sweep on laminar flow. R.A.E. Tech. Memo Aero.255, 1952.
29.	Butler, S.F.J.	Transition on a Swept Back Wing. R.A.E. Tech.Note Aero 2324. 1954.
30.	Anscombe, A. Butler, S.F.J.	The Effect of Sweepback on the Laminar Boundary Layer. R.A.E. T.N. Aero 2335.
31.	Hartree, D.R.	Procs. of Cambridge Phil.Soc. 33. Part II. 223. 1937.
32.	Cooke	Procs. of Cambridge Phil.Soc. 46. 645. 1950.
33.	Gray, W.E.	The nature of the boundary layer Flow at the nose of a swept back Wing R.A.E. Tech. Memo Aero 256. 1952.
34.	Owen P.R. Randall, D.G.	Boundary Layer Transition on a Swept Back Wing. R.A.E. Tech Memo Aero 277. 1952.

35. Wild, J.M. — The Boundary Layer of Yawed Infinite Wings. Journal of Aero. Sc. 16. 41. 1949.

36. Rott, N. / Crabtree, L.F. — Simplified Laminar Boundary Layer Calculations for Bodies of Revolution and for Yawed Wings. Journal of Aero. Sc. 19. 553. 1952.

APPENDIX I

Pilot's Handling Techniques

by

B. F. Russell.

1. The Effects of the Experimental Wing on the Handling of Lancaster P.A.474.

The Lancaster handles normally in the air with the wing set at zero incidence, except that it is more directionally stable and the rate of roll is reduced.

2. The Effects of Cross-Wind

In the presence of a cross wind, both take off and landing are more difficult than normal. Take off in such conditions requires a large amount of differential throttle, whilst on landing it was found that "kicking the drift off" had to be left very late since although the aircraft will respond initially tb the rudder, it tends to return to the original heading. The maximum cross wind in which a landing was made was 25 KTS at 20° to starboard.

3. The Wing at Incidence

It was found that the aircraft could be trimmed to maintain zero sideslip with the wing set at any incidence within -10° to $+10^\circ$ and for speeds (I.A.S.) in the range 90 KTS - 195 KTS. A combination of large incidence and high speed gave rise to vibration and slight rudder buffet.

4. Technique

Leave engine r.p.m. constant, and adjust boost to maintain height at the required speed; trim elevator, rudder, and ailerons. Check A.S.I. altimeter, sideslip indicator, and directional gyro.

(Note: A small continuous change of heading is permissable providing the yawmeter is maintained at zero).

APPENDIX II

A.2. Calculation of the Distributions of Velocity and Pressure Over the Wing at Zero Incidence

A.2.1. The Actual Wing Section: Two Dimensional Case. (Incompressible Flow)

It is sufficient for our purpose to consider the wing at zero incidence and hence since the section is symmetrical the circulation in such a configuration is also zero. Under these conditions the wing thickness distribution may be represented by an equivalent source distribution such that along an elementary length dx of the chord line the total source strength is $\sigma'(x)dx$.

Thus for the actual wing section in two dimensional flow and in the coordinate system shown in fig.15, we may write the perturbation potential in the form :-

$$\bar{w} = -\frac{1}{2\pi}\int_{-a_1}^{a_2}\sigma'(\xi)\ln(\bar{z}-\xi)d\xi \qquad (A.2.1.)$$

where $\bar{z} \triangleq x + iy$.

The velocity components at the chord line are given by:-

$$u(x) = -\mathcal{Re}\left\{\frac{d\bar{w}}{d\bar{z}}\right\} = \frac{1}{2\pi}\int_{-a_1}^{a_2}\frac{\sigma'(\xi)\,d\xi}{(x-\xi)} \qquad (A.2.2.)$$

$$\text{and} \quad v(x) = \mathcal{Im}\left\{\frac{d\bar{w}}{d\bar{z}}\right\} = \mathrm{Lt}_{y\to 0}\ \frac{1}{2\pi}\int_{-a_1}^{a_2}\frac{y\sigma'(\xi)d\xi}{(x-\xi)^2+y^2}$$

$$\text{i.e.} \quad v(x) = \frac{1}{2}\sigma'(x)\ \text{sign}\ y \qquad (A.2.3.)$$

Now the boundary condition for the wing section contour to be a streamline is given by:

$$\frac{v(x)}{U_0} = \frac{dy}{dx} \qquad (A.2.4.)$$

and if the section ordinates are given by:

$$y_t = f(x) \qquad (A.2.5)$$

then from (A.2.4.) and (A.2.5.) we easily obtain:

$$\sigma'(x) = 2U_0\, f'(x) \qquad (A.2.6.)$$

Thus equation (A.2.2) may be written in the form:-

$$\frac{U(x)}{U_o} = \frac{1}{\pi}\int_{-a_1}^{a_2} \frac{y_t'(\xi)d\xi}{(x-\xi)} \tag{A.2.7}$$

Now

$$y_{tn}' = \frac{-b\xi}{a_n^2\sqrt{1-\frac{\xi^2}{a_n}}} \qquad \begin{array}{l} n = 1.\ \text{for } -a_1 \leq \xi \leq 0 \\ n = 2.\ \text{for } o \leq \xi \leq a_2 \end{array} \tag{A.2.8}$$

and on substituting for y_t' in (A.2.7.) we obtain:-

$$\frac{U(x)}{U_o} = \frac{b}{\pi}\sum_{n=1}^{2} \left| (-1)^{2-n}\frac{1}{a_n}\int_0^1 \frac{\xi\, d\xi}{\sqrt{1-\xi_2}\left\{\xi+(-1)^{n-1}\frac{x}{a}\right\}}\right| \tag{A.2.9}$$

This expression (A.2.9.) may be integrated and yields

$$\frac{U(x)}{U_o} = \frac{b}{\pi}\sum_{n=1}^{2} (-1)^{2-n}\frac{1}{a_n}\left|\frac{\pi}{2} + \frac{(-1)^n\frac{x}{a_n}}{\sqrt{1-\frac{x^2}{a_n}}}\operatorname{sech}^{-1}\frac{x}{a_n}\right| \tag{A.2.10}$$

- so that the total velocity at the chordline is given by.

$$\frac{q(x,o)}{U_o} = 1 + \frac{U(x)}{U_o} \tag{A.2.11}$$

To calculate the velocity at the wing surface, $q(x,y)$, we note from ref.21. that the two integrals:

$$\oint q(x,y)\sqrt{dx^2+dy^2} \quad , \quad \oint q(x,o)dx$$

which give the values of the circulation round the aerofoil, must be equal. Hence it is plausible to assume that locally

$$\therefore\ q(x,y)\sqrt{dx^2+dy^2} = q(x,o)\,dx \tag{A.2.12}$$

so that the velocity at the surface is given by

$$q(x,y) = \frac{q(x,o)}{\sqrt{1+\left(\frac{dy}{dx}\right)^2}} = \frac{q(x,o)}{B_x} \tag{A.2.13}$$

Thus on combining (A.2.10), (A.2.11), and (A.2.13), we obtain the following expression for the velocity distribution over the actual section:-

$$\frac{q}{U_o} = \frac{q(x,y)}{U_o} = \frac{1}{B_x}\left\{1 + \frac{b}{\pi}\sum_{n=1}^{2}(-1)^{2-n}\frac{1}{a_n}\left(\frac{\pi}{2} + \frac{(-1)^n \frac{x}{a_n}}{\sqrt{1-\frac{x^2}{a_n}}}\ \mathrm{sech}^{-1}\ \frac{x}{a_n}\right)\right\} \qquad (A.2.14.)$$

- in which:

$$B_x = \sqrt{1 + \frac{b^2\ x^2}{a_n^2\ (a_n^2 - x^2)}}\ , \qquad \begin{array}{l} n = 1 \text{ for } -a_1 \leqslant x \leqslant o \\ n = 2 \text{ for } o \leqslant x \leqslant a_2 \end{array}$$

The calculation of the pressure coefficient is performed using the relationship:

$$C_p\ (x,y) = 1 - \left\{\frac{q(x,y)}{U_o}\right\}^2 \qquad (A.2.15.)$$

A.2.2. The "Effective" Wing Section. Two Dimensional Case (Incompressible Flow)

Referring to fig.15. we have in this case:

$$y'_{t_2} = \frac{-b}{a_2^2\sqrt{1-\frac{\xi^2}{a_2^2}}} \qquad \text{for } o \leqslant \xi \leqslant a_2 \text{ , for the rear ellipse (shown}$$

dotted), and for the trailing edge fairing

$$y'_{t_3} = -\tan a.$$

so that

$$d = \frac{a_2^2}{1} \qquad (A.2.16.)$$

giving the necessary conditions for surface continuity.

There are three domains of intigration to be considered in the evaluation of the perturbation component U(x) and we find on proceeding as in (A.2.1.) that :-

$$\frac{U(x)}{U_o} = -\frac{b}{\pi a_1}\int_{-1}^{o}\frac{\xi\ d\xi}{\sqrt{1-\xi^2}\left(\frac{x}{a_1}-\xi\right)} - \frac{b}{\pi\ a_2}\int_{o}^{d}\frac{\xi\ d\xi}{\sqrt{a^2-\xi^2}(x-\xi)} - \frac{\tan a}{\pi}\int_{d}^{1}\frac{d\xi}{(x-\xi)} \qquad (A.2.17)$$

The integral terms in (A.2.17) may be evaluated and after some manipulation the following expression for $q(x,o)$ may be derived:

$$\frac{q(x,o)}{U_0} = \left\{ 1 - \frac{b}{\pi a_1}\left(\frac{\pi}{2} - \frac{x}{a_1\sqrt{1-\frac{x^2}{a_1^2}}} \operatorname{sech}^{-1}\frac{x}{a_1} \right) + \frac{b}{\pi a_2}\left(\sin^{-1}\frac{d}{a_2} + \frac{x}{a_2\sqrt{1-\frac{x^2}{a_2^2}}}\, l_n.\, D \right) \right.$$

$$\left. + \frac{\tan \alpha}{\pi}\, l_n. \left| \frac{x-l}{x-d} \right| \right\} \qquad (A.2.18.)$$

- where D is given by:-

$$D = \frac{\left(1 + \sqrt{1 - \frac{x^2}{a_2^2}}\right)\left(1 - \frac{a_2^2}{lx}\right)}{\left(1 - \frac{x}{l} + \sqrt{1-\frac{x^2}{a_2^2}}\,\sqrt{1 - \frac{a_2^2}{l^2}}\right)}$$

Here also the velocity at the surface is given by (A.2.13.) with

$$B_x = \sqrt{1 + \frac{b^2\, x^2}{a_n^2\,(a_n^2 - x^2)}}\,, \qquad \begin{array}{l} n = 1, \text{ for } -a_1 \leqslant x \leqslant o \\ n = 2, \text{ for } o \leqslant x \leqslant d \end{array}$$

$$B_x = \sqrt{1 + \tan^2 \alpha} \qquad \text{for } d \leqslant x < l.$$

$$B_x = \infty \qquad \text{for } x = l.$$

- and the pressure coefficient is calculated from (A.2.15.)

A.3.3. The Infinite Sheared Wing. at Zero Incidence (Actual & "Effective" Sections)

For the wing of infinite span sheared by an angle Λ (the section remaining unaltered in the direction of the undisturbed stream) the undisturbed stream has components $U_0 \cos \Lambda$ and $U_0 \sin \Lambda$ normal to and parallel to the leading edge respectively. Since the wing surface is a stream surface to the flow $U_0 \sin \Lambda$ which is consequently unaffected by the wing thickness distribution, the velocity perturbation will thus depend upon the streaming of the component $U_0 \cos \Lambda$ over the surface characterised by the ordinates $y_1 = f_1(x_1)$.

The calculation procedure used in determining the velocity distributions for both the actual and "effective" sections, each being respectively considered as the streamwise section of a wing of infinite span, is identical in principle with that in paras A.2.1. and A.2.2, the results obtained in this case being as follows:

For the actual section we have:-

$$\frac{q_1(x_1\,,\,y_1)}{U_0} = \frac{1}{B_{x_1}}\left\{\cos\Lambda + \frac{b}{\pi}\sum_{n=1}^{2}(-1)^{2-n}\cdot\frac{1}{a_n}\left(\frac{\pi}{2} + \frac{(-1)^n\frac{x}{a_n}}{\sqrt{1-\frac{x^2}{a_n^2}}}\operatorname{sech}^{-1}\frac{x}{a_n}\right)\right\}$$

(A.2.19)

- where in this case B_{x_1} is given by:-

$$B_{x_1} = \sqrt{1 + \frac{1}{\cos^2\Lambda}\left(\frac{dy}{dx}\right)^2} \qquad (A.2.20)$$

The total velocity at the wing surface is given by:

$$\frac{q(x,y)}{U_0} = \sqrt{\left(\frac{q_1}{U_0}\right)^2 + \sin^2\Lambda}\ . \qquad (A.2.21.)$$

and the pressure coefficient by:-

$$C_p\,(x,y) = 1 - \left\{\frac{q}{U_0}\,(x,y)\right\}^2 \qquad (A.2.22.)$$

For the "effective" section we have:-

$$\frac{q_1(x_1\,,0)}{U_0} = \left\{\cos\Lambda - \frac{b}{\pi a_1}\left(\frac{\pi}{2} - \frac{x}{a_1\sqrt{1-\frac{x^2}{a_1^2}}}\operatorname{sech}^{-1}\frac{x}{a_1}\right) + \frac{b}{\pi a_2}\left(\sin^{-1}\frac{d}{a_2} + \frac{x}{\sqrt[2]{1-\frac{x^2}{a_2^2}}}\ln D\right)\right.$$
$$\left. + \frac{\tan\alpha}{\pi}\ln\left|\frac{x-1}{x-d}\right|\right\}$$

(A.2.23.)

with $\frac{q_1(x_1,y_1)}{U_0}$ $C_p(x,y)$, determined using (A.2.20) and (A.2.22).

The distributions of pressure $C_p(x,y)$ calculated for the two sections may be seen in fig.17.

APPENDIX III

A.3 The calculation of the Steady State Three Dimensional Boundary Layer for the Sheared Wing of Infinite Span by the Method of Series

A.3.1 The General Case

Referring to the coordinate system $x_2\, y_2\, z_2$ (see fig 14) we may, according to several authors (e.g. ref. 22), write down the equations of motion for the three dimensional boundary layer in the form

$$u_2 \frac{\partial u_2}{\partial x} + v_2 \frac{\partial u_2}{\partial y_2} + w_2 \frac{\partial u_2}{\partial z_2} = -\frac{1}{\rho}\frac{\partial p}{\partial x_2} + \nu \frac{\partial^2 u}{\partial y_2^2}$$

$$u_2 \frac{\partial w_2}{\partial x_2} + v_2 \frac{\partial w_2}{\partial y_2} + w_2 \frac{\partial w_2}{\partial z_2} = -\frac{1}{\rho}\frac{\partial p}{\partial z_2} + \nu \frac{\partial^2 w_2}{\partial y_2^2} \qquad - (A.3.1)$$

$$\frac{\partial u_2}{\partial x_2} + \frac{\partial v_2}{\partial y_2} + \frac{\partial w_2}{\partial z_2} = 0$$

in which the boundary conditions are

$$\begin{aligned} y_2 &= 0, \quad u_2 = v_2 = w_2 = 0 \\ y_2 &= \infty, \quad u_2 = U_2, \quad w_2 = W_2 \end{aligned} \qquad (A.3.2)$$

Now for the sheared wing we have to close approximation

$$\begin{aligned} U_2 &= U_2(x_2), \quad W_2 = W_0 = \text{constant} \\ &\text{and } \frac{1}{\rho}\frac{\partial p}{\partial x_2} = U_2 \frac{dU_2}{dx_2} \end{aligned} \qquad (A.3.3)$$

so that the system of equations (A.3.1) may be reduced to

$$u_2 \frac{\partial u_2}{\partial x_2} + v_2 \frac{\partial u_2}{\partial y_2} = U_2 \frac{dU_2}{dx_2} + \nu \frac{\partial^2 u}{\partial y_2^2}$$

$$u_2 \frac{\partial w_2}{\partial x_2} + v_2 \frac{\partial w_2}{\partial y_2} = \nu \frac{\partial^2 w_2}{\partial y_2^2} \qquad (A.3.4)$$

$$\frac{\partial u_2}{\partial x_2} + \frac{\partial v_2}{\partial y_2} = 0$$

with the boundary conditions again as given by (A.3.2)

Now the three dimensional boundary layer on a sheared wing at zero lift may be calculated in a similar way to that for a cylinder whose axis is at right angles to the main stream, by treating the chordwise (normal to the leading edge) and spanwise flow components separately. Such a procedure is assumed permissible since the equations for steady flow in the boundary layer (A.3.4) show no dependence upon z_2 (ref.4). It is important however to note that in applying this principle of independence we are referring strictly to steady flow. In the case of disturbed flow, a dependence upon z_2 is implicitly inferred in the equations of motion (ref. 16).

Thus following the usual procedure we take

$$U_2(x_2) = \sum_{n=0}^{m} A_{2n+1} \cdot x_2^{2n+1} \quad , \; n = 0,1,2,\ldots m \qquad \text{(A.3.5)}$$

$$\text{and } W_2 = W_0 \quad \text{constant}$$

and if the stream function is expressed in the form

$$\psi(x_2, y_2) = \sqrt{\frac{\nu}{A_1}} \; A_1 x_2 f_1(\eta) + 4A_3 x_2^3 f_3(\eta) + \ldots \qquad \text{(A.3.6)}$$

$$\text{where} \quad = y \sqrt{\frac{A_1}{\nu}} \quad . \qquad \text{(A.3.6a)}$$

then according to ref. 22 the velocity components $u_2(x_2, y_2)$, $v_2(x_2 y_2)$ may be expressed as a Blasius' series, the flow being independent of z_2 such that

$$u_2(x_2, y_2) = A_1 x_2 f_1'(\eta) + 4A_3 x_2^3 f_3'(\eta) +$$

$$v_2(x_2, y_2) = - \sqrt{\frac{\nu}{A_1}} \Big\{ A_1 f_1(\eta) + 12 A_3 x^2 f_3(\eta) + \ldots\ldots \qquad \text{(A.3.7)}$$

$$w_2(x_2, y_2) = W_0 \Big\{ g_0(\eta) + \frac{A_3}{A_1} x^2 g_2(\eta) + \ldots\ldots.$$

in which the prime denotes differentiation with respect to η, and the functions g_0, g_0, ..., satisfy the differential equations

$$g_0'' + f_1 g_0' = 0 \qquad \text{(A.3.8)}$$

$$g_2 + f_1 g_2' - 2f_1' g_2 = -12 f_3 g_0'$$

the boundary condition to be satisfied being

$$\eta = 0 \quad g_0 = 0, \quad g_2 = 0.$$
$$\eta = \quad g_0 = 1. \quad g_2 = 0. \qquad \text{(A.3.9)}$$

Now according to Prandtl (ref.19) the equation for g_0 may be solved by direct integration to yield

$$g_0(\eta) = \frac{\int_0^\eta \exp.\left\{ - \int_0^\eta f_1 \; d\eta \right\}. \; d\eta}{\int_0^\infty \exp.\left\{ - \int_0^\eta f_1 \; d\eta \right\} \; d\eta} \qquad \text{(A.3.10)}$$

The functions f_1, f_3, .. f_1', f_3', ..., are extensively tabulated (refs. 1, 7.22 for example) whilst g_0, g_2, ..., may be found in refs. 20 and 22.

The problem of calculating the three dimensional boundary layer is therefore one of expressing the external velocity distribution (as given by theory or experiment) as the power series given by A.3.5. i.e. as

$$U_2(x_2) = \sum_{n=0}^{m} A_{2n+1} \; x_2^{2n+1}$$

- the summation having the upper bound m imposed by the at present somewhat restricted range of tabulated values for the functions g_0, g_2, ..., and by the extent of mechanical work involved in performing the necessary computations in cases where the boundary layer is required over a considerable distance from the stagnation line. If however we need only concern ourselves with relatively short distances from the stagnation line then by a judicious choice of the expression for the above series, satisfactory to the degree of accuracy required, the boundary layer may be readily calculated.

A.3.2. Application to the Particular Case.

For the wing under consideration it can easily be shown that since the leading edge portion is of elliptic section (fig.4.) the distance along the wing surface (from the stagnation line at zero incidence) in a direction normal to the leading edge is given by an integral of the form

$$x_2 = b \int_0^\phi \sqrt{1 + n^2 \sin^2 \theta} \; . \quad d\theta \qquad \text{(A.3.11)}$$

- where $n^2 + \left\{\frac{a^2}{b^2} - 1\right\} > 0$

which is an incomplete elliptic integral of the second kind (written in Legendres notation) and which may be evaluated following a reduction of the integrant to a Jacobian elliptic function, i.e. by writing

$$x_2 = b\int_0^{\phi} \sqrt{1 + n^2 \sin^2 \theta}.\ d\theta = b\,k' \int_0^{u_1} n\,d^2\,u\ du.$$

- in the notation of ref. 18.

Thus we find x_2 given by

$$x_2 = \frac{b}{k'}\left\{E(u_1) - k^2 \operatorname{sn} u_1 \operatorname{cd} u_1\right\} \qquad \begin{array}{l} 0 < k < 1 \\ 0 < \phi < \frac{\pi}{2} \end{array}$$

the calculation being facilitated by reference to tables of the elliptic functions. The results obtained are shown in fig.18.

We note in passing that the integrand of (A.3.11) could alternatively be expressed as a series in θ using a Binomial expansion and x_2 derived following a term by term integration, but the method offers no advantage in the circumstances.

It is indeed evident that there is no simple way of analytically expressing $U_2(x_2)$ as a readily calculable function of x_2 satisfying the form requirements of (A.3.5.) and so at the expense of accuracy we may approximate by reducing the problem to one of mechanical curve fitting.

The measured and calculated distributions of velocity over a section normal to the leading edge are shown in fig.19, the measured distribution being deduced from the experimental results obtained for the mid semi span station. The agreement between theory and experiment is excellent so that we may expect the external streamline of the viscous flow case to approximate very closely in direction to that calculated for potential flow. (see fig.20) over the sheared wing of infinite span. This leads to the observation that the external streamline is only curved to any significant extent for a very short distance along the wing surface (cf.para,2.4.) and thus the secondary flow effects in which we are interested may be expected to achieve prime significance in a region of similar length (Ref.17). On the supposition that such a condition is true we note that for a very short distance along the leading edge both the experimental and theoretical distributions of velocity may be very accurately represented by an expression of the form

$$Q_2 = \frac{U_2(x_2)}{U \cos\Lambda} = \sin\frac{\pi x_2}{5} = \frac{\pi x_2}{5} - \frac{1}{6}\left(\frac{\pi x}{5}\right)^3 + \dots, \qquad 0 \leqslant x_2 < 2.5. \tag{A.3.12}$$

(see fig.19 for comparison), where x_2 is quoted in dimensional form (inches) since we are only concerned with a particular case.

Thus the external flow conditions may be expressed as

$$\frac{1}{U_0 \cos\Lambda}\sum_{n=0}^{m} A_{2n+1}\, x_2^{2n+1} = \frac{\pi x_2}{5} - \frac{1}{6}\left(\frac{\pi}{5}\right)^3 x_2^3 + \frac{1}{120}\left(\frac{\pi}{5}\right)^5 x_2^5 - \dots \tag{A.3.13}$$

so that

$$A_1 = \frac{\pi}{5} \times \ U_0 \ \cos \Lambda, \ A_3 = -\frac{1}{6} \left(\frac{\pi}{5}\right)^3 \ U_0 \ \cos \Lambda, \ A_5 = \frac{1}{120} \left(\frac{\pi}{5}\right)^5 \ U_0 \cos \Lambda \ . \qquad (A.3.14)$$

and hence the two components of interest in the boundary layer are given by substituting for A_1, A_3, etc. into (A.3.7)

The distribution of velocity calculated on this basis together with the profiles obtained by resolution on the co-ordinate system ξ_1 ζ_1 of the external streamline, may be seen in Fig.21. They receive discussion in para 2.6.

APPENDIX IV

The Three Dimensional Boundary Layer for the Potential Flow

$$Q_2 = \frac{U_2 \ (x_2)}{U_0 \cos \Lambda} = A_1 x_2^m \ .$$

A particular case of a laminar boundary layer flow which is amenable to analytical treatment is that associated with a potential velocity distribution of the type

$$Q_2 = \frac{U_2(x_2)}{U_0 \cos \Lambda} = A_1 x_2^m \ .$$

where A_1 and m are constants. (A.4.1)

Such a distribution is a little more than just of academic interest in relation to the present work for we note that both A_1 and m can be chosen to not only permit the calculation of the boundary layer (by the use of existing tables), but also to approximately represent the velocity distribution over the swept back wing at zero incidence. (See Fig.19)

Since $Q_2 \sim x_2^m$, the velocity distributions at various positions (x_2) may be universally represented (Ref.22.) following the choice of suitable scaling factors for u_2 , w_2 and y_2 . The choice for three dimensional flow being

$$\eta = y_2 \ \sqrt{\frac{m+1}{2} \cdot \frac{U_2}{\nu x_2}} \qquad (A.4.2.)$$

- with the velocity components given in the form

$$\left.\begin{aligned} u_2 &= U_0 \cos\Lambda Q_2 f'(\eta_1). \\ w_2 &\quad W_0\, G(\eta_1)\,. \end{aligned}\right\} \qquad (A.4.3.)$$

The differential equations of the boundary layer obtained for this type of flow have been studied by Hartree (ref.31) and Cooke (ref.32.) who provided tables of the functions $f'(\eta_1)$ and $G(\eta_1)$ for a range of values for m.

Choosing $A = 0.89$ and $m = \frac{1}{9}$ (which is convenient for our purpose), the calculated distributions of velocity in the boundary layer together with the profiles obtained by resolution on to the co-ordinate system ξ_1, ζ_1 of the external streamline (calculated for $Q_1 = A\ x_2^m$) may be seen in fig.22. They are discussed in para. 2.6.3.[2]

TABLE I

THE CHORDWISE LOCATION OF THE STATIC PRESSURE TAPPINGS IN THE SWEPT BACK HALF WING

Hole number	Distance from the leading edge along axis of	$\frac{x}{c_o}$ % *
1	0	0
1a	0.325	0.378
1b	0.650	0.756
1c	0.975	1.135
2	1.3000	1.512
3	2.6000	3.03
4	5.2	6.04
5	7.8	9.06
6	10.4	12.10
7	13	15.12
8	19.5	22.70
9	26	30.25
10	32.5	37.80
11	39	45.40
12	45.5	52.90
13	50.6	58.80

* The reason for the numerically inconvenient values of $\frac{x}{c_o}$ is due to the distances along x as tabulated in the second column being referred, during the wing design stage, to the 'effective' chord, and not to the actual chord as is here chosen. Thus for example hole number 10 corresponds to a chordwise position of $37.8\,\% \times \frac{86}{130} = 25\,\%$ referred to the 'effective chord'.

TABLE II

DISTRIBUTION OF STATIC PRESSURE OVER SWEPT BACK WING. REYNOLDS NUMBER RANGE: $0.884 - 1.916 \times 10^6$/ft.

The suffix U denotes upper surface
The suffix L denotes lower surface

	HOLE No.	$\alpha = 0^\circ$ C_{P_U}	$\alpha = 2^\circ$ C_{P_U}	$\alpha = 2^\circ$ C_{P_L}	$\alpha = 4^\circ$ C_{P_U}	$\alpha = 4^\circ$ C_{P_L}	$\alpha = 6^\circ$ C_{P_U}	$\alpha = 6^\circ$ C_{P_L}	$\alpha = 8^\circ$ C_{P_U}	$\alpha = 8^\circ$ C_{P_L}	$\alpha = 10^\circ$ C_{P_U}	$\alpha = 10^\circ$ C_{P_L}
WING TIP STATION (See Fig. 8)	1	+0.473	+0.463	+0.387	+0.333	+0.182	+0.147	-0.080	-0.209	-0.552	-0.642	-0.949
	1a	+0.425	+0.278	+0.442	+0.019	+0.357	-0.318	+0.283	-0.822	+0.105	-1.297	+0.119
	1b	+0.291	+0.115	+0.375	-0.161	+0.448	-0.501	+0.436	-0.919	+0.344	-1.387	+0.196
	1c	+0.183	-0.080	+0.312	-0.329	+0.412	-0.614	+0.445	-1.001	+0.437	-1.466	+0.390
	2	+0.124	-0.092	+0.276	-0.336	+0.393	-0.583	+0.448	-0.944	+0.482	-1.306	+0.468
	3	-0.005	-0.180	+0.150	-0.379	+0.273	-0.569	+0.349	-0.835	+0.432	-1.098	+0.467
	4	-0.087	-0.228	+0.027	-0.366	+0.138	-0.504	+0.212	-0.680	+0.307	-0.854	+0.360
	5	-0.154	-0.265	-0.088	-0.385	+0.044	-0.496	+0.116	-0.635	+0.209	-0.770	+0.265
	6	-0.150	-0.247	-0.067	-0.339	+0.015	-0.428	+0.078	-0.540	+0.161	-0.644	+0.213
	7	-0.158	-0.238	-0.087	-0.318	-0.013	-0.392	+0.039	-0.485	+0.113	-0.569	+0.164
	8	-0.190	-0.249	-0.141	-0.300	-0.087	-0.348	-0.044	-0.416	+0.016	-0.467	+0.056
	9	-0.184	-0.222	-0.150	-0.261	-0.106	-0.292	-0.078	-0.339	-0.029	-0.380	+0.002
	10	-0.188	-0.216	-0.160	-0.245	-0.130	-0.272	-0.104	-0.302	-0.068	-0.331	-0.042
	11	-0.186	-0.208	-0.166	-0.227	-0.144	-0.249	-0.127	-0.270	-0.093	-0.291	-0.071
	12	-0.205	-0.217	-0.185	-0.228	-0.167	-0.236	-0.154	-0.263	-0.129	-0.276	-0.108
	13	-0.212	-0.223	-0.199	-0.231	-0.183	-0.233	-0.172	-0.259	-0.144	-0.262	-0.133
MID SEMI SPAN STATION (See Fig. 8)	1	+0.391	+0.478	+0.415	+0.340	+0.211	+0.150	-0.050	-0.228	-0.528	-0.675	-0.934
	1a	+0.452	+0.305	+0.481	+0.034	+0.422	-0.306	+0.326	-0.825	+0.131	-1.304	+0.165
	1b	+0.304	+0.118	+0.422	-0.179	+0.477	-0.537	+0.461	-0.981	+0.371	-1.477	+0.217
	1c	+0.199	-0.032	+0.340	-0.337	+0.444	-0.648	+0.479	-1.058	+0.466	-1.556	+0.428
	2	+0.140	-0.085	+0.287	-0.339	+0.413	-0.588	+0.472	-0.960	+0.513	-1.330	+0.500
	3	+0.026	-0.159	+0.166	-0.367	+0.298	-0.556	+0.378	-0.833	+0.466	-1.098	+0.500
	4	-0.064	-0.209	+0.052	-0.365	+0.166	-0.501	+0.243	-0.693	+0.347	-0.877	+0.401
	5	-0.119	-0.248	-0.020	-0.371	+0.084	-0.482	+0.158	-0.628	+0.259	-0.771	+0.316
	6	-0.131	-0.240	-0.047	-0.344	+0.047	-0.439	+0.114	-0.560	+0.209	-0.677	+0.266
	7	-0.144	-0.237	-0.066	-0.328	+0.015	-0.408	+0.078	-0.514	+0.166	-0.612	+0.220
	8	-0.183	-0.242	-0.121	-0.318	-0.054	-0.382	-0.003	-0.452	+0.071	-0.522	+0.121
	9	-0.190	-0.234	-0.141	-0.292	-0.089	-0.338	-0.043	-0.395	+0.019	-0.448	+0.061
	10	-0.210	-0.240	-0.169	-0.287	-0.124	-0.325	-0.091	-0.369	-0.035	-0.407	+0.001
	11	-0.212	-0.231	-0.178	-0.272	-0.145	-0.298	-0.113	-0.328	-0.069	-0.358	-0.038
	12	-0.219	-0.234	-0.197	-0.269	-0.167	-0.286	-0.149	-0.310	-0.106	-0.326	-0.077
	13	-0.243	-0.260	-0.221	-0.279	-0.200	-0.295	-0.181	-0.314	-0.149	-0.323	-0.120
WING ROOT STATION (See Fig. 8)	1	+0.524	+0.501	+0.485	+0.382	+0.298	+0.224	+0.096	-0.086	-0.290	-0.455	-0.610
	1a	+0.460	+0.338	+0.493	+0.108	+0.464	-0.199	+0.398	-0.650	+0.223	-1.062	+0.047
	1b	+0.316	+0.144	+0.428	-0.118	+0.487	-0.432	+0.497	-0.827	+0.438	-1.241	+0.326
	1c	+0.231	+0.025	+0.356	-0.247	+0.454	-0.511	+0.499	-0.850	+0.503	-1.269	+0.453
	2	+0.138	-0.081	+0.279	-0.311	+0.406	-0.539	+0.467	-0.874	+0.527	-1.175	+0.531
	3	+0.040	-0.139	+0.168	-0.322	+0.296	-0.494	+0.374	-0.738	+0.471	-0.977	+0.510
	4	-0.058	-0.196	+0.053	-0.331	+0.168	-0.457	+0.243	-0.627	+0.348	-0.792	+0.405
	5	-0.079	-0.193	+0.012	-0.299	+0.113	-0.400	+0.186	-0.532	+0.282	-0.659	+0.335
	6	-0.102	-0.200	-0.019	-0.293	+0.068	-0.381	+0.134	-0.492	+0.226	-0.597	+0.281
	7	-0.112	-0.197	-0.039	-0.282	+0.044	-0.358	+0.102	-0.451	+0.190	-0.541	+0.243
	8	-0.150	-0.214	-0.089	-0.278	-0.024	-0.333	+0.026	-0.403	+0.104	-0.469	+0.152
	9	-0.163	-0.219	-0.115	-0.269	-0.061	-0.315	-0.017	-0.371	+0.050	-0.420	+0.091
	10	-0.186	-0.229	-0.149	-0.271	-0.099	-0.308	-0.063	-0.352	-0.001	-0.392	+0.033
	11	-0.206	-0.239	-0.168	-0.271	-0.127	-0.299	-0.099	-0.334	-0.047	-0.369	-0.013
	12	-0.234	-0.261	-0.206	-0.291	-0.173	-0.317	-0.150	-0.338	-0.107	-0.367	-0.075
	13	-0.255	-0.277	-0.228	-0.302	-0.203	-0.323	-0.179	-0.339	-0.138	-0.364	-0.113

TABLE III

MEASURED CHORDWISE LOADINGS CORRESPONDING TO TABLE II

	$\alpha = 2^\circ$	$\alpha = 4^\circ$	$\alpha = 6^\circ$	$\alpha = 8^\circ$	$\alpha = 10^\circ$
1	+0.076	+0.151	+0 226	+0.343	+0.307
1a	+0.164	+0.338	+0.601	+0.927	+1.416
1b	+0.260	+0.609	+0.827	+1.263	+1.583
1c	+0.392	+0.741	+1.059	+1.438	+1.856
2	+0.369	+0.728	+1.031	+1.426	+1.774
3	+0.330	+0.652	+0.918	+1.267	+1.565
4	+0.255	+0.504	+0.715	+0.988	+1.214
5	+0.211	+0.431	+0.613	+0.844	+1.036
6	+0.176	+0.354	+0.506	+0.701	+0.857
7	+0.152	+0.305	+0.432	+0.603	+0.733
8	+0.103	+0.212	+0.304	+0.432	+0.523
9	+0.072	+0.155	+0.213	+0.310	+0.383
10	+0.056	+0.115	+0.160	+0.234	+0.289
11	+0.042	+0.083	+0.122	+0.178	+0.220
12	+0.032	+0.061	+0.082	+0.135	+0.168
13	+0.024	+0.045	+0.057	+0.115	+0.130

Wing Tip Station

	$\alpha = 2^\circ$	$\alpha = 4^\circ$	$\alpha = 6^\circ$	$\alpha = 8^\circ$	$\alpha = 10^\circ$
1	+0.063	+0.128	+0.200	+0.300	+0.259
1a	+0.176	+0.388	+0.632	+0.956	+1.469
1b	+0.304	+0.656	+0.998	+1.352	+1.694
1c	+0.372	+0.781	+1.127	+1.524	+1.984
2	+0.372	+0.752	+1.060	+1.474	+1.830
3	+0.325	+0.665	+0.934	+1.299	+1.599
4	+0.261	+0.531	+0.744	+1.040	+1.278
5	+0.229	+0.454	+0.636	+0.887	+1.087
6	+0.193	+0.391	+0.550	+0.769	+0.943
7	+0.170	+0.343	+0.486	+0.680	+0.832
8	+0.121	+0.263	+0.380	+0.524	+0.643
9	+0.094	+0.202	+0.295	+0.418	+0.509
10	+0.071	+0.164	+0.237	+0.334	+0.408
11	+0.053	+0.126	+0.185	+0.259	+0.320
12	+0.037	+0.102	+0.137	+0.204	+0.249
13	+0.039	+0.080	+0.114	+0.165	+0.202

Mid Semi Span Station

	$\alpha = 2^\circ$	$\alpha = 4^\circ$	$\alpha = 6^\circ$	$\alpha = 8^\circ$	$\alpha = 10^\circ$
1	+0.030	+0.084	+0.128	+0.204	+0.155
1a	+0.155	+0.356	+0.597	+0.873	+1.109
1b	+0.284	+0.605	+0.929	+1.265	+1.567
1c	+0.331	+0.701	+1.010	+1.353	+1.722
2	+0.360	+0.717	+1.006	+1.402	+1.706
3	+0.307	+0.618	+1.867	+1.208	+1.487
4	+0.249	+0.499	+0.700	+0.975	+1.197
5	+0.204	+0.412	+0.585	+0.813	+0.994
6	+0.182	+0.361	+0.515	+0.718	+0.878
7	+0.158	+0.326	+0.459	+0.641	+0.817
8	+0.125	+0.254	+0.359	+0.508	+0.621
9	+0.104	+0.208	+0.298	+0.421	+0.511
10	+0.080	+0.171	+0.245	+0.352	+0.425
11	+0.070	+0.144	+0.201	+0.286	+0.356
12	+0.055	+0.118	+0.167	+0.234	+0.292
13	+0.049	+0.100	+0.144	+0.200	+0.251

Wing Root Station

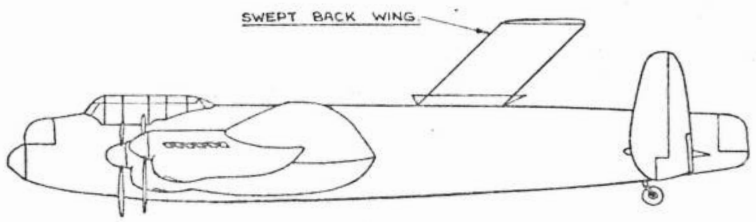

FIG. 1 . ARRANGEMENT OF AIRCRAFT & WING.

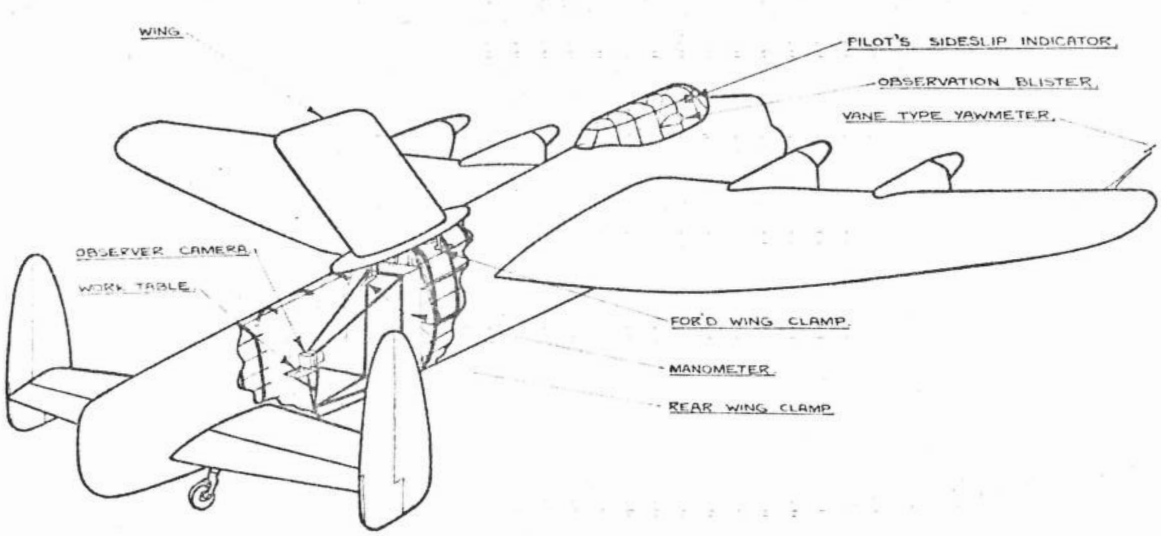

FIG. 2. LAYOUT OF EQUIPMENT IN AIRCRAFT.

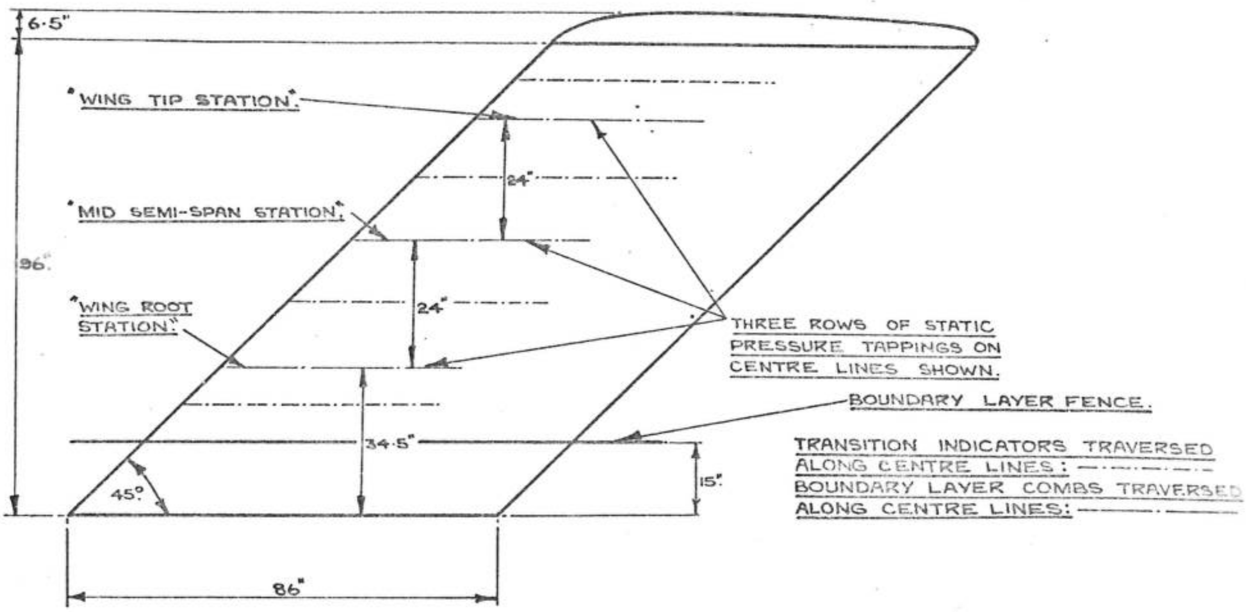

FIG. 3. GENERAL PLANFORM DIMENSIONS OF WING.

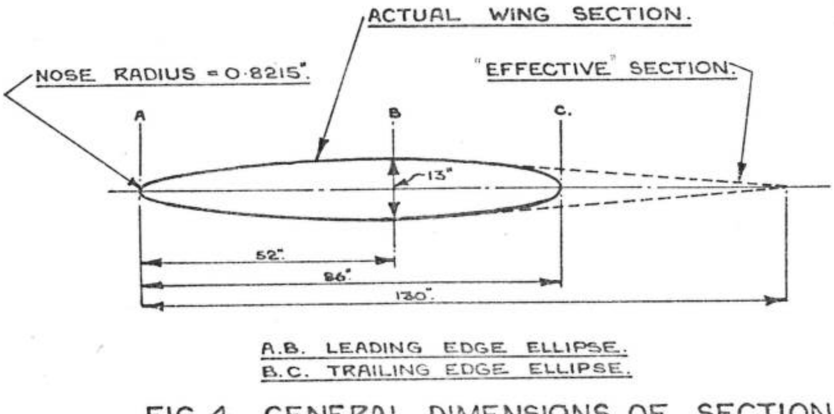

A.B. LEADING EDGE ELLIPSE.
B.C. TRAILING EDGE ELLIPSE.

FIG. 4. GENERAL DIMENSIONS OF SECTION.

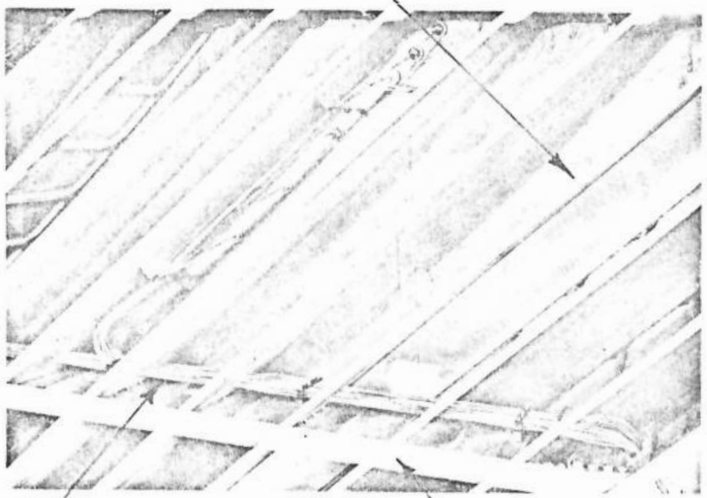

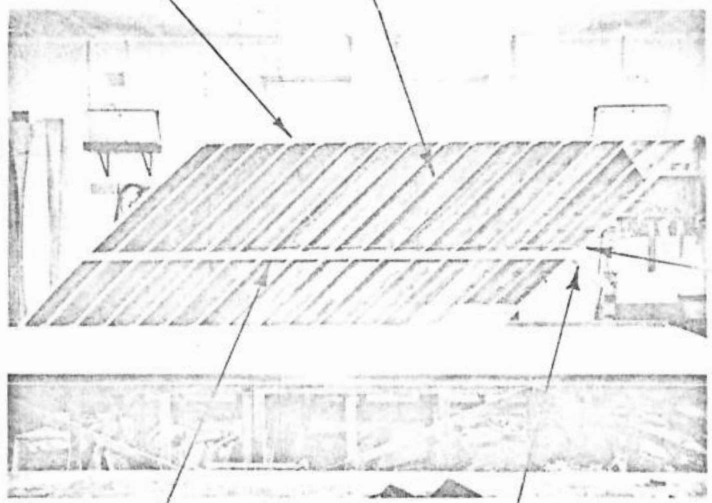

FIG 5a. THE WING DURING CONSTRUCTION.

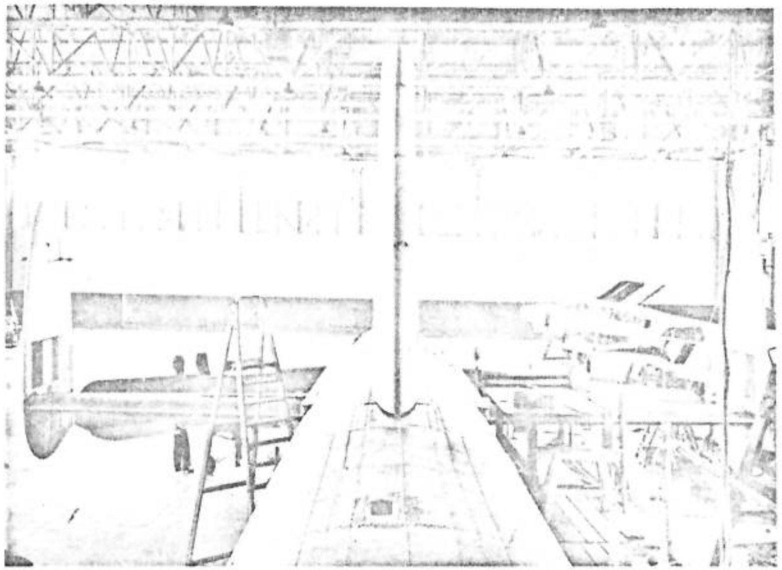

FIGURE 5 b. THE SWEPT WING NEARING COMPLETION AND IN POSITION ON THE FUSELAGE

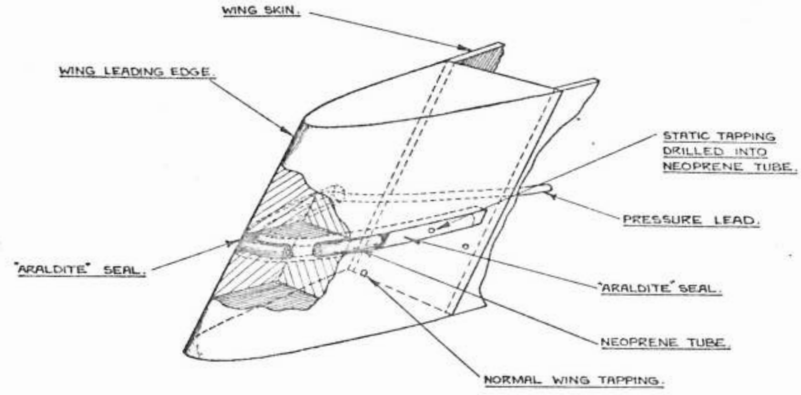

FIG. 6a. STATIC PRESSURE TAPPINGS AT LEADING EDGE OF SWEPT BACK WING.

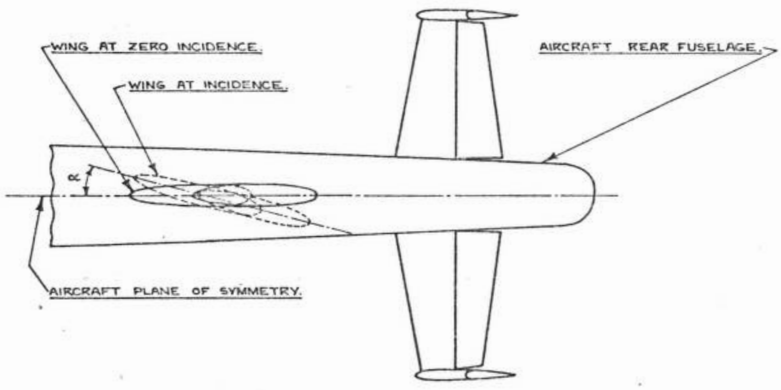

FIG 6b. SWEPT WING INCIDENCE SETTING.

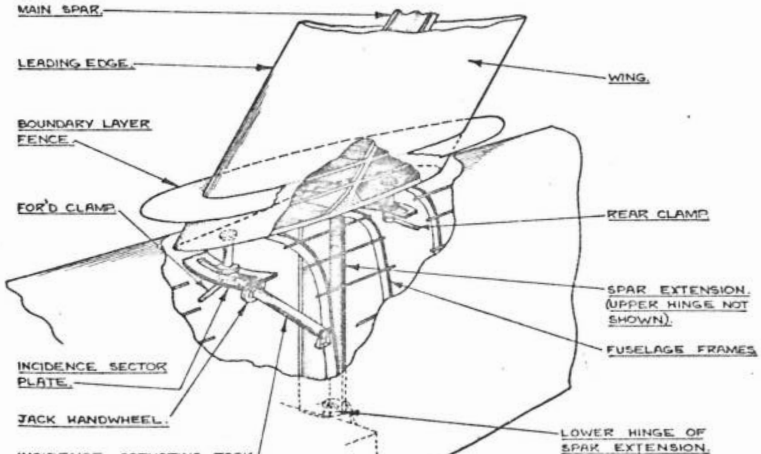

FIG. 6c. INCIDENCE ACTUATING JACK & SECTOR PLATE.

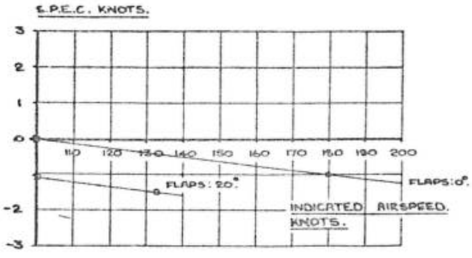

FIG.7. STATIC PRESSURE ERROR CORRECTION CURVE FOR LANCASTER P.A. 474.

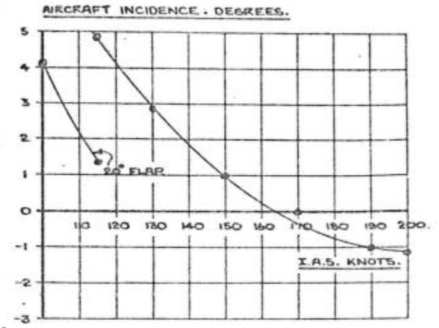

FIG. 7a. VARIATION OF AIRCRAFT INCIDENCE WITH INDICATED AIRSPEED AT 44,000 lb. A.U.W.

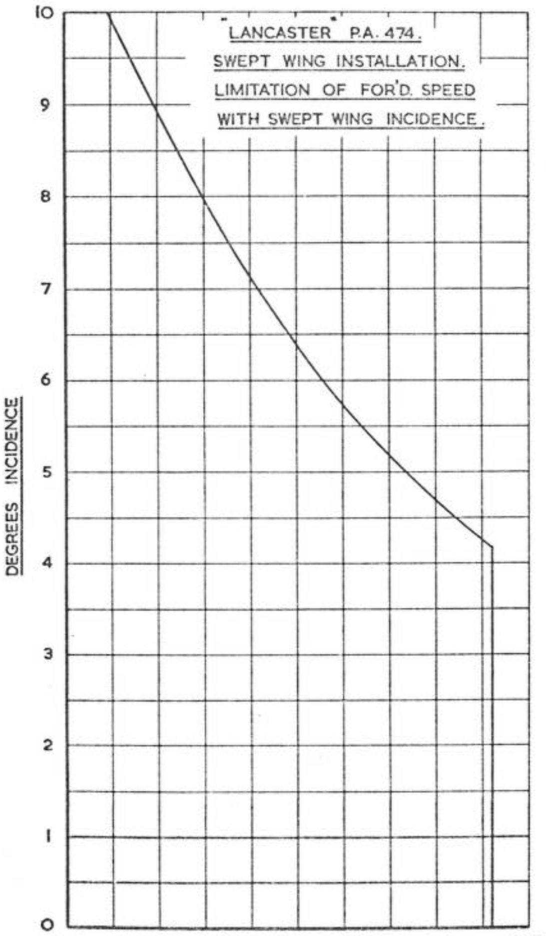

FIG. 8. AIRCRAFT SPEED ~ WING INCIDENCE BOUNDARY CURVE.

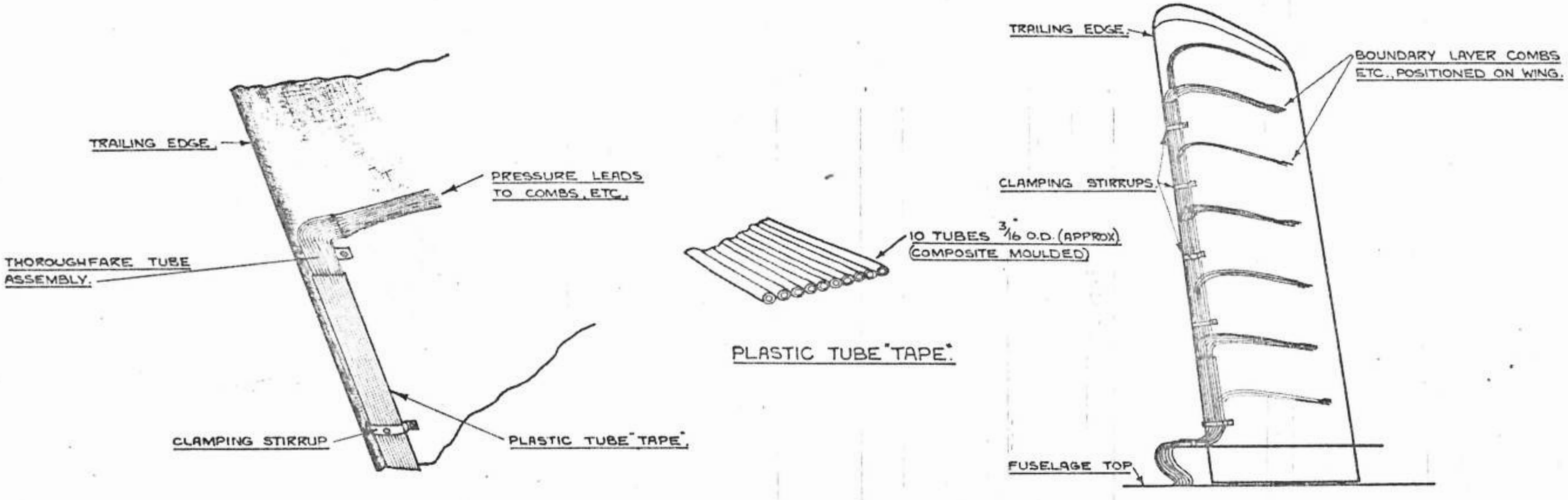

FIG.9. PIPE WORK AT THE TRAILING EDGE.

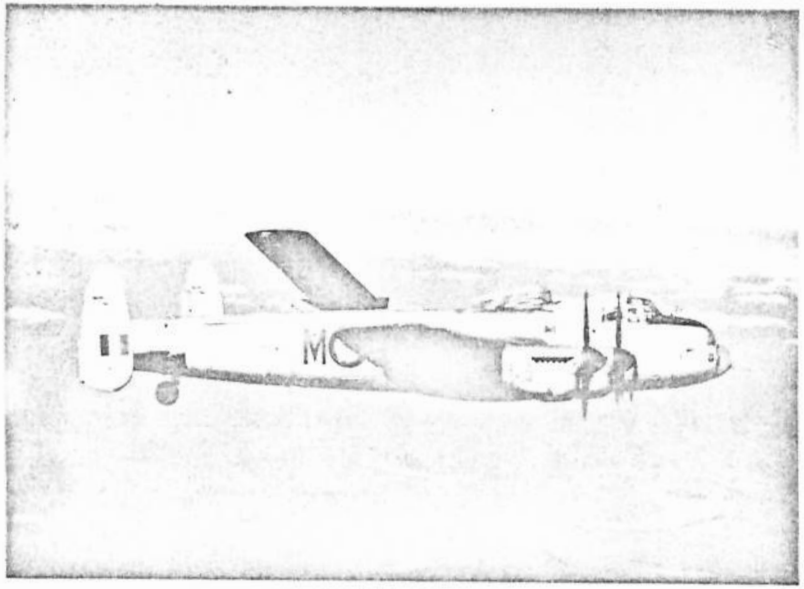

FIGURE 10

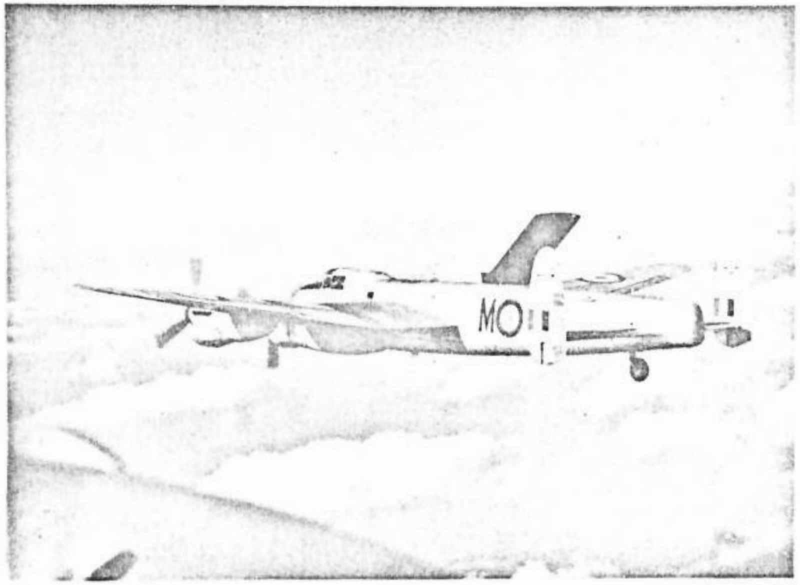

FIGURE 11

LANCASTER P. A. 474 IN FLIGHT

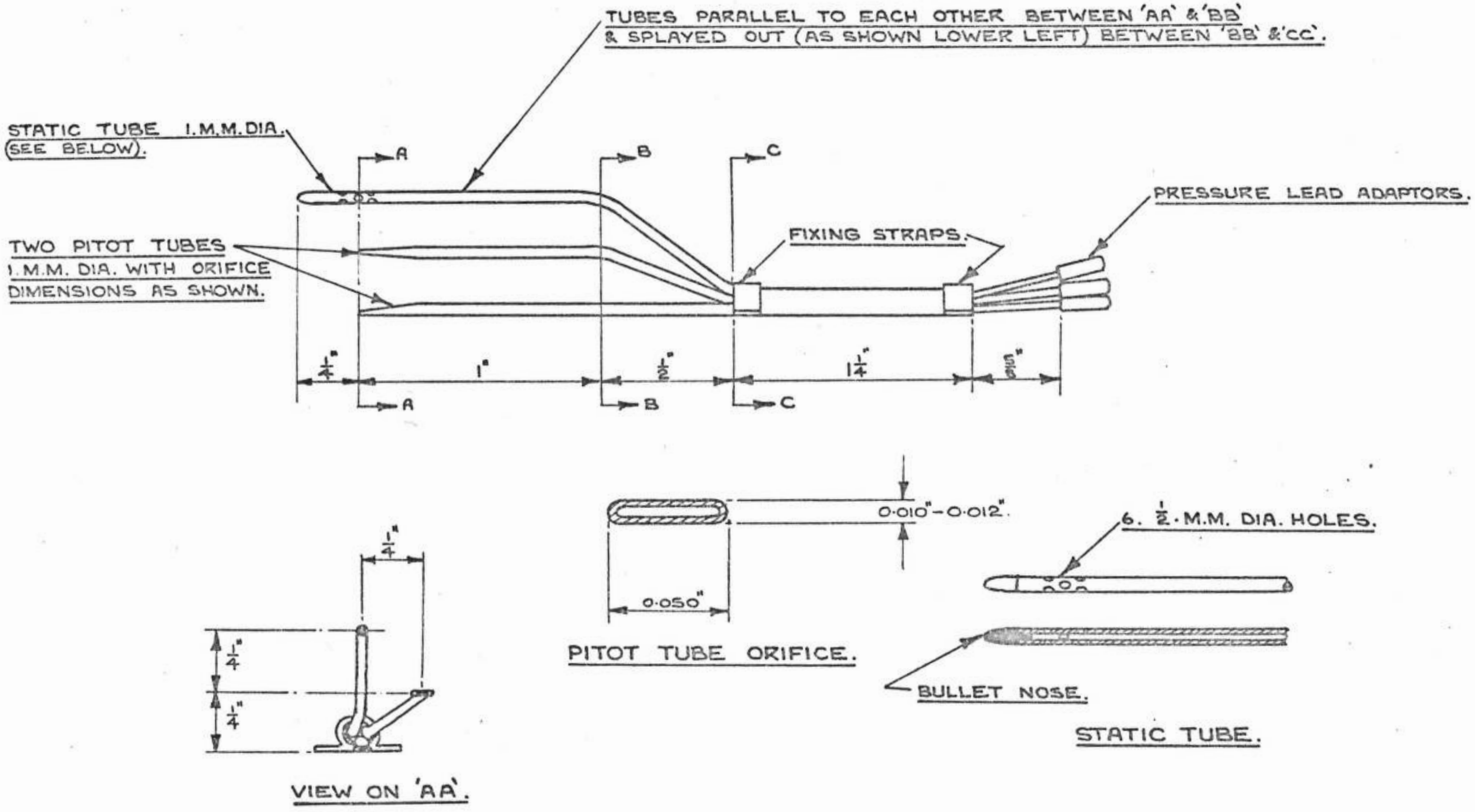

FIG.12. TRANSITION INDICATOR.

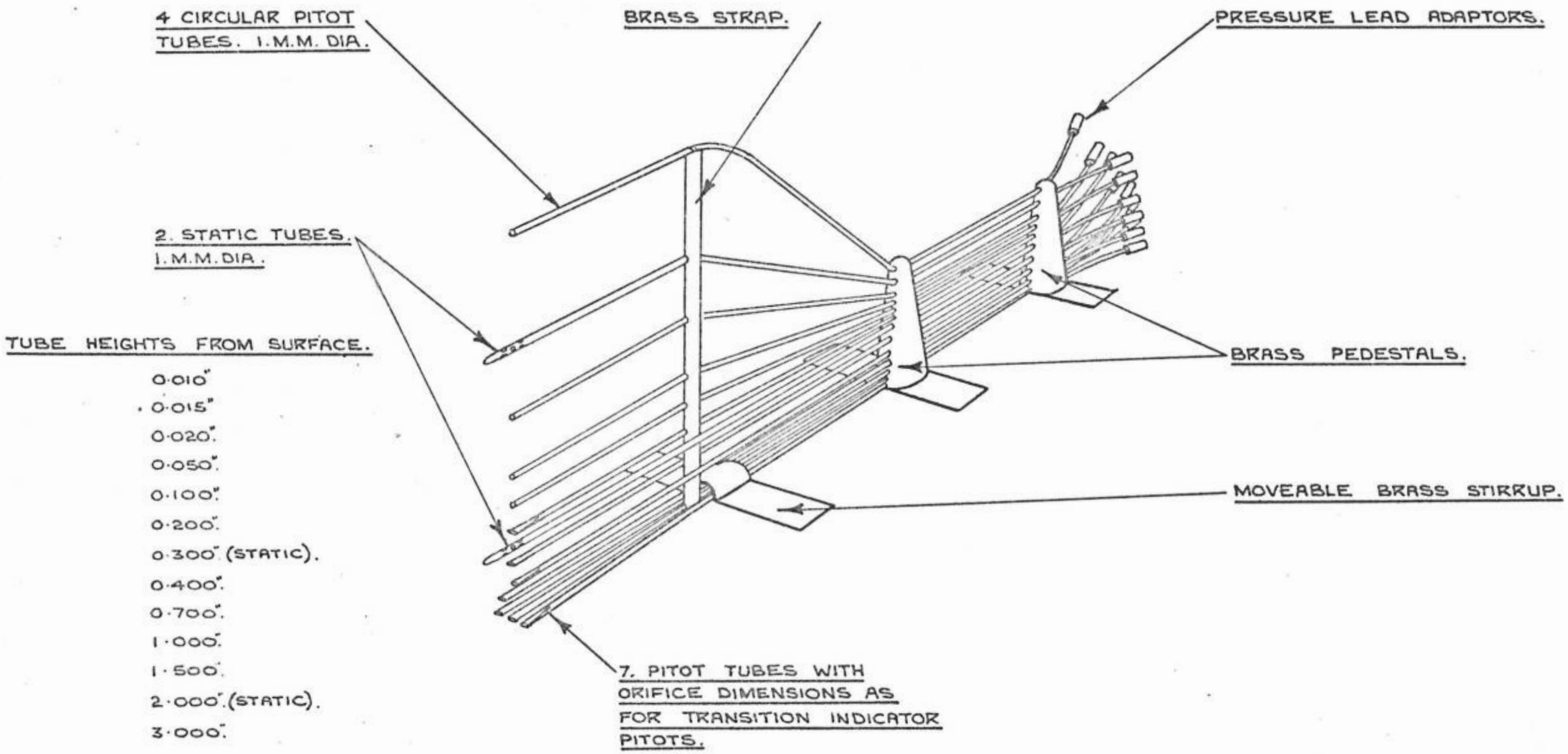

FIG. 13. BOUNDARY LAYER COMB.

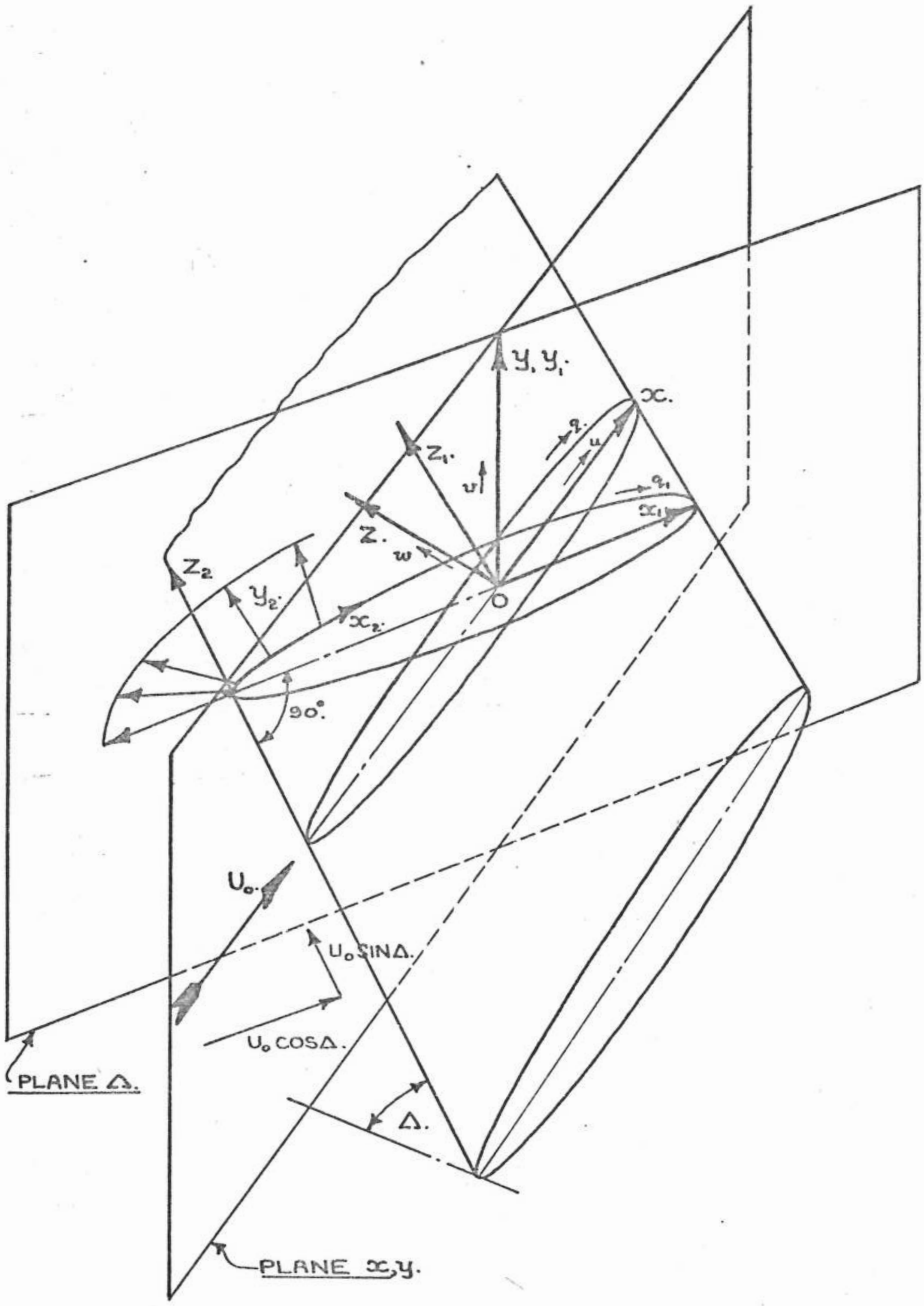

FIG. 14. SYSTEMS OF AXES USED.

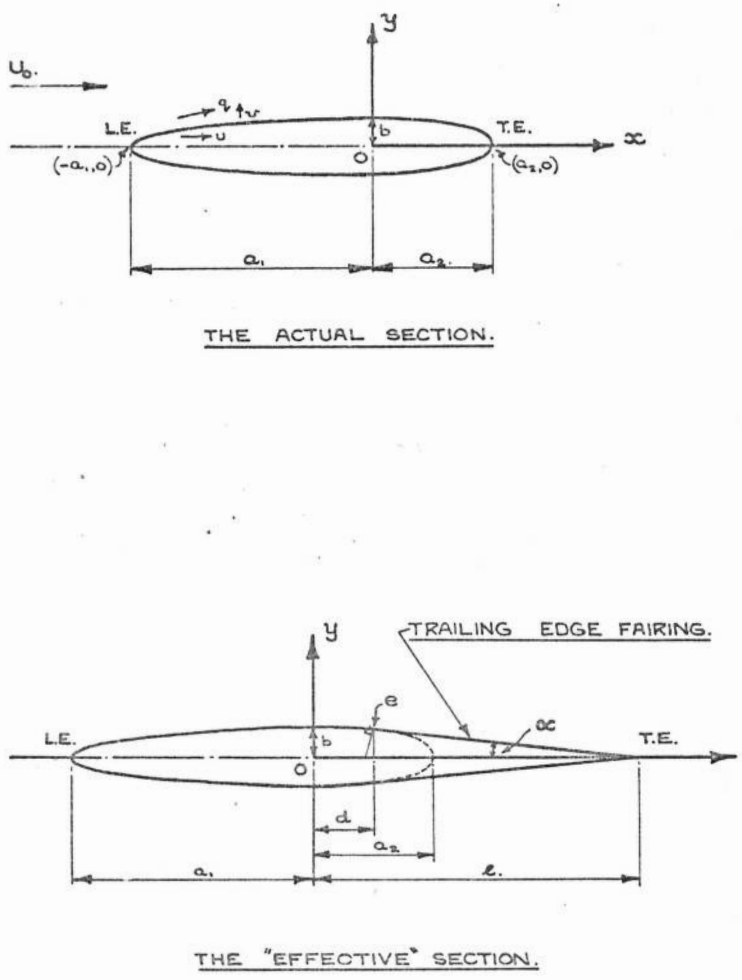

FIG.15. WING SECTIONS CONSIDERED IN § 2.3 .

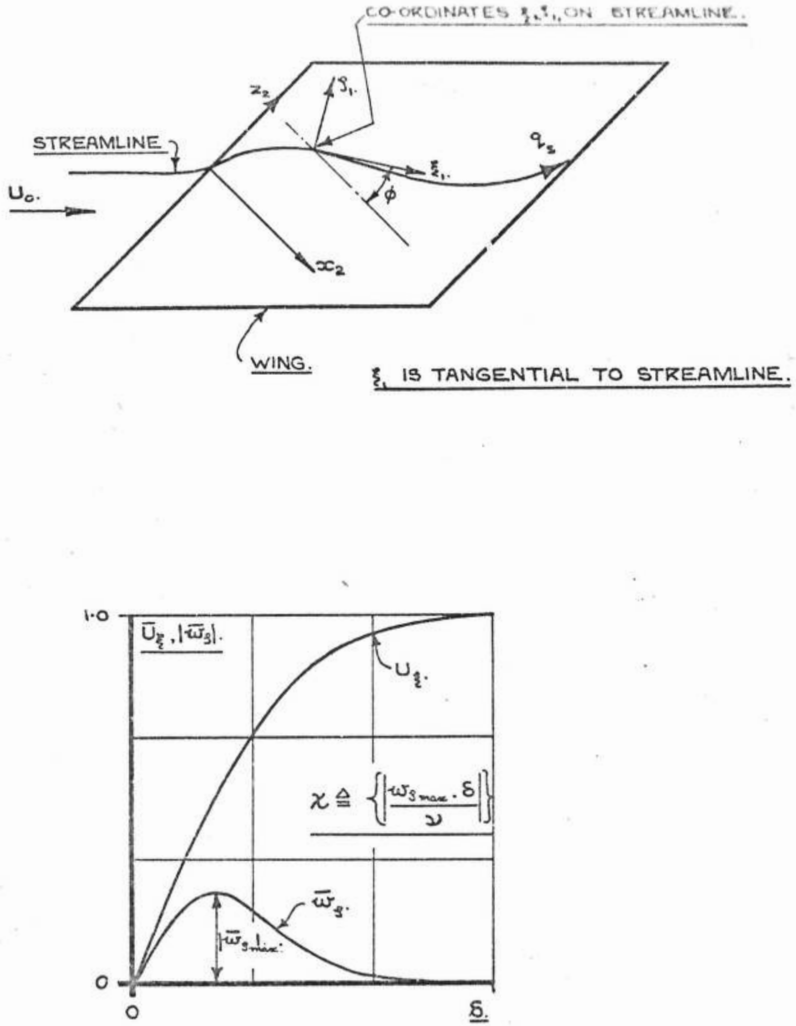

FIG.16. THE BOUNDARY LAYER IN RELATION TO THE EXTERNAL STREAMLINE.

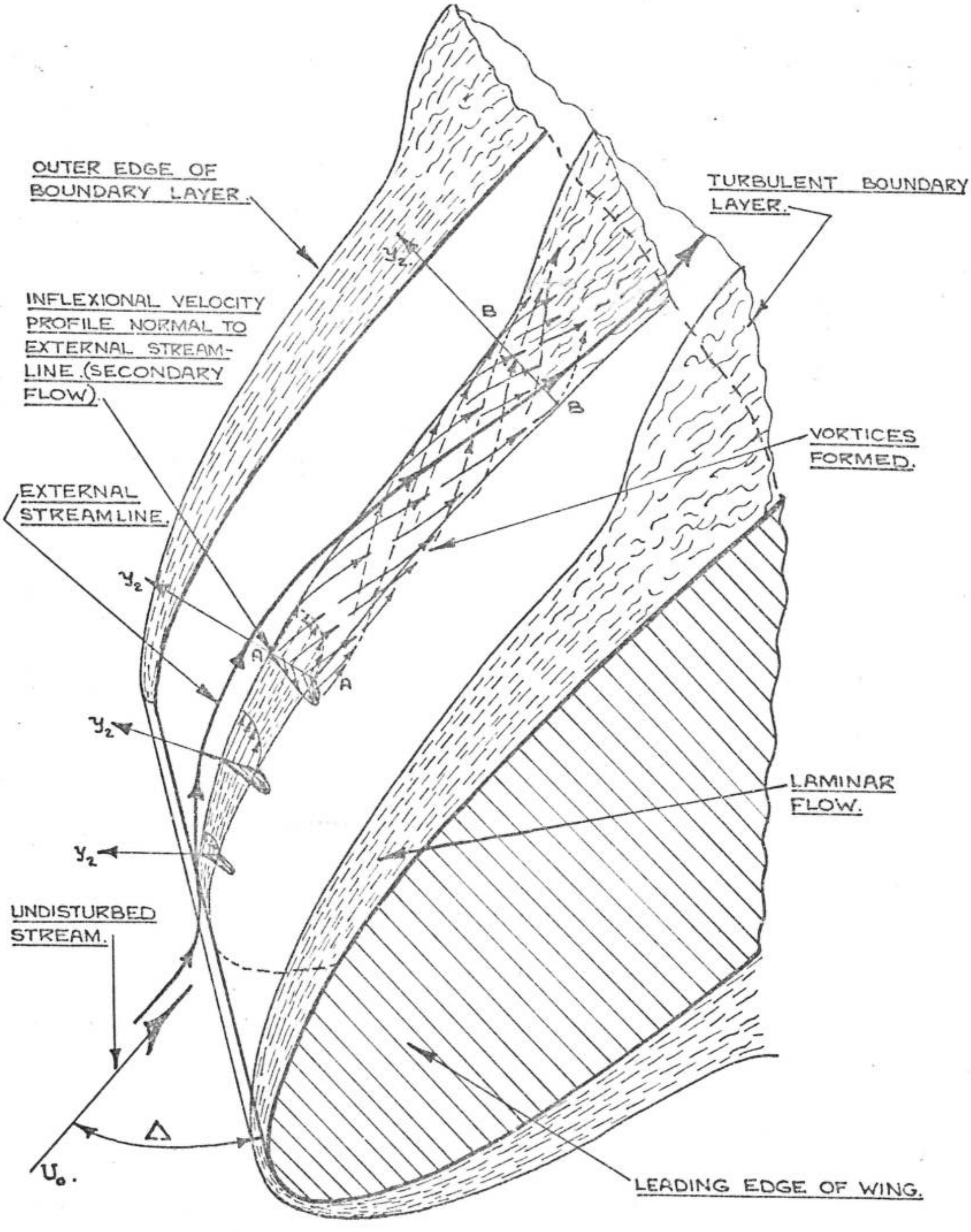

A.A. INSTABILITY DEVELOPS IN THE SECONDARY FLOW.

A.A.–B.B. GROWTH OF VORTEX FORMATION.

B.B. BOUNDARY LAYER TRANSITION BEGINS.

FIG.16a. GENERAL ELEMENTS OF THE LEADING EDGE VORTEX FORMATION PRODUCING INSTABILITY IN THE LAMINAR BOUNDARY LAYER.

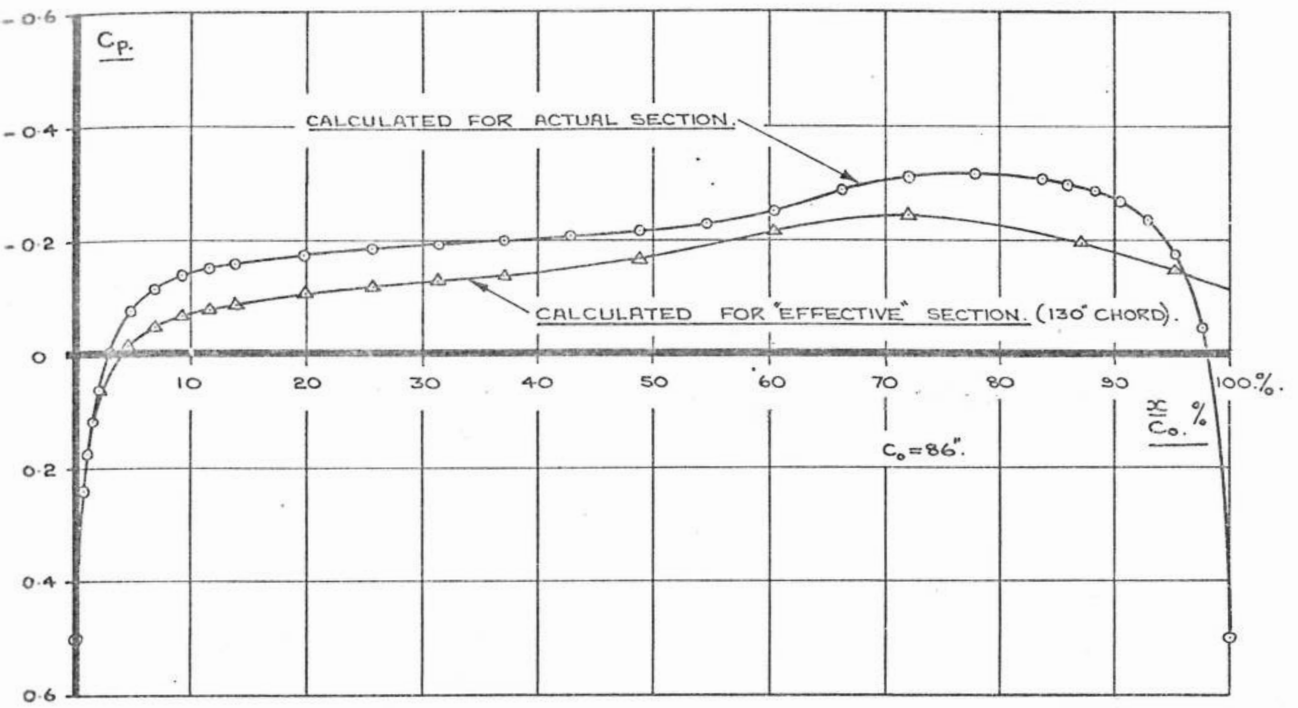

FIG. 17. CALCULATED DISTRIBUTIONS OF PRESSURE.

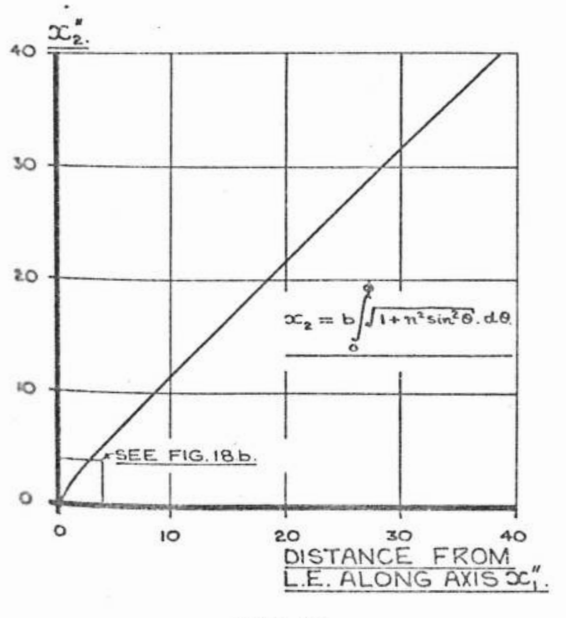

FIG. 18a.

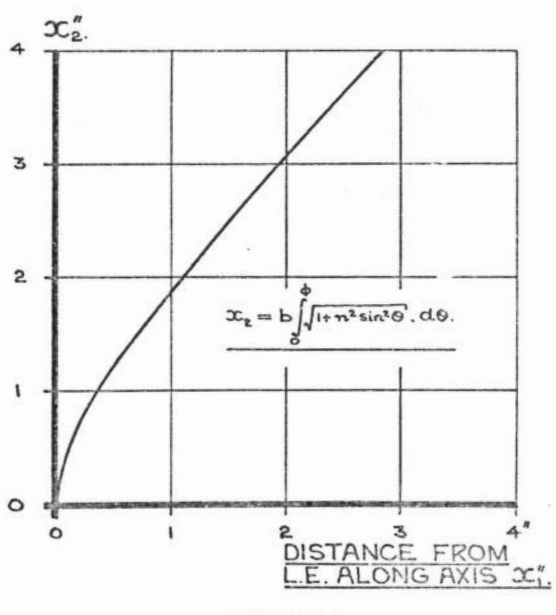

FIG. 18b.

FIGS. 18 . THE DISTANCE x_2 AS CALCULATED FROM EQN. A.3.11.

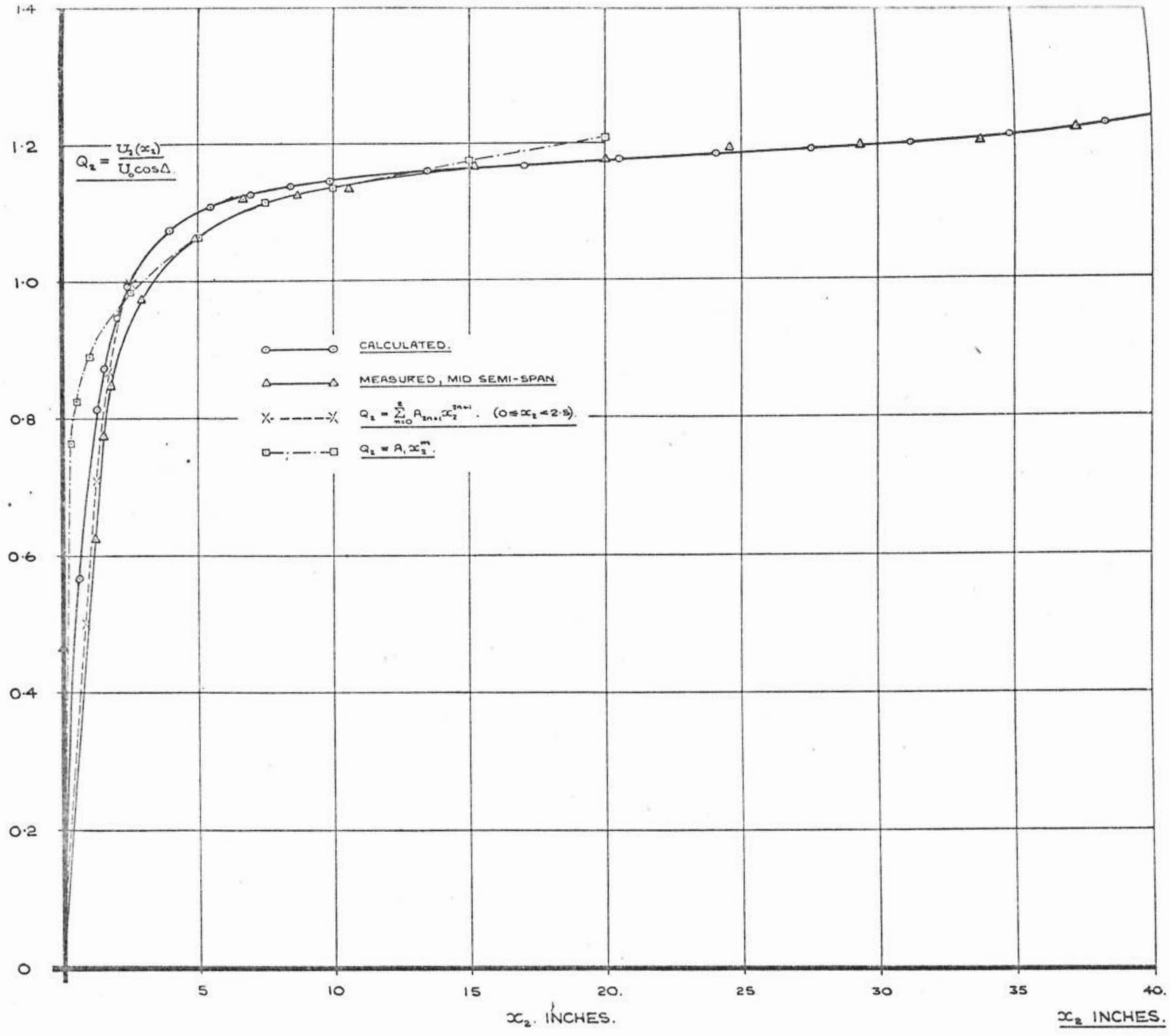

FIG.19. DISTRIBUTIONS OF VELOCITY: CALCULATED, MEASURED, & APPROXIMATIONS.

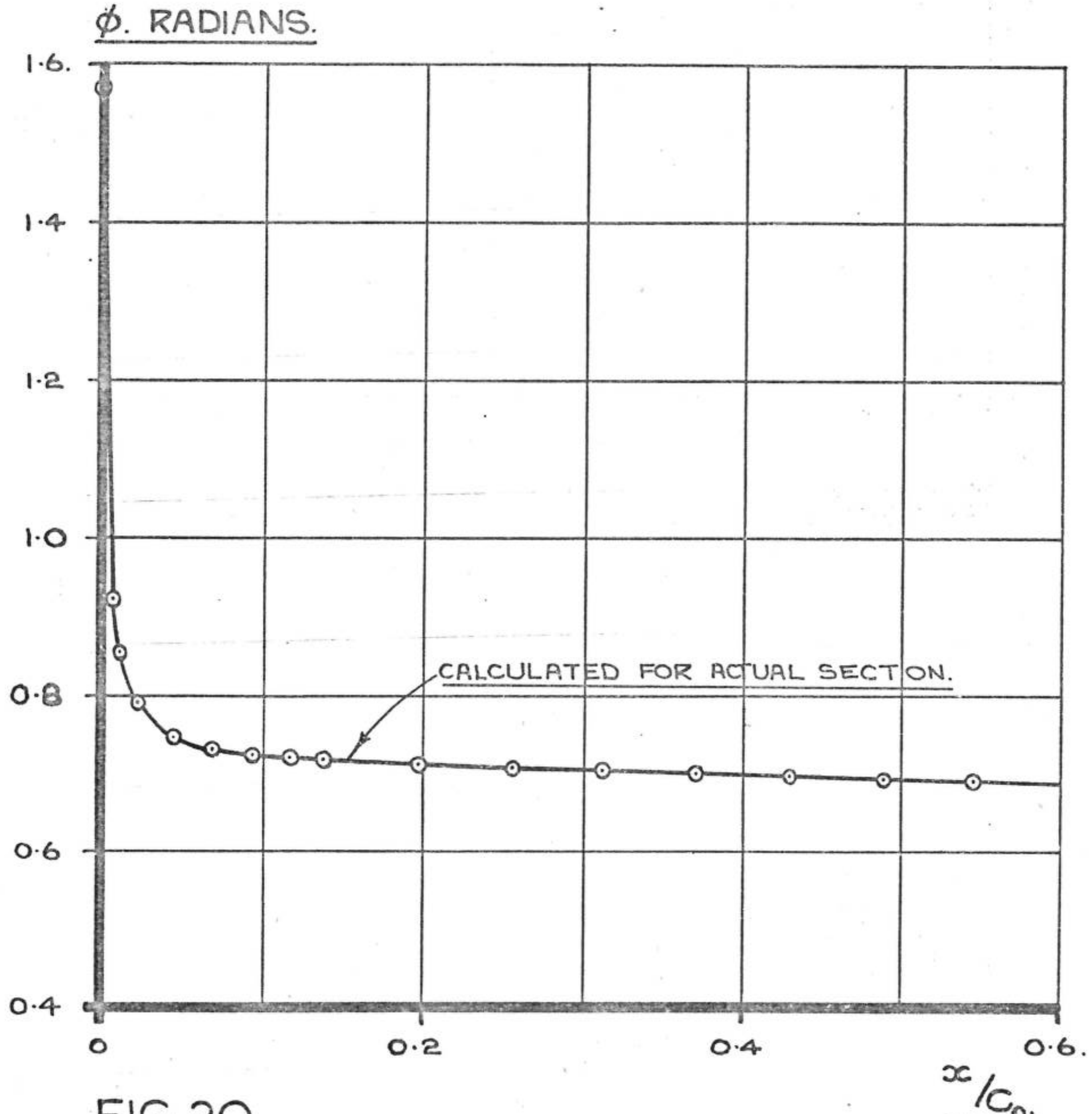

FIG. 20.

THE DIRECTION OF THE POTENTIAL FLOW STREAMLINE RELATIVE TO THE AXIS x_2.

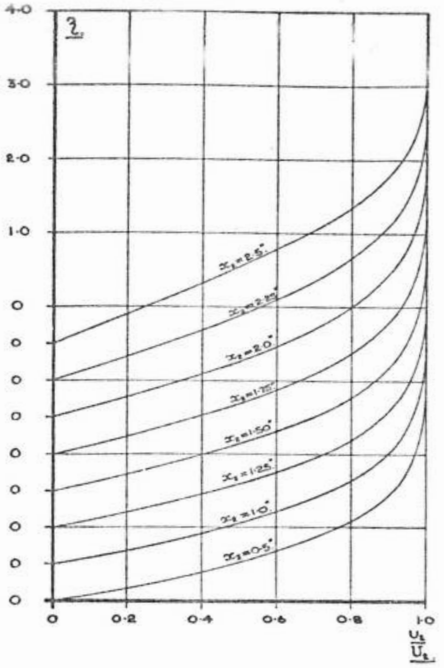

FIG. 21a. THE CALCULATED LAMINAR BOUNDARY LAYER FOR FLOW ALONG THE AXIS x_2, CLOSE TO LEADING EDGE.

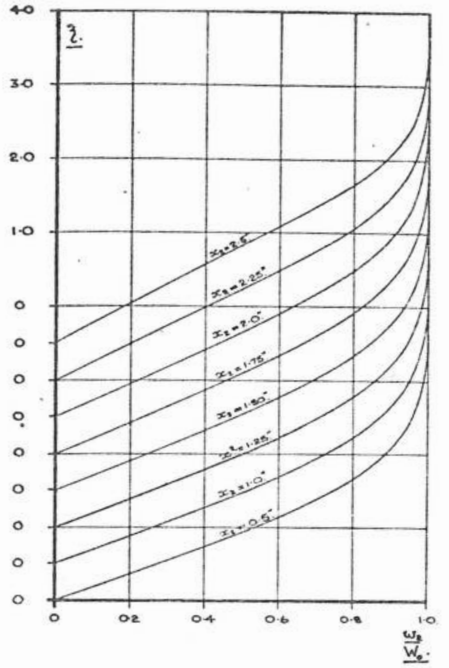

FIG. 21b. THE CALCULATED LAMINAR BOUNDARY LAYER FOR FLOW ALONG THE SPAN (PARALLEL TO L.E.), CLOSE TO L.E.

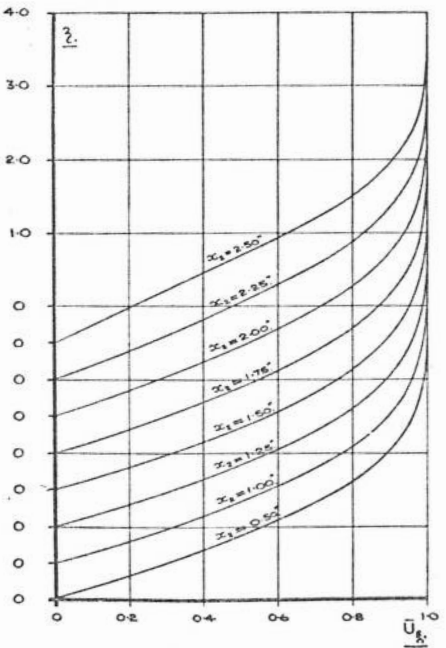

FIG. 21c. THE CALCULATED LAMINAR BOUNDARY LAYER REFERRED TO THE EXTERNAL STREAMLINE.

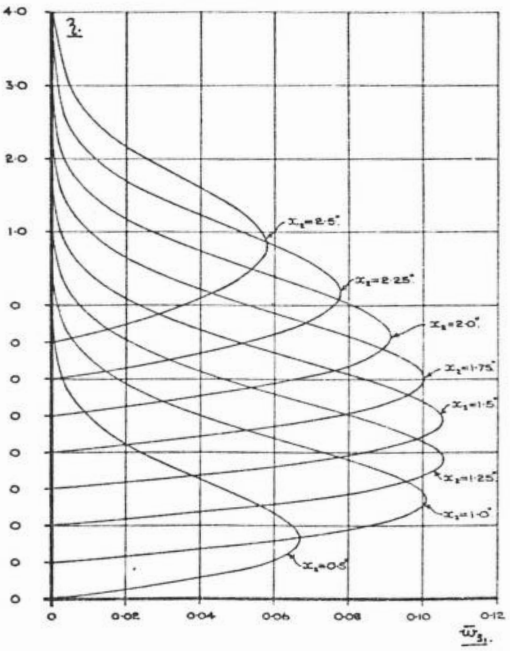

FIG. 21d. THE CALCULATED LAMINAR BOUNDARY LAYER NORMAL TO THE EXTERNAL STREAMLINE: SECONDARY FLOW.

FIG. 21. THE LAMINAR BOUNDARY LAYER FOR $U_2(x_2) = U_e \cos\Lambda \sum_{n=0}^{m} A_{2n+1} x_2^{2n+1}$.

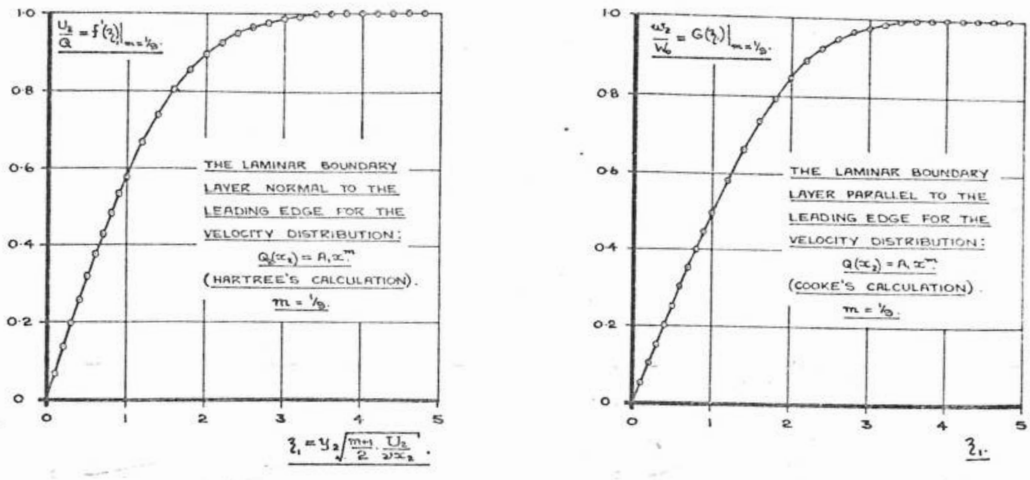

FIG.22a. THE LAMINAR BOUNDARY LAYER FOR $Q(x_2) = A_1 x_2^m$.

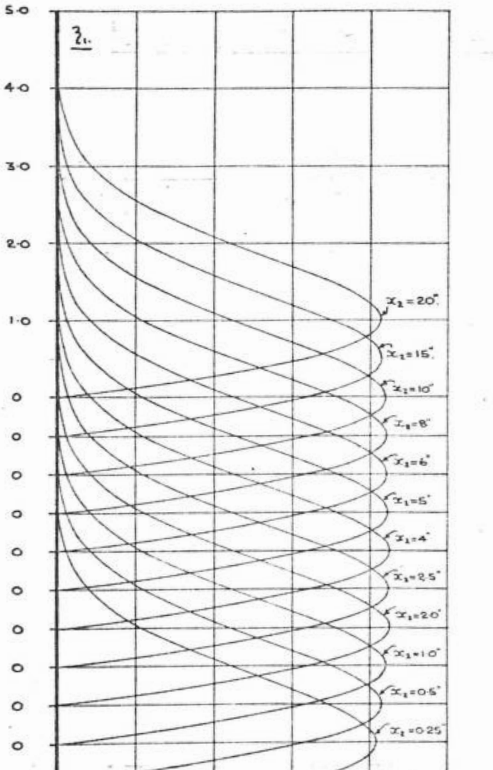

FIG.22c. THE CALCULATED LAMINAR BOUNDARY LAYER NORMAL TO THE EXTERNAL STREAMLINE: SECONDARY FLOW.

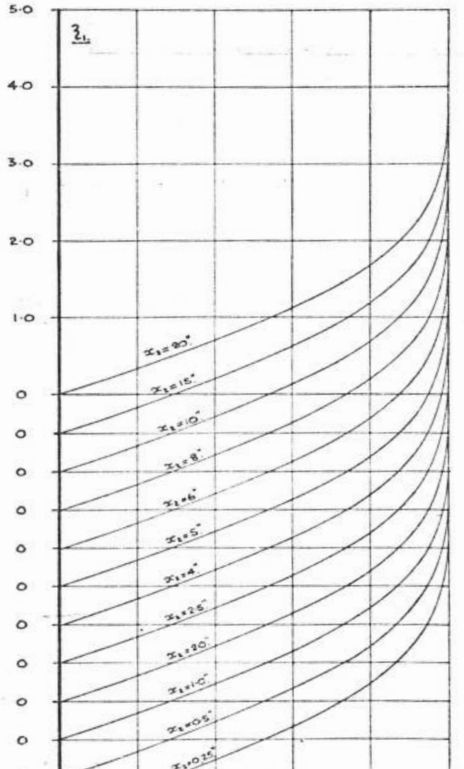

FIG.22b. THE CALCULATED LAMINAR BOUNDARY LAYER REFERRED TO THE EXTERNAL STREAMLINE.

FIG.22. THE LAMINAR BOUNDARY LAYER FOR $Q_2(x_2) = A_1 x^m$.

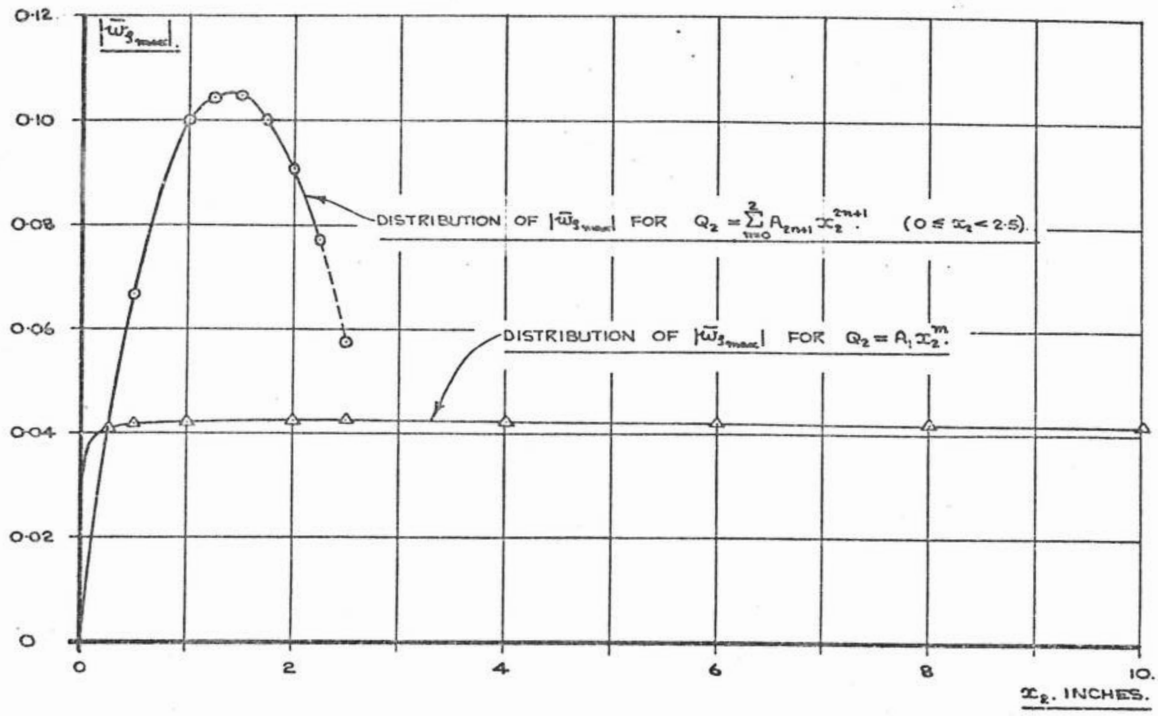

FIG. 23. DISTRIBUTION OF $|\bar{w}_{\zeta_{max}}|$.

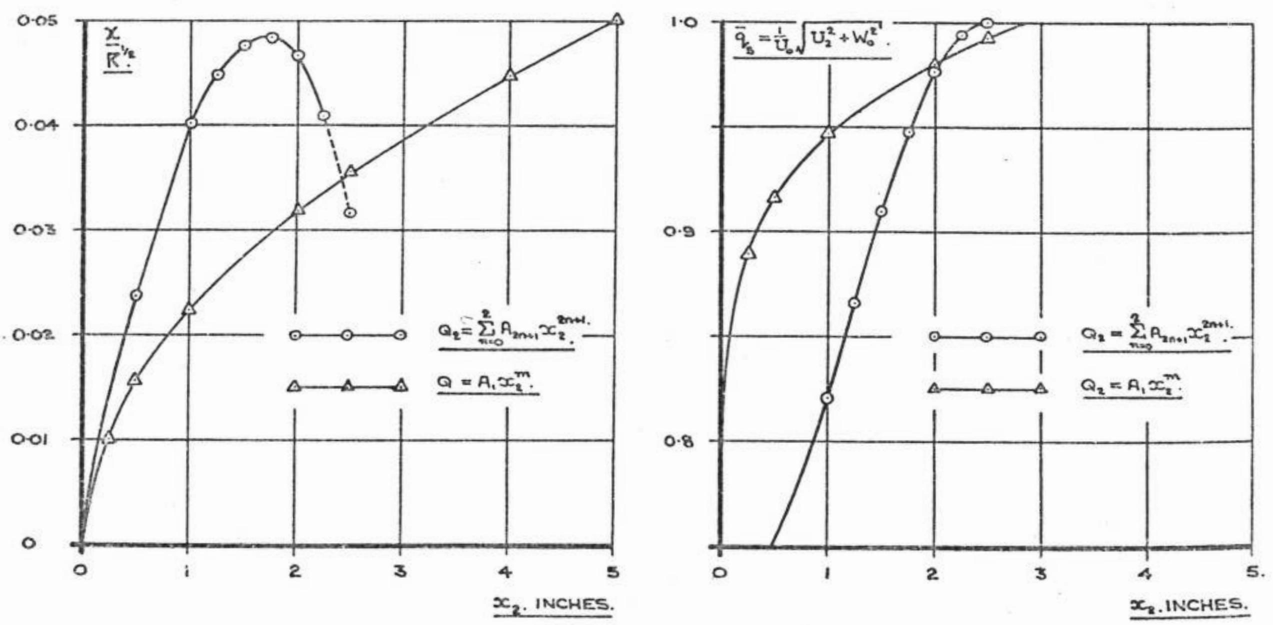

FIG. 24. SECONDARY FLOW REYNOLDS NUMBERS & VELOCITY ALONG THE EXTERNAL STREAMLINE.

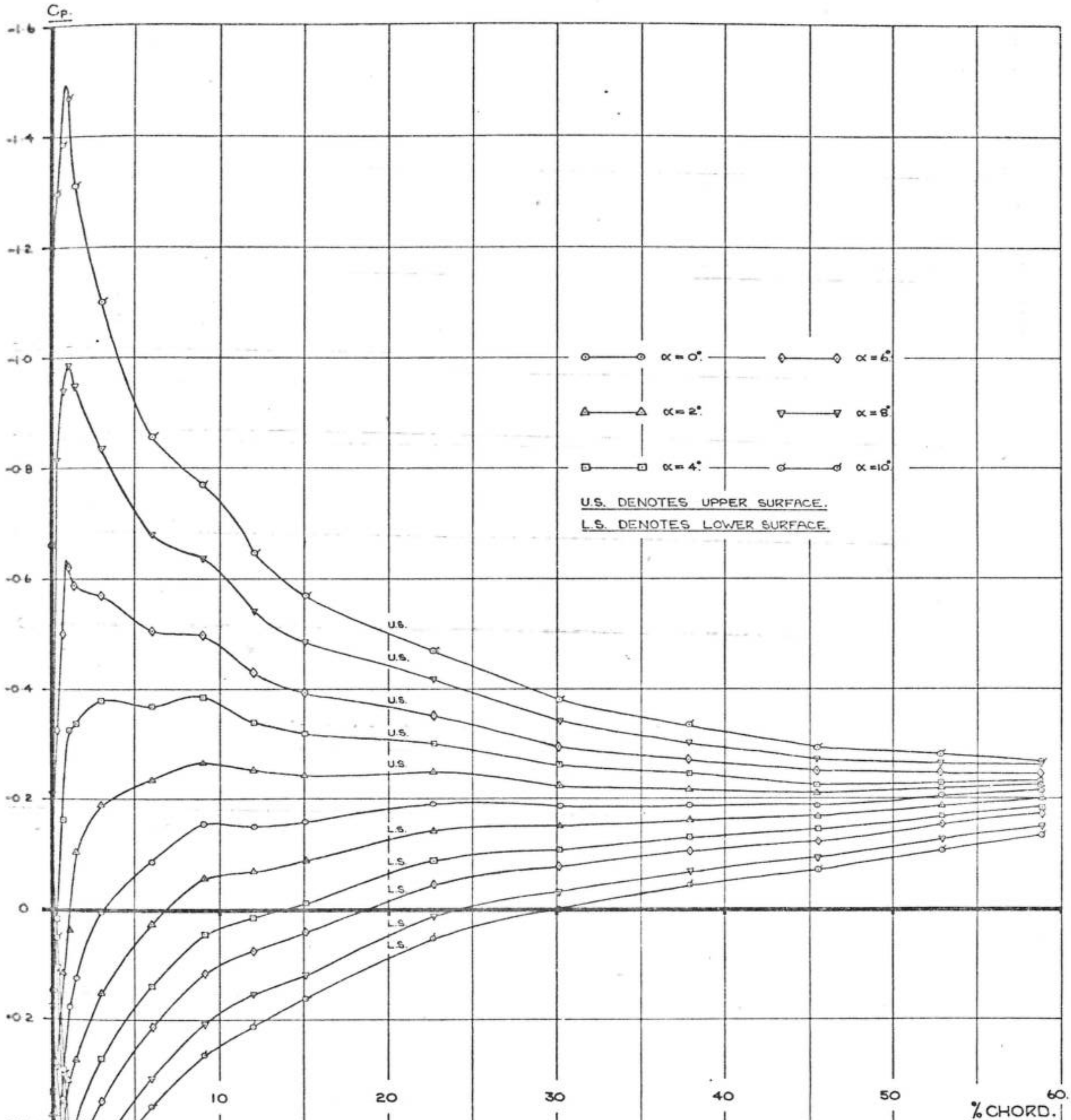

WING TIP STATION

FIG. 25 a.

STATIC PRESSURE DISTRIBUTION OVER THE SWEPT BACK HALF WING FOR THE REYNOLDS NUMBER RANGE $0{\cdot}884 \times 10^6 - 1{\cdot}916 \times 10^6$ PER FOOT. UPPER AND LOWER SURFACES.

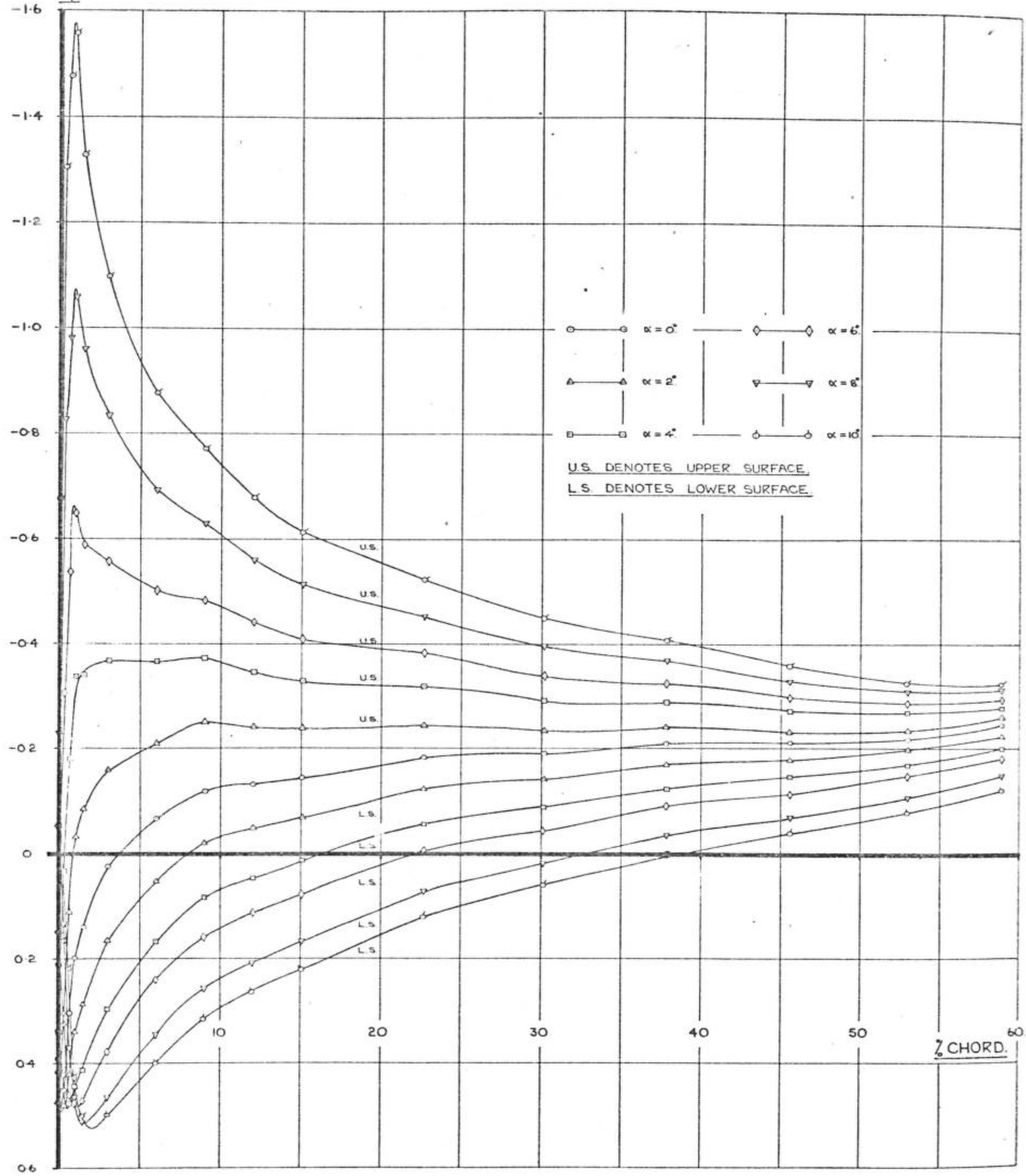

MID SEMI-SPAN STATION

FIG. 25. b.

STATIC PRESSURE DISTRIBUTION OVER THE SWEPT BACK HALF WING
FOR THE REYNOLDS NUMBER RANGE
$0{\cdot}884 \times 10^6 - 1{\cdot}916 \times 10^6$ PER FOOT. UPPER AND LOWER SURFACES.

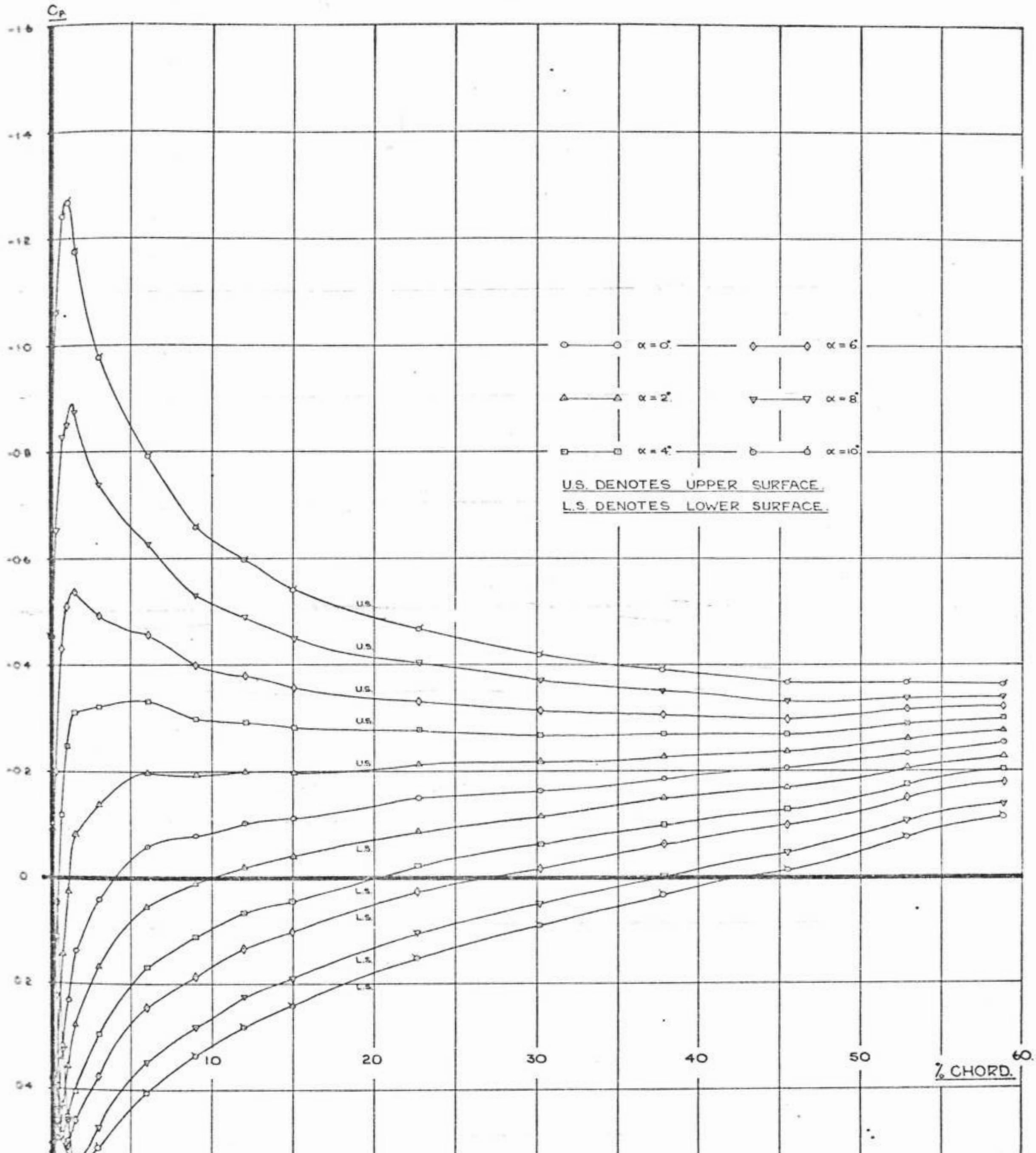

WING ROOT STATION

FIG. 25.c.

STATIC PRESSURE DISTRIBUTION OVER THE SWEPT BACK HALF WING
FOR THE REYNOLDS NUMBER RANGE
$0{\cdot}884 \times 10^6 - 1{\cdot}916 \times 10^6$ PER FOOT. UPPER AND LOWER SURFACES.

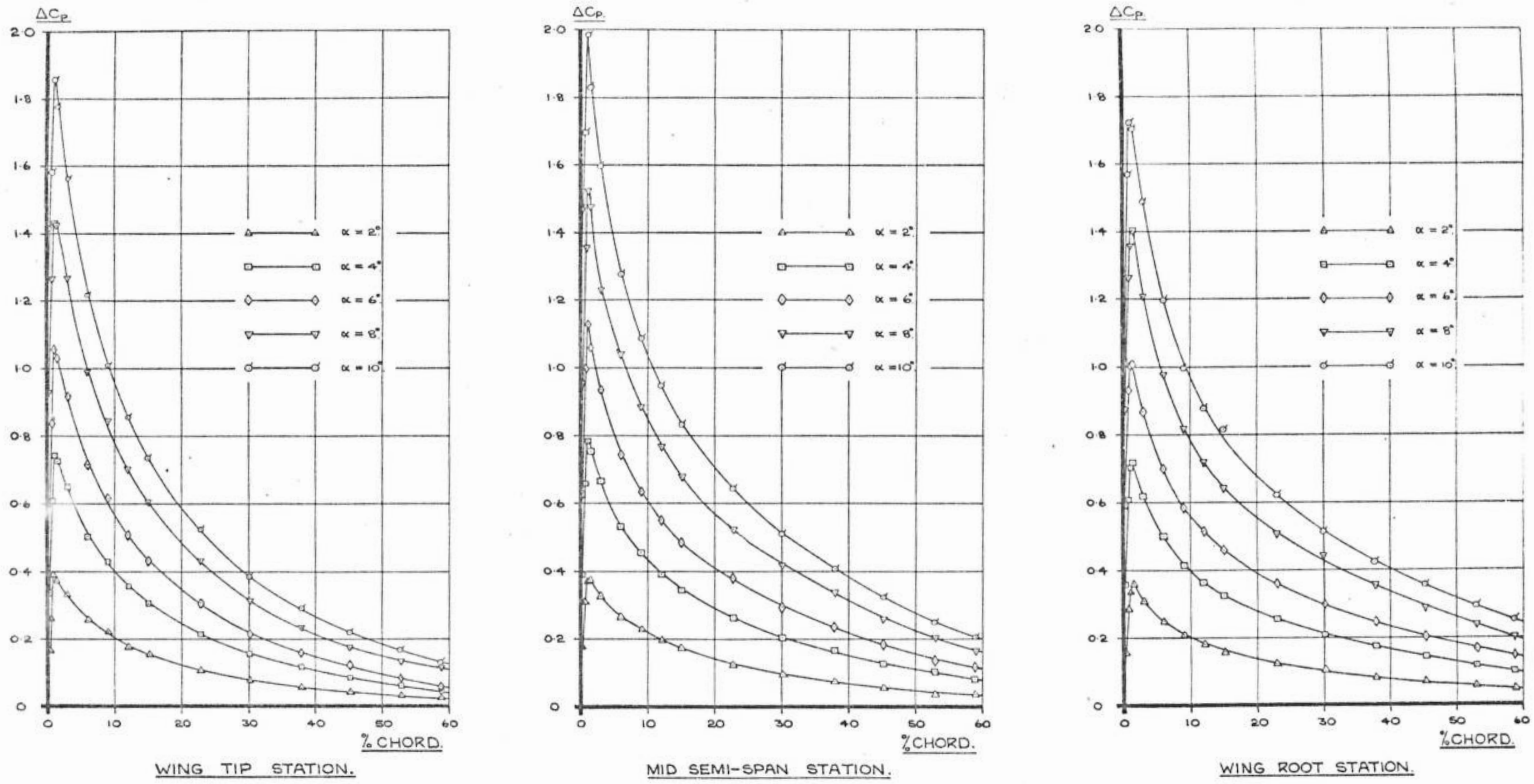

FIG. 26. MEASURED CHORDWISE LOADINGS: ΔC_p, ON SWEPT BACK HALF WING FOR THE REYNOLDS NUMBER RANGE $0{\cdot}884 \times 10^6 - 1{\cdot}916 \times 10^6$ PER FOOT.

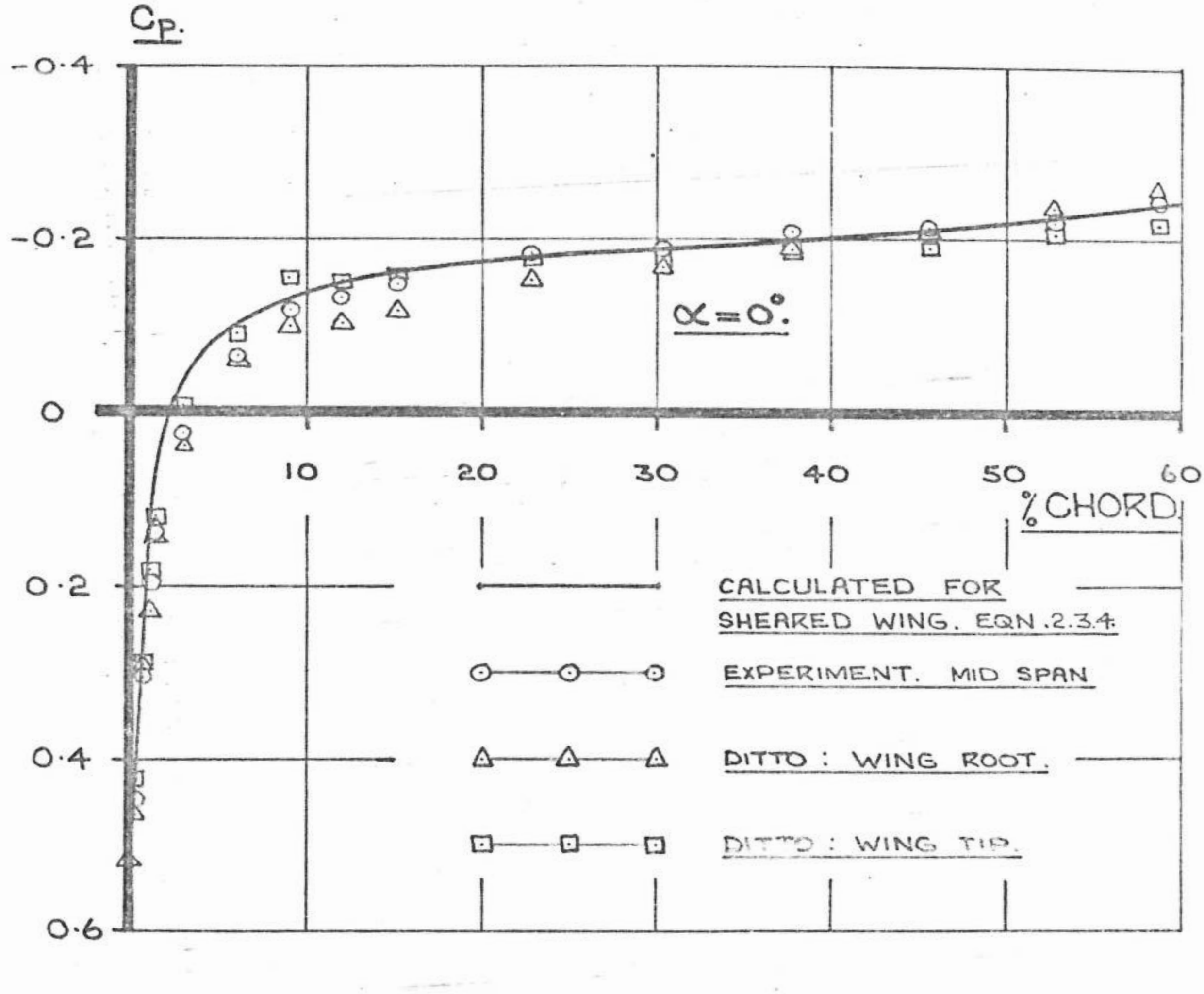

FIG. 27. COMPARISON OF MEASURED AND CALCULATED DISTRIBUTIONS OF STATIC PRESSURE UP TO MAX^{M} THICKNESS POSITION.

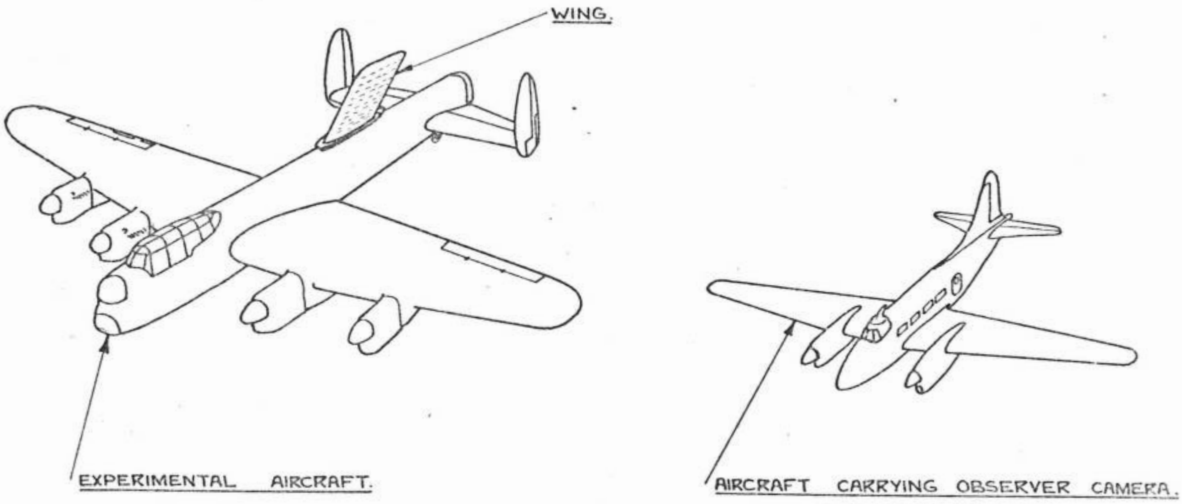

FIG.28a. TUFT OBSERVATIONS IN FLIGHT.

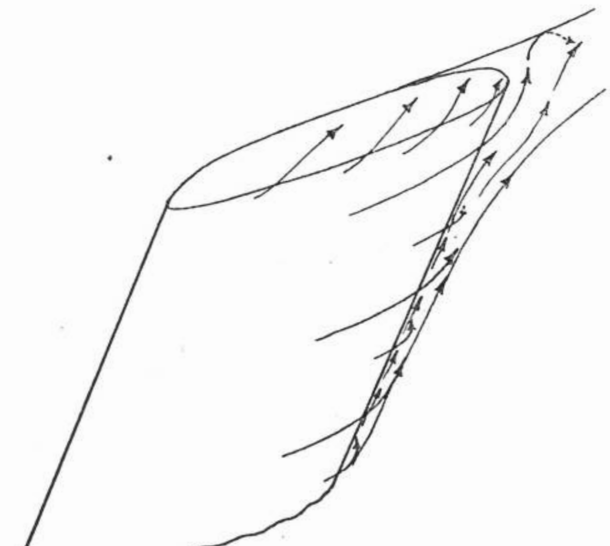

FIG. 28C. FLOW AT THE TRAILING EDGE.
(LOWER SURFACE SHOWN).

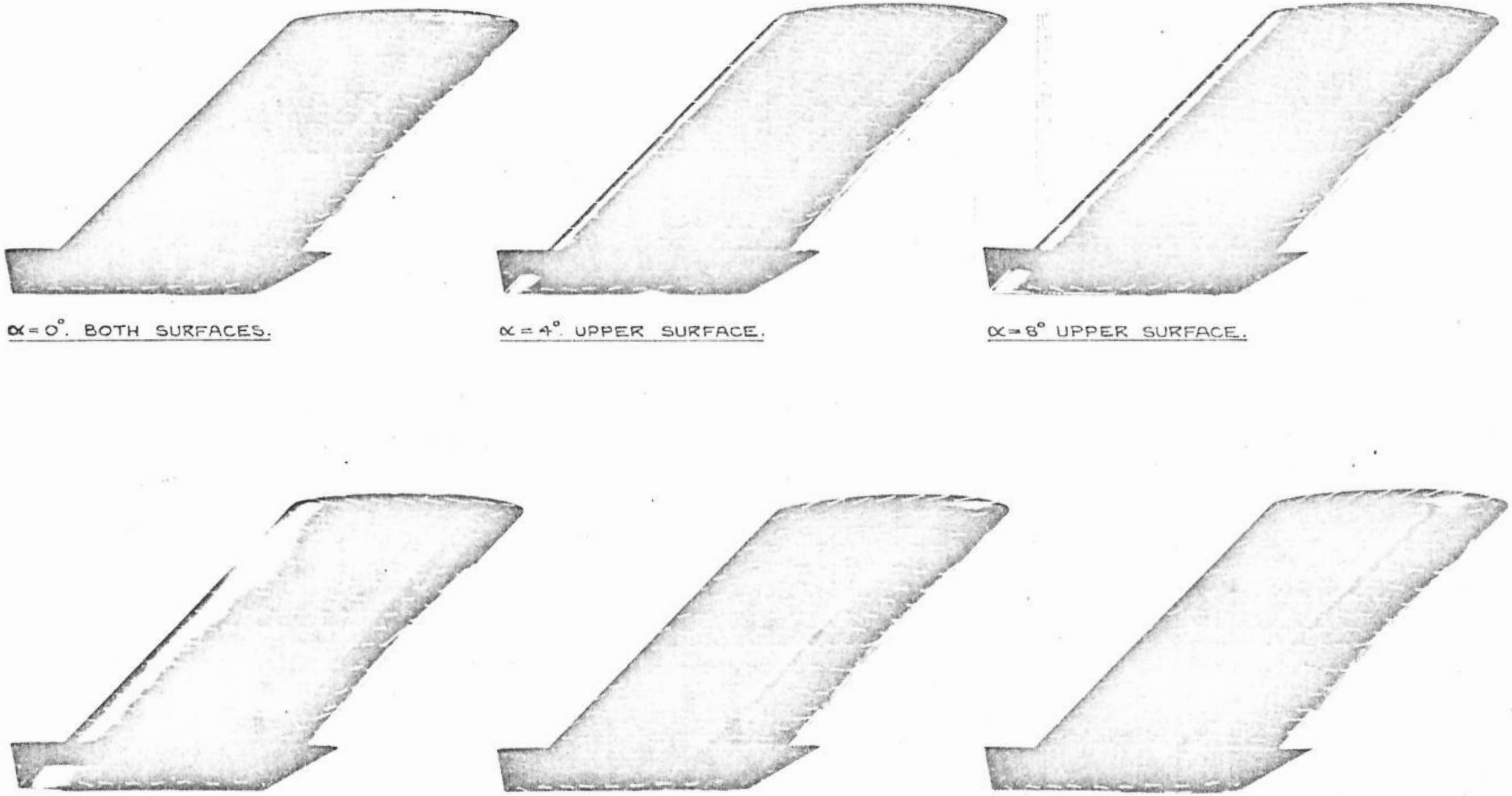

$\alpha = 0^\circ$. BOTH SURFACES.

$\alpha = 4^\circ$ UPPER SURFACE.

$\alpha = 8^\circ$ UPPER SURFACE.

$\alpha = 10^\circ$. UPPER SURFACE.

$\alpha = 6^\circ$. LOWER SURFACE.

$\alpha = 10^\circ$. LOWER SURFACE.

FIG. 28 b. TUFT OBSERVATIONS : SPECIMEN RESULTS.

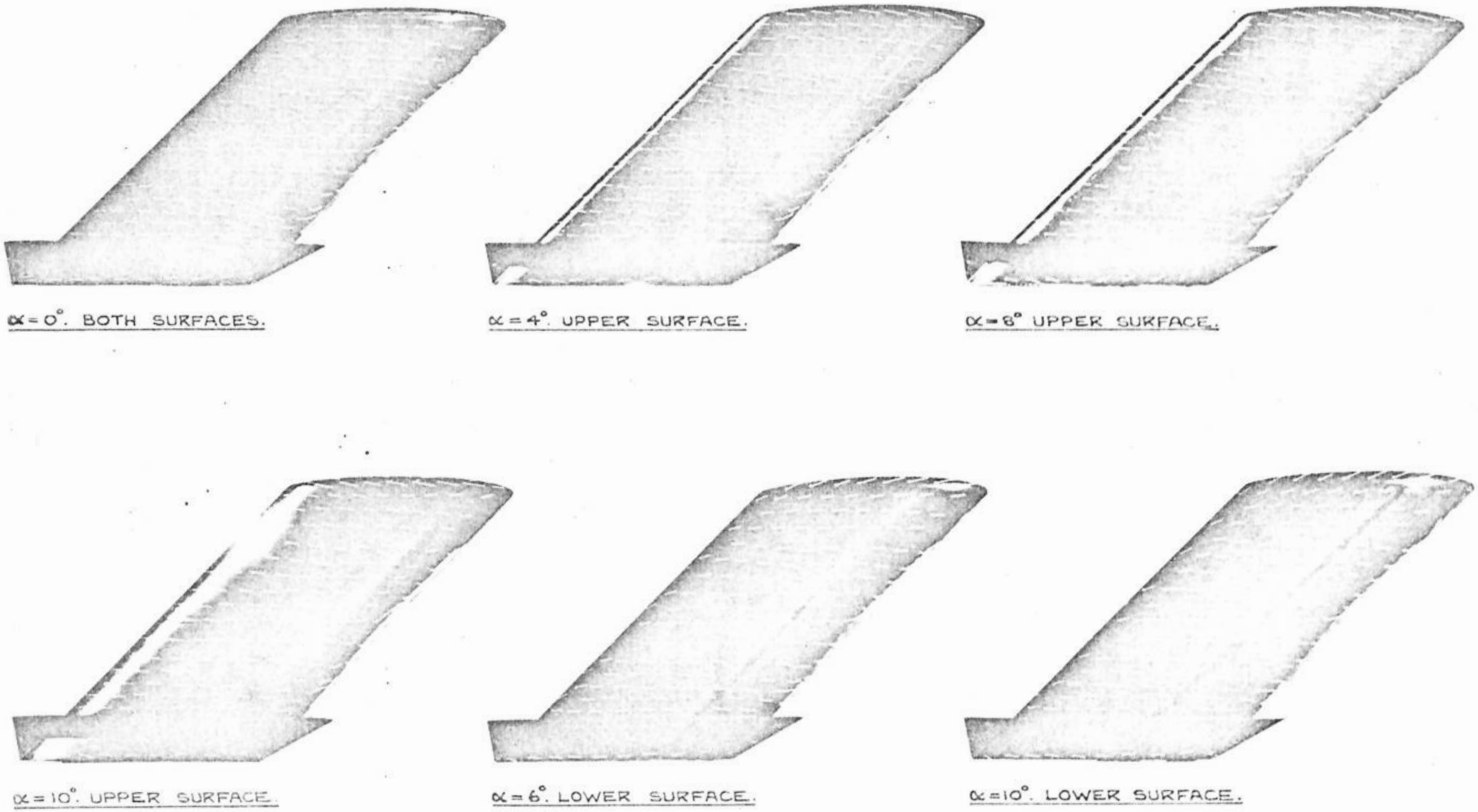

FIG. 28 b. TUFT OBSERVATIONS : SPECIMEN RESULTS.

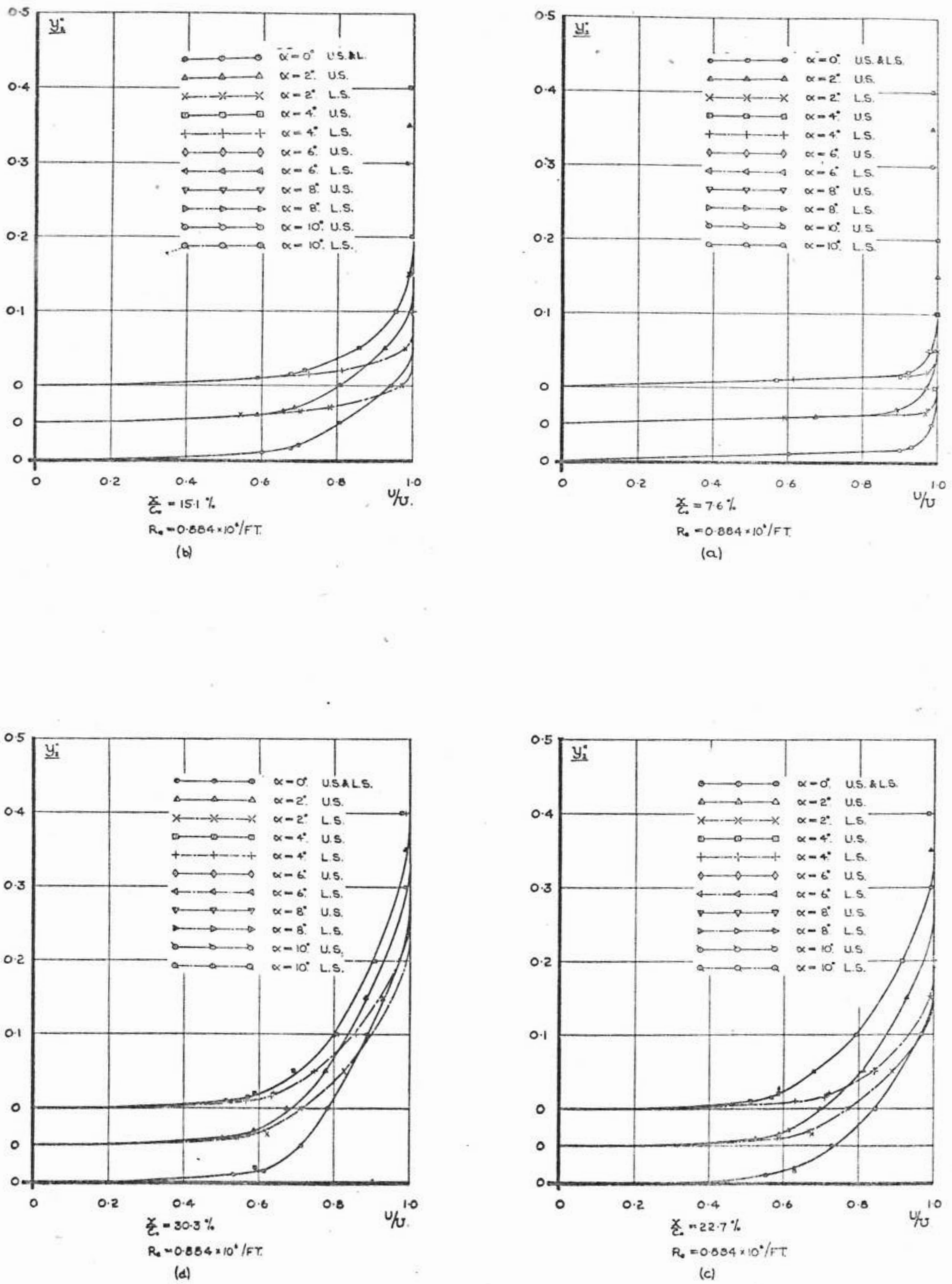

FIG 29. BOUNDARY LAYER VELOCITY PROFILES. WING ROOT STATION.

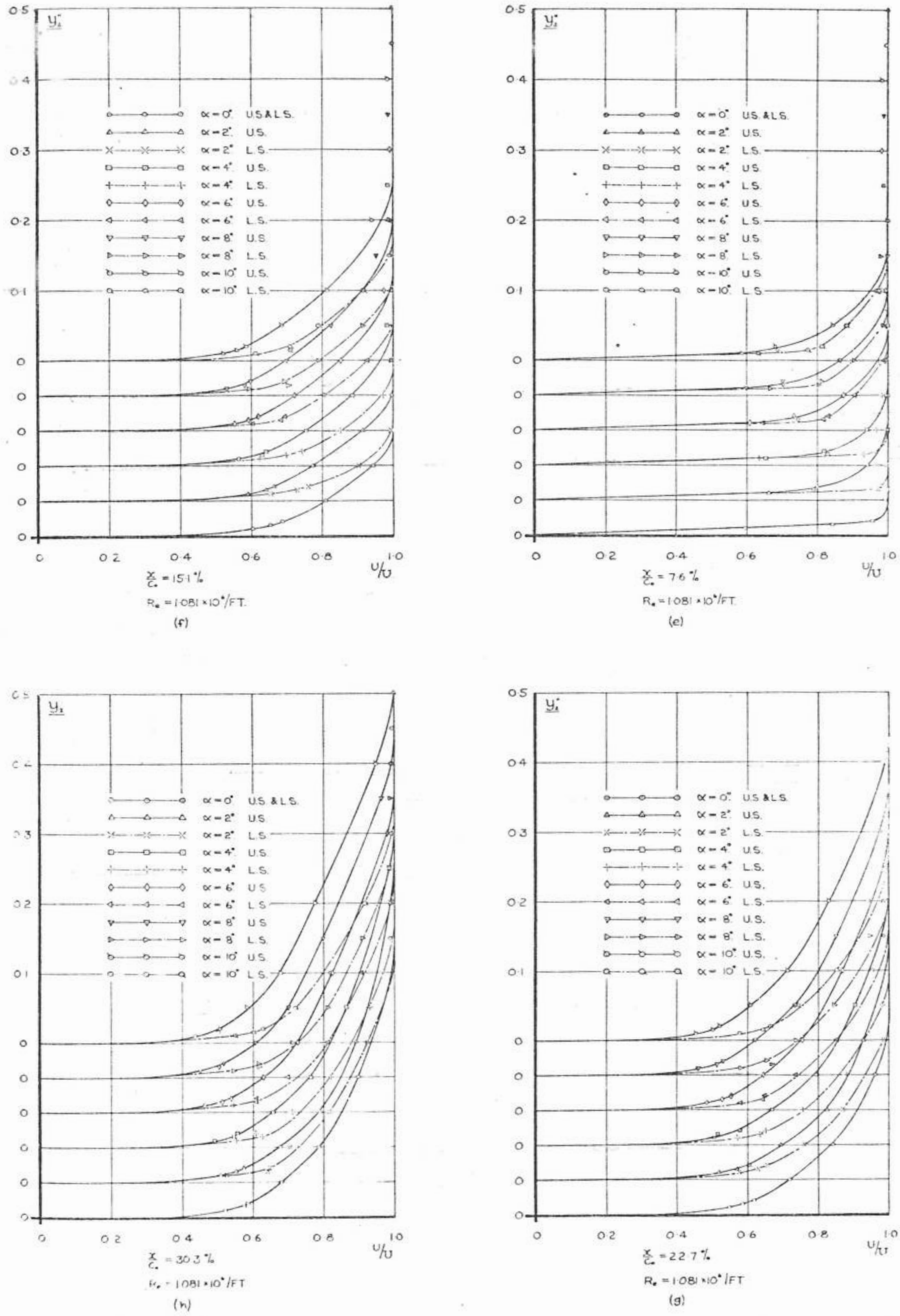

FIG 29. BOUNDARY LAYER VELOCITY PROFILES. WING ROOT STATION.

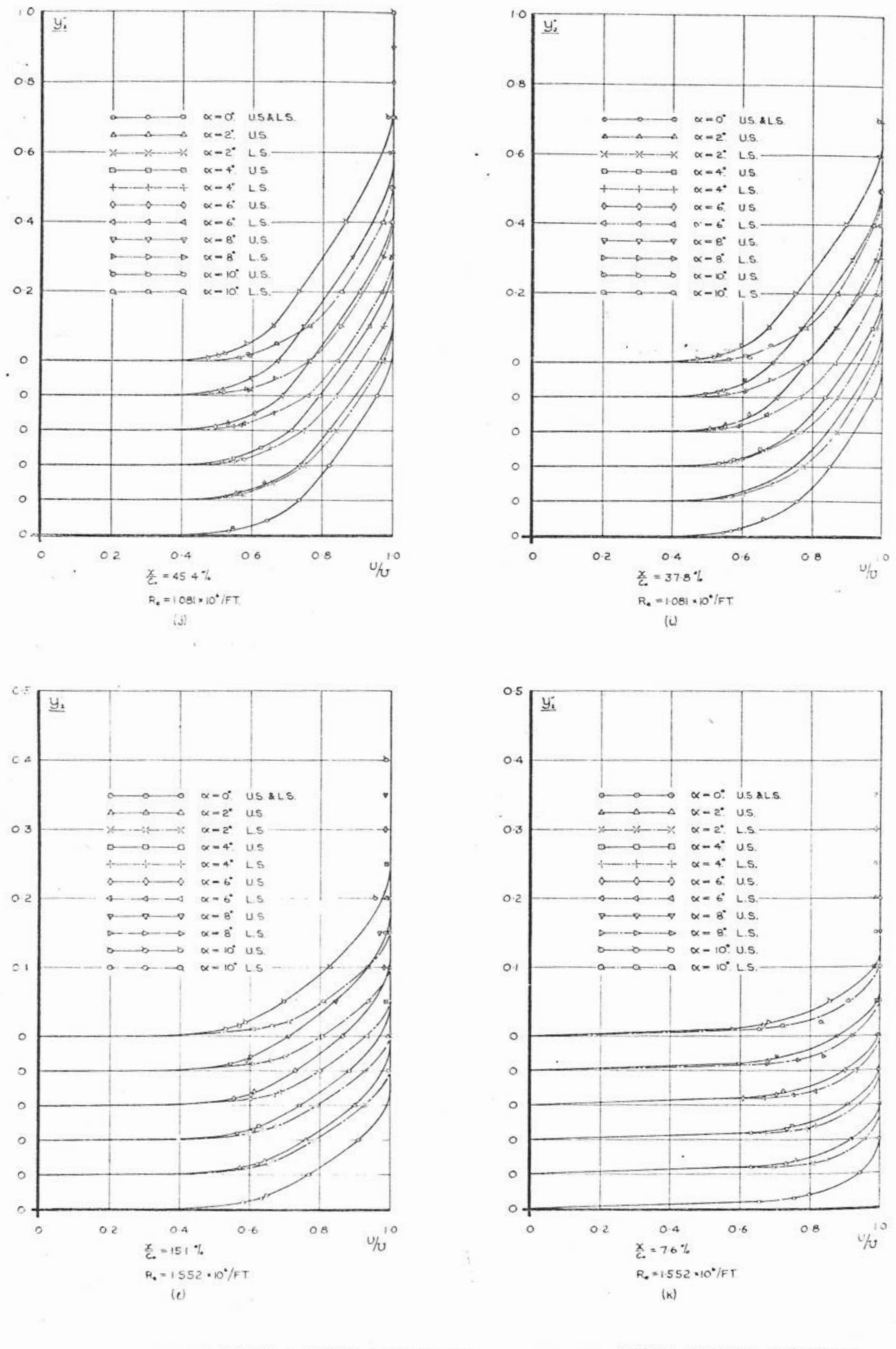

FIG 29. BOUNDARY LAYER VELOCITY PROFILES. WING ROOT STATION.

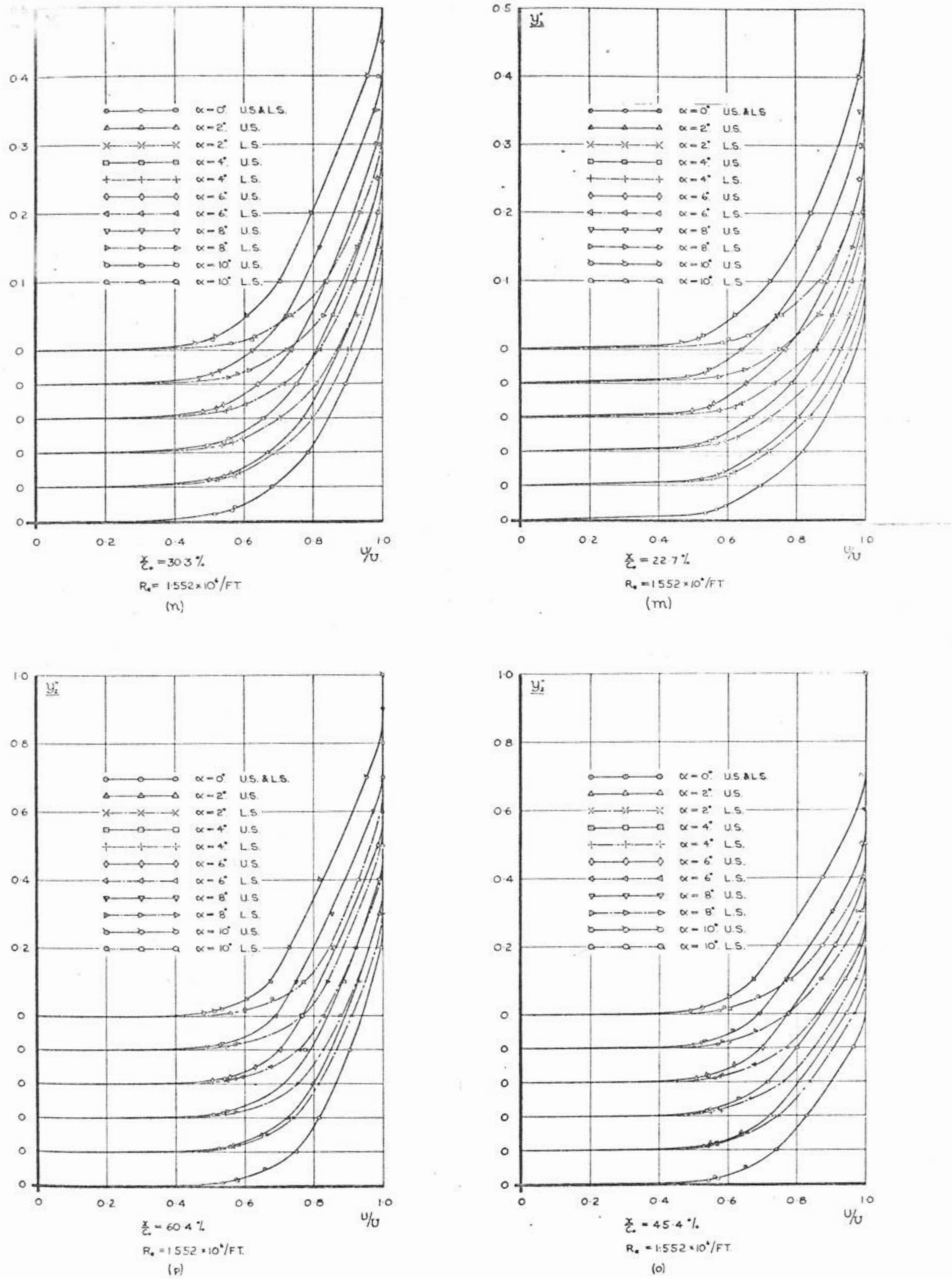

FIG 29. BOUNDARY LAYER VELOCITY PROFILES. WING ROOT STATION.

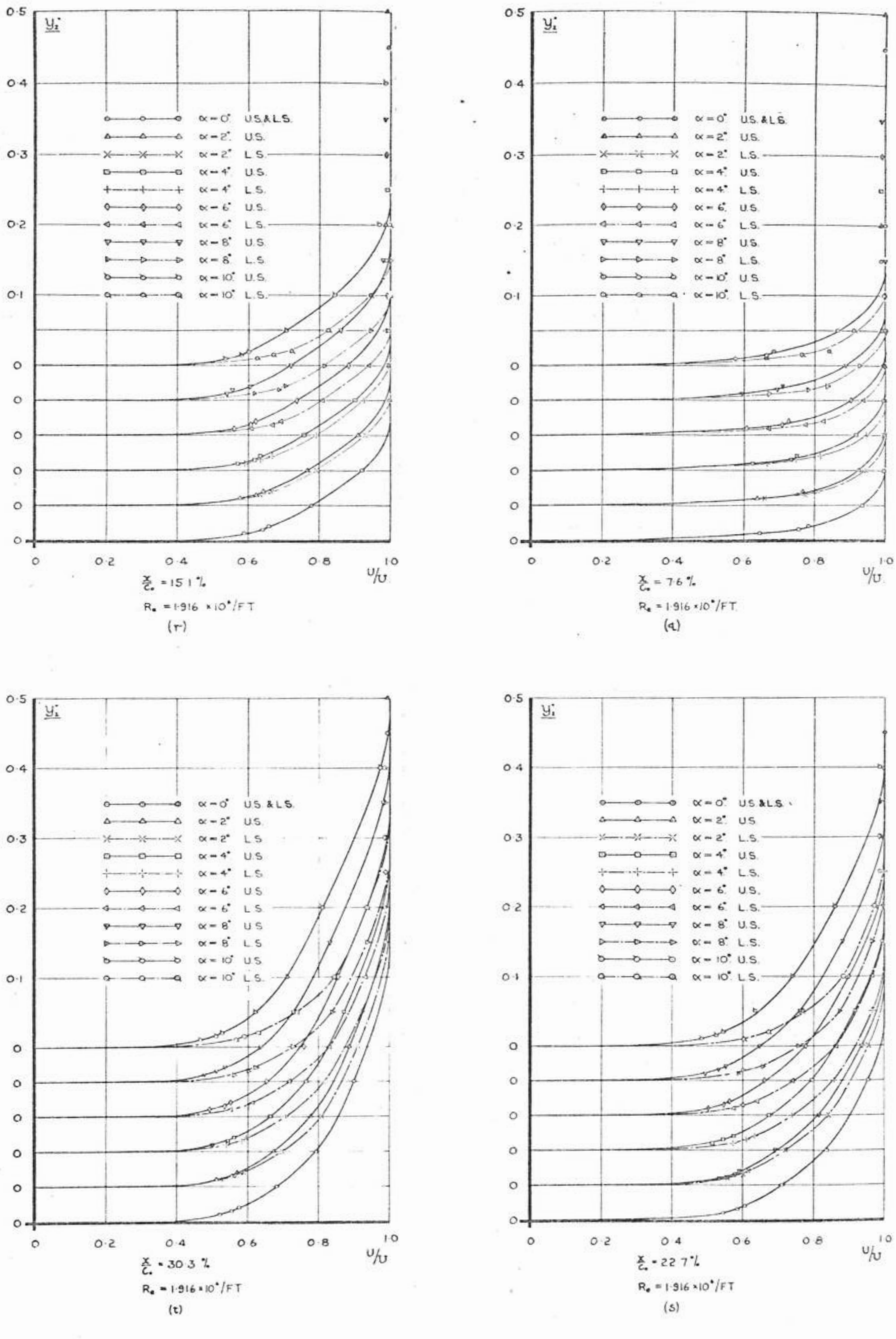

FIG 29. BOUNDARY LAYER VELOCITY PROFILES. WING ROOT STATION.

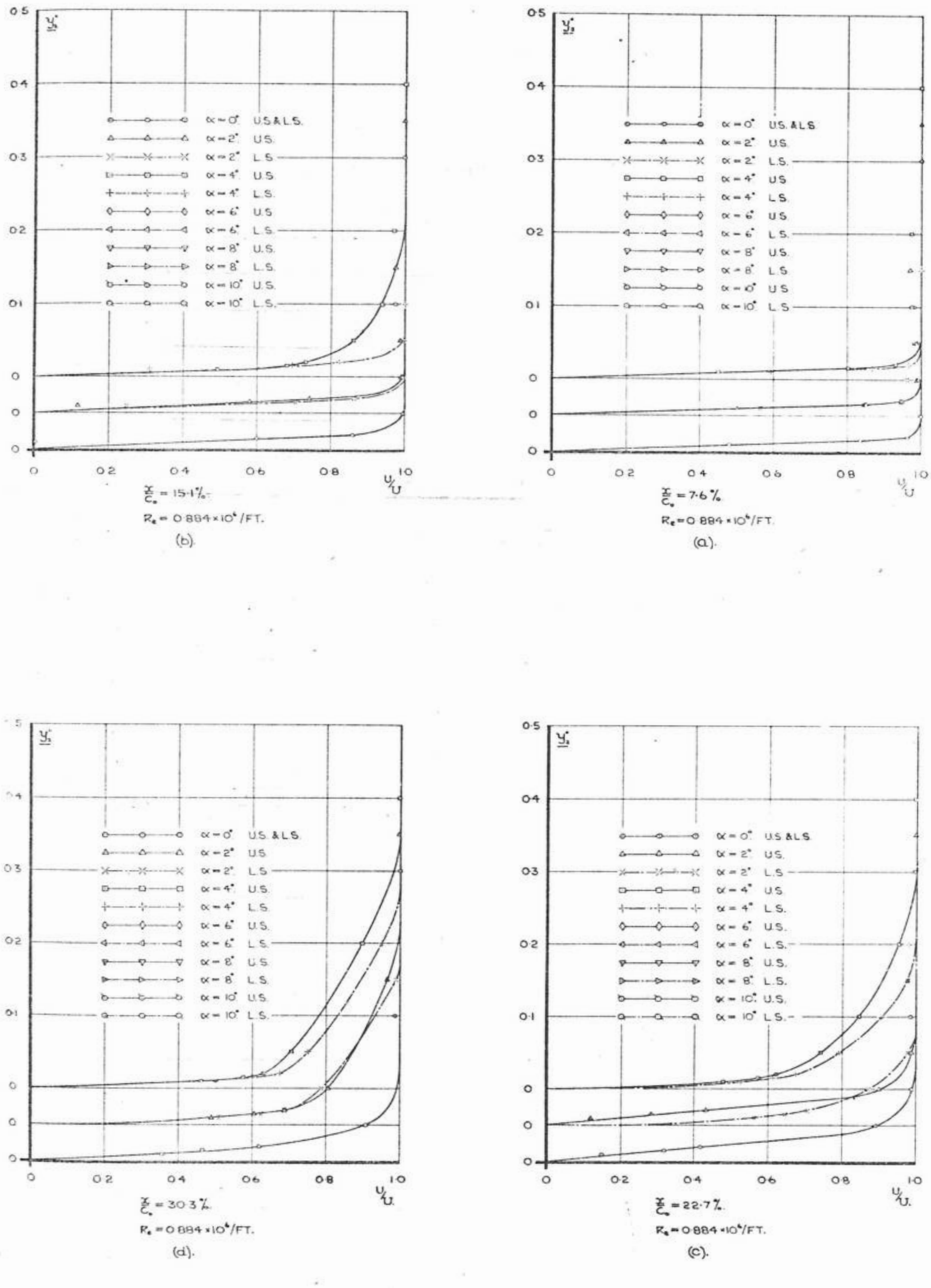

FIG 30 BOUNDARY LAYER VELOCITY PROFILES. MID SEMI-SPAN STATION.

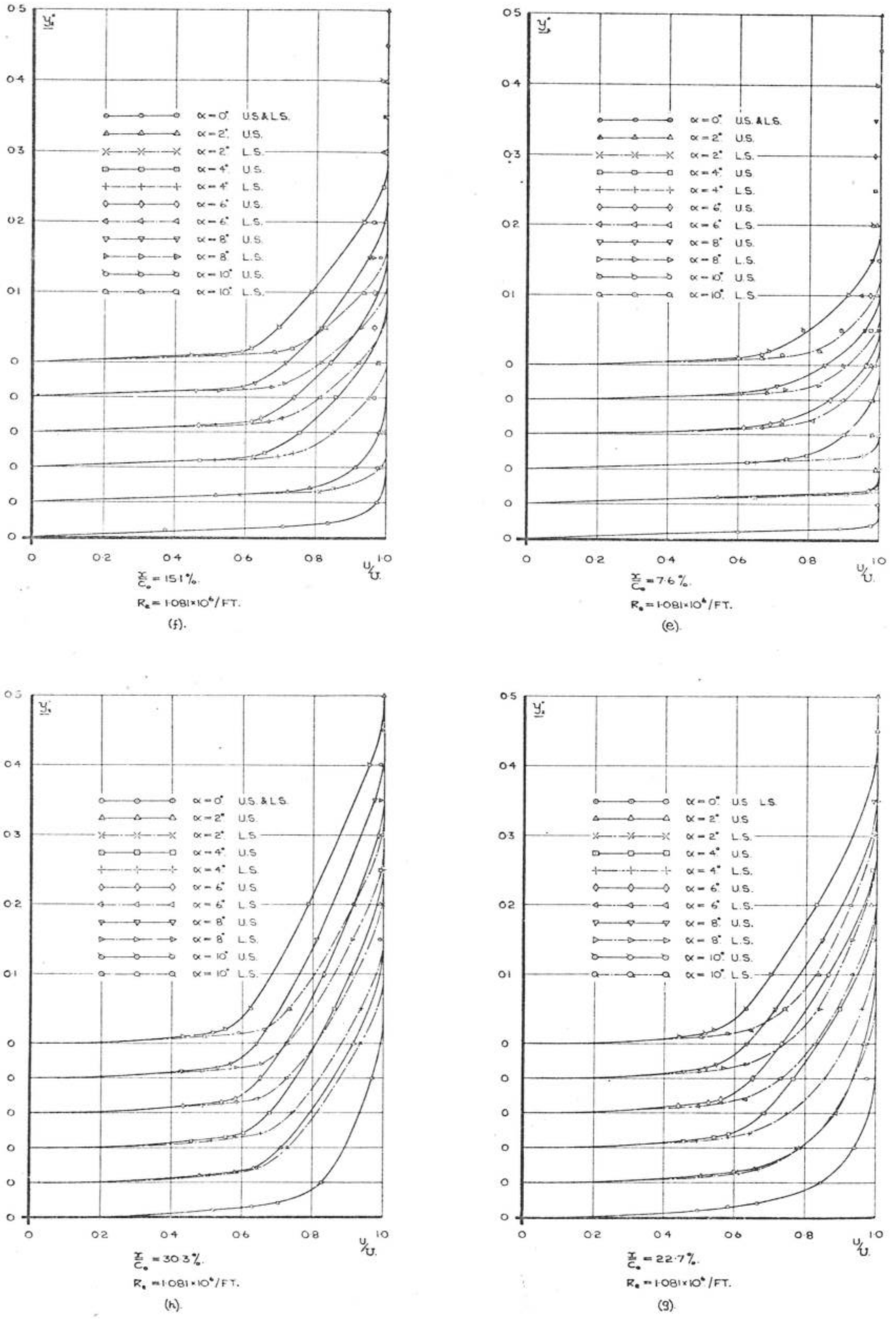

FIG 30 BOUNDARY LAYER VELOCITY PROFILES. MID SEMI-SPAN STATION.

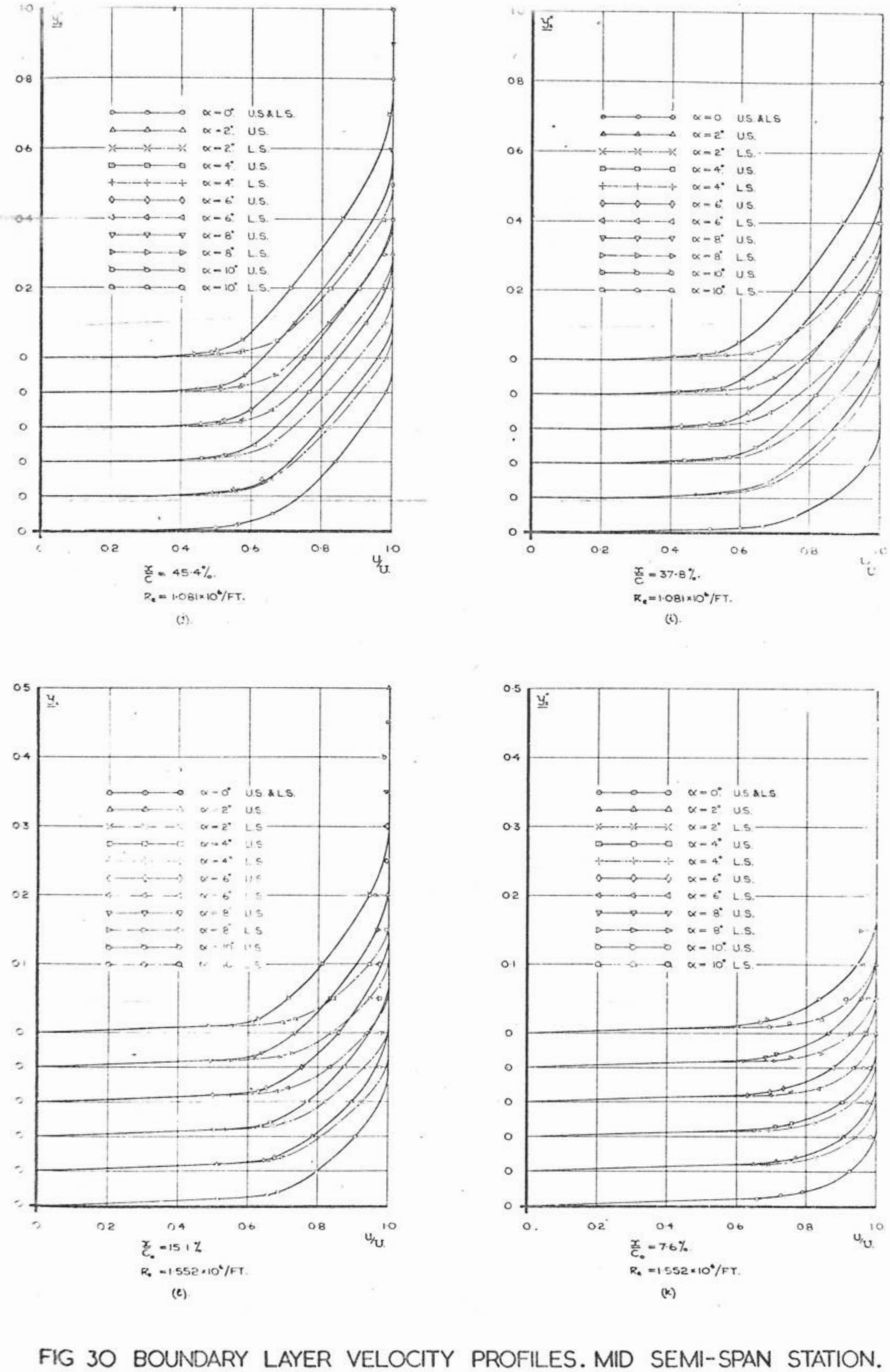

FIG 30 BOUNDARY LAYER VELOCITY PROFILES. MID SEMI-SPAN STATION.

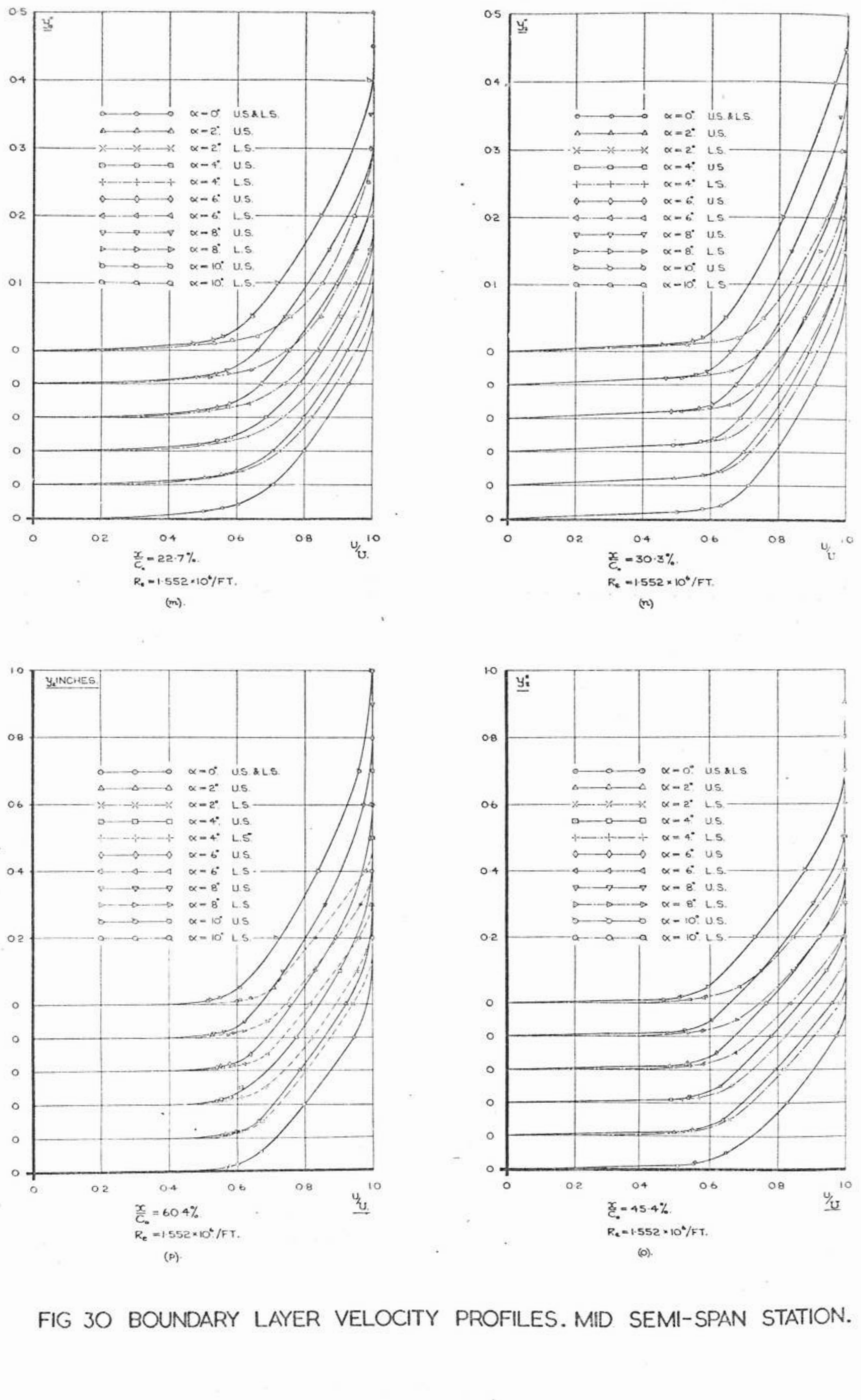

FIG 30 BOUNDARY LAYER VELOCITY PROFILES. MID SEMI-SPAN STATION.

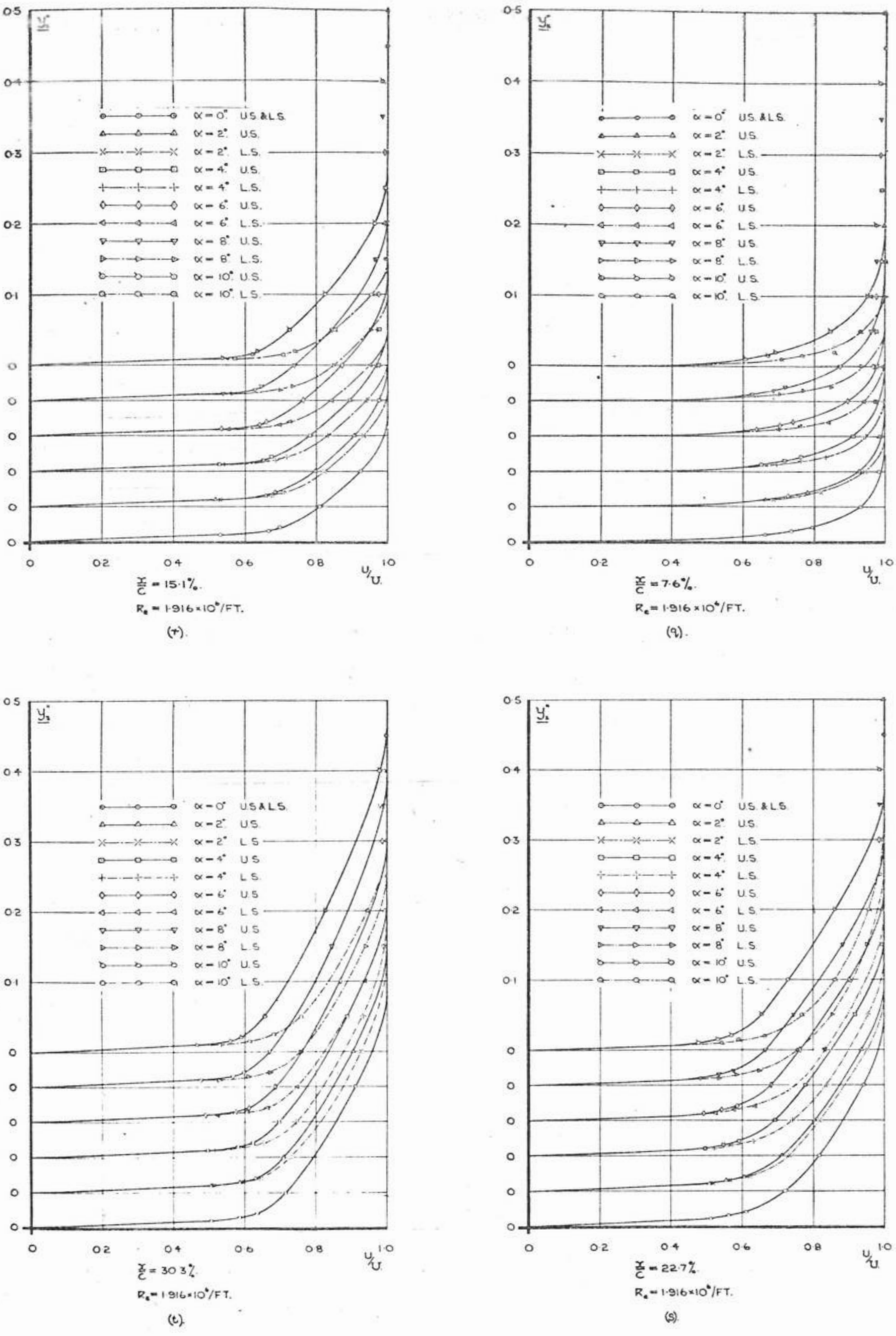

FIG 30 BOUNDARY LAYER VELOCITY PROFILES. MID SEMI-SPAN STATION.

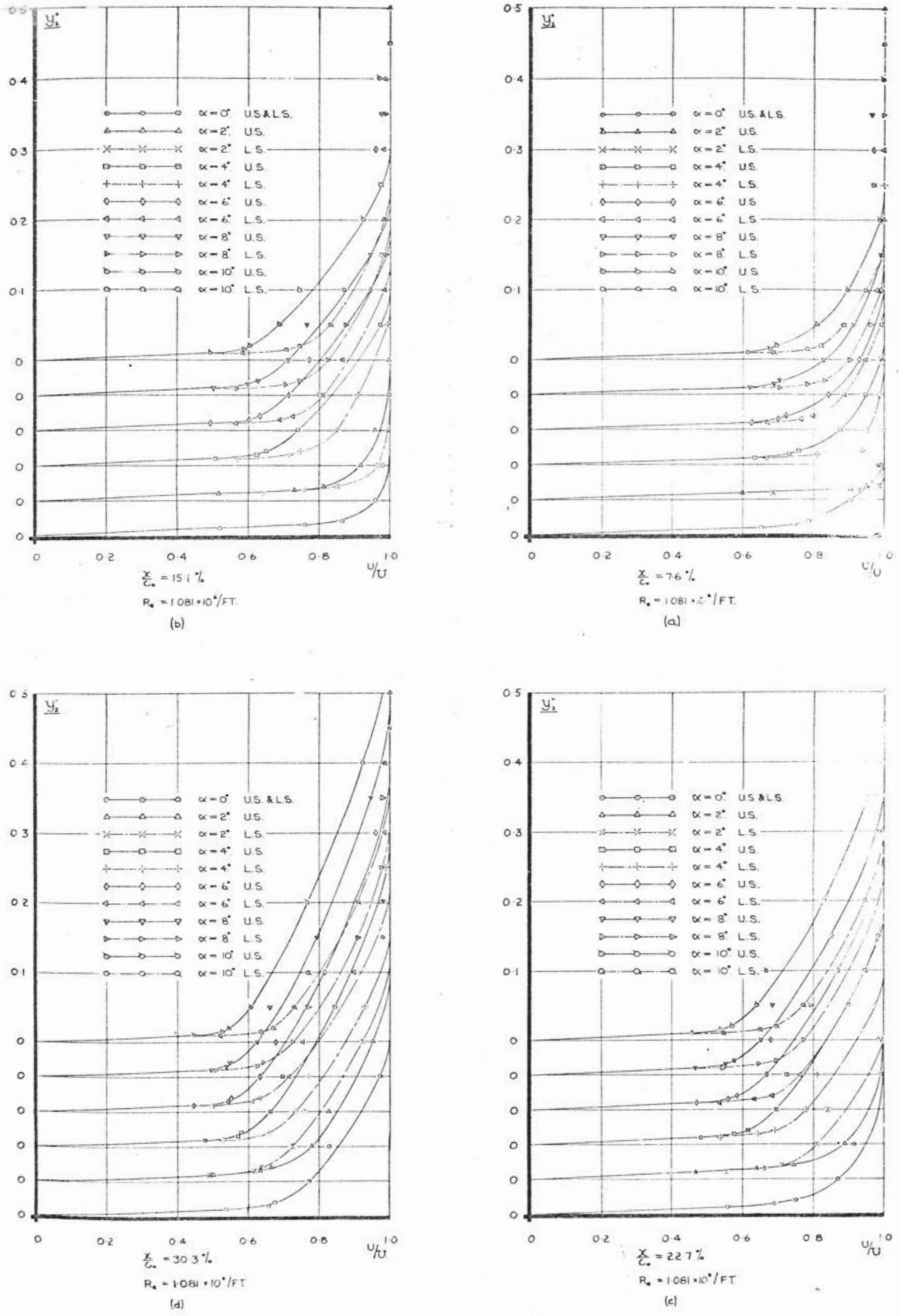

FIG 31 BOUNDARY LAYER VELOCITY PROFILES. WING TIP STATION.

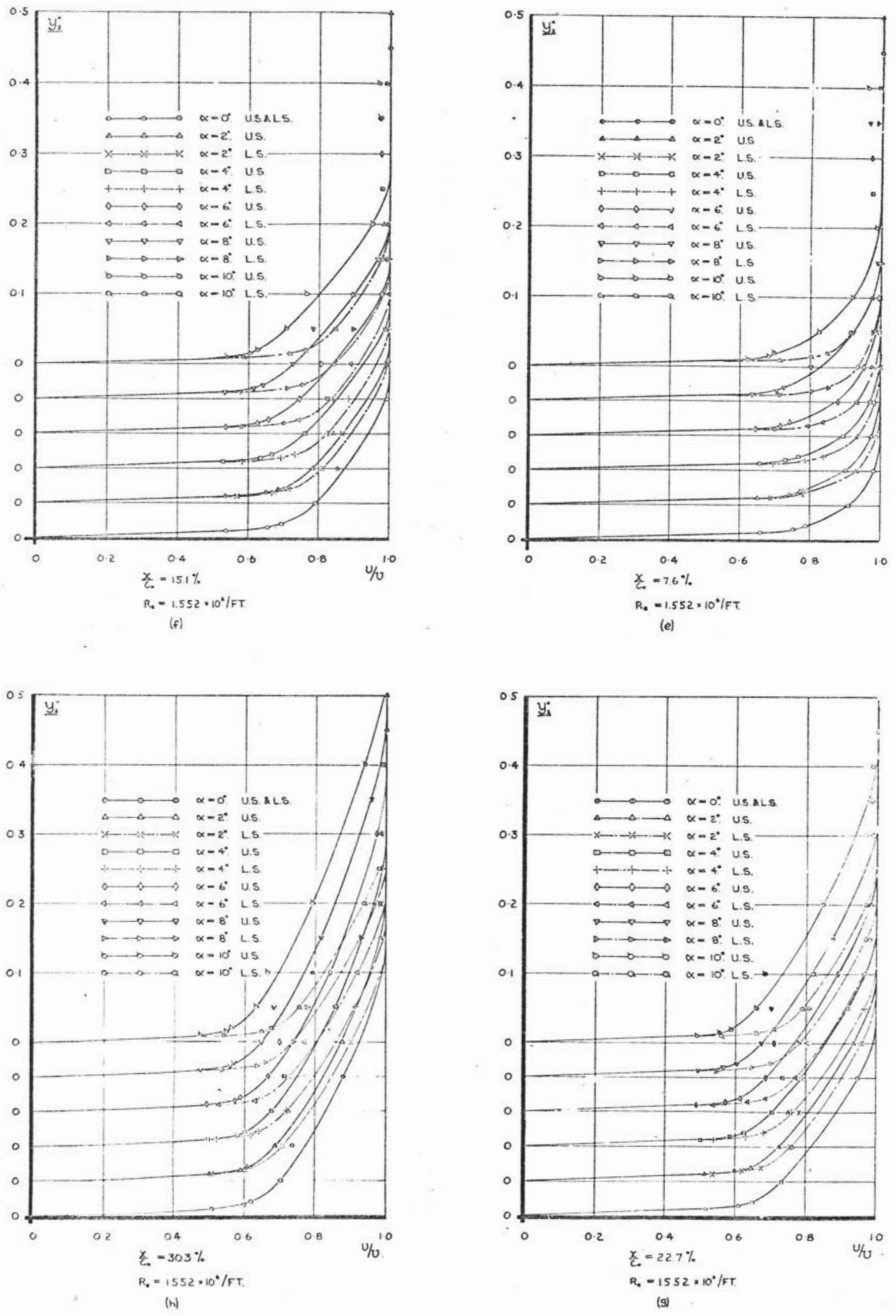

FIG 31 BOUNDARY LAYER VELOCITY PROFILES. WING TIP STATION.

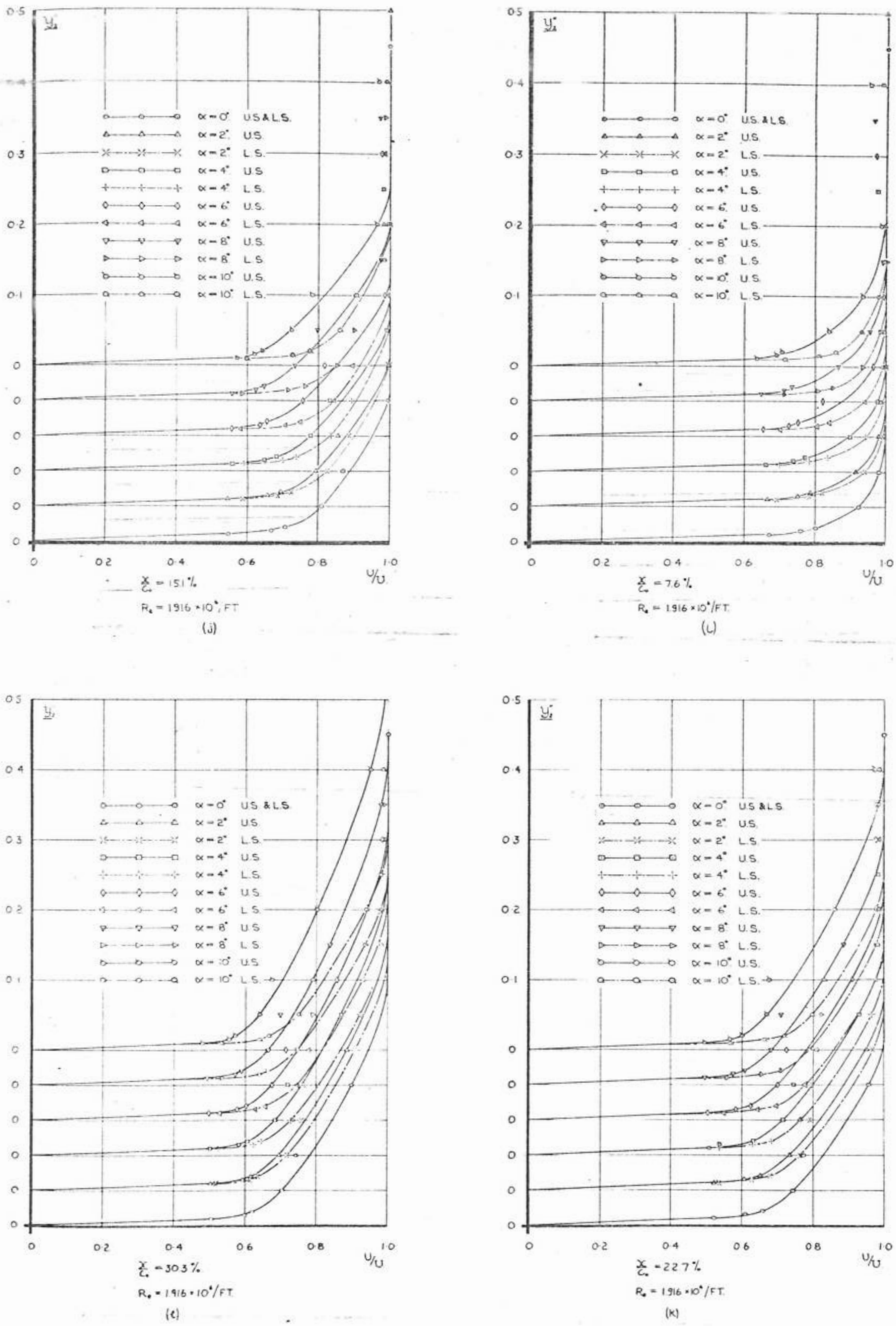

FIG 31 BOUNDARY LAYER VELOCITY PROFILES. WING TIP STATION.

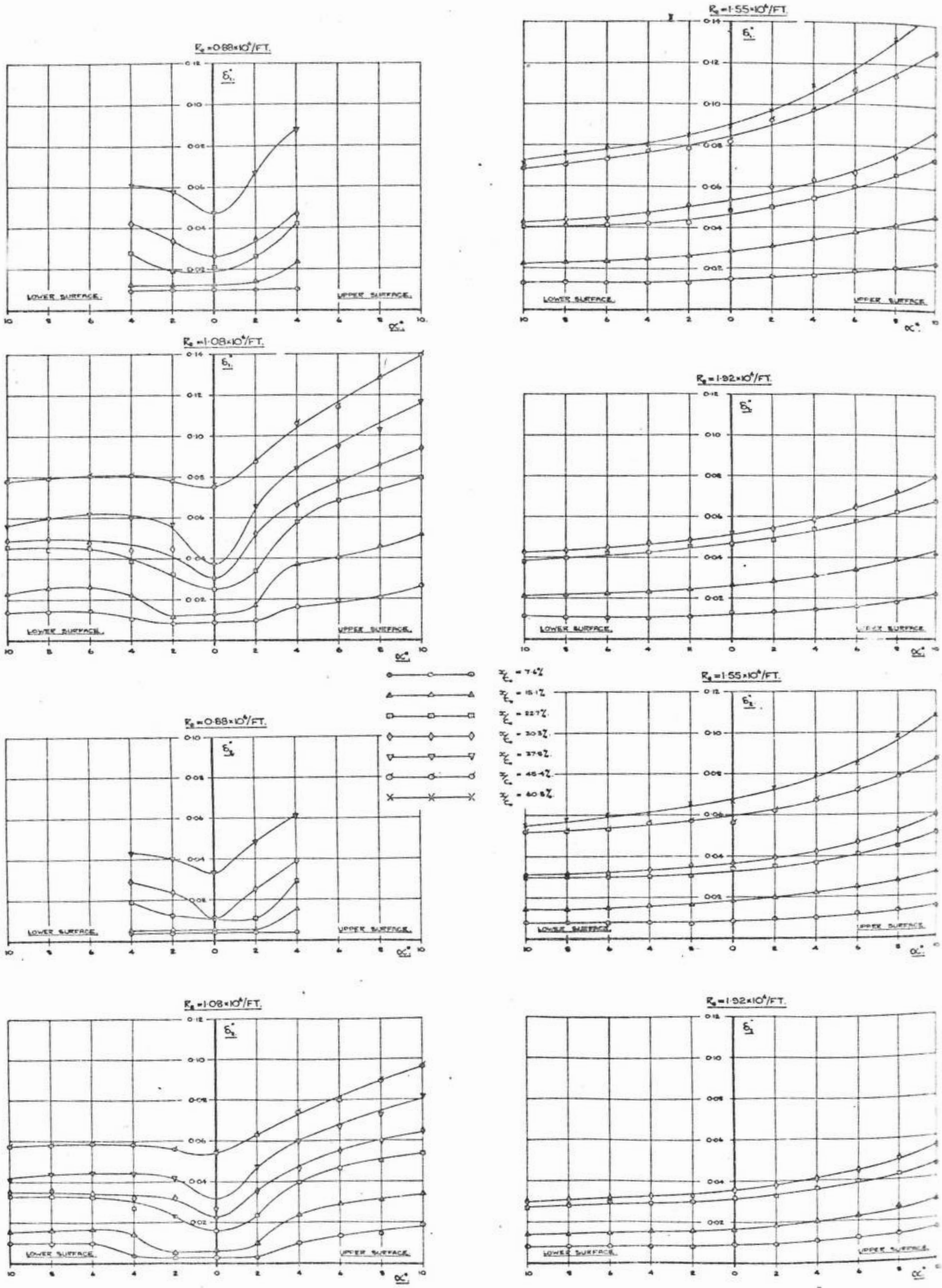

FIG. 32. DISPLACEMENT & MOMENTUM THICKNESS VARIATION.
MID SEMI-SPAN STATION.

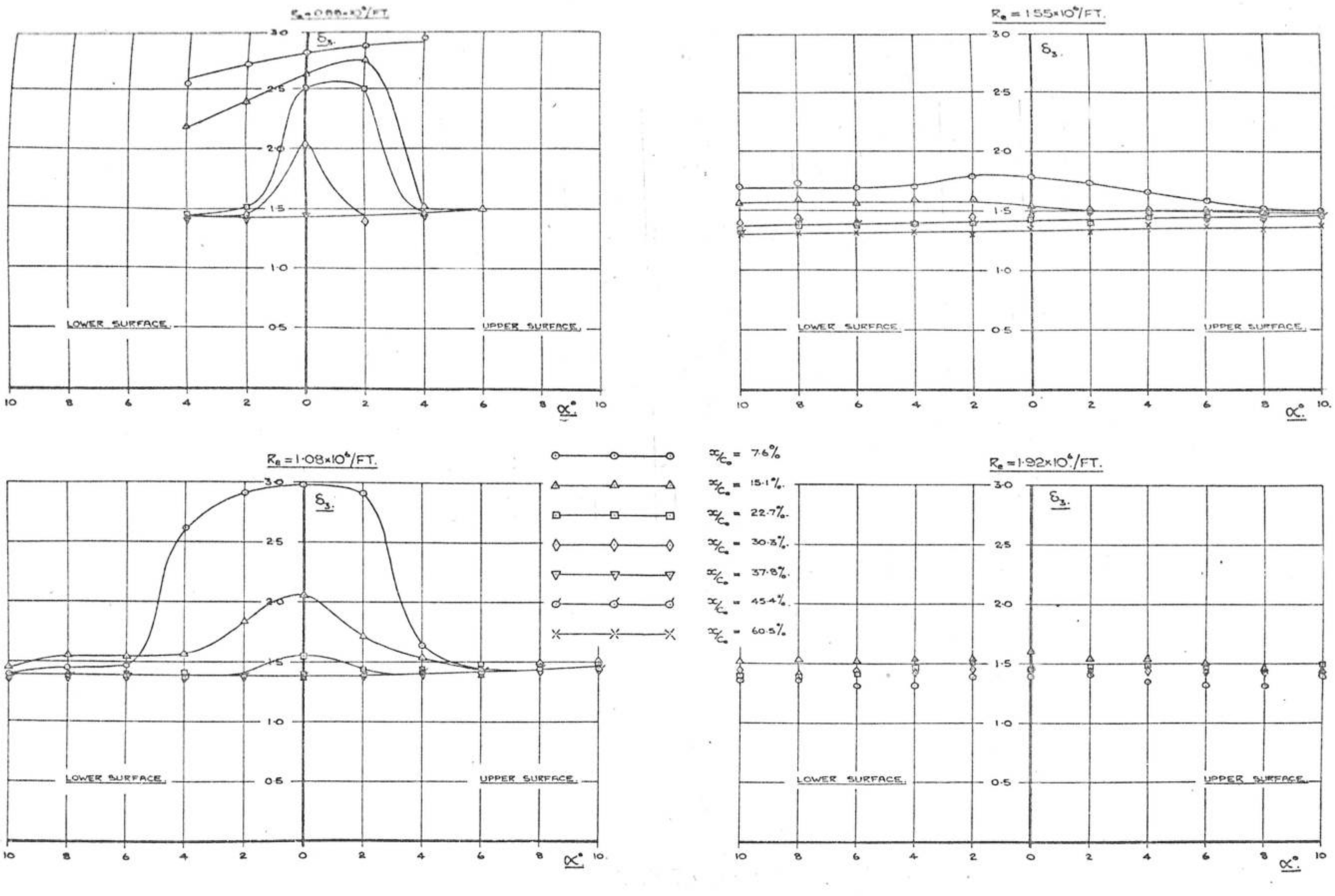

FIG. 33. SHAPE PARAMETER VARIATION. MID-SEMI-SPAN STATION.

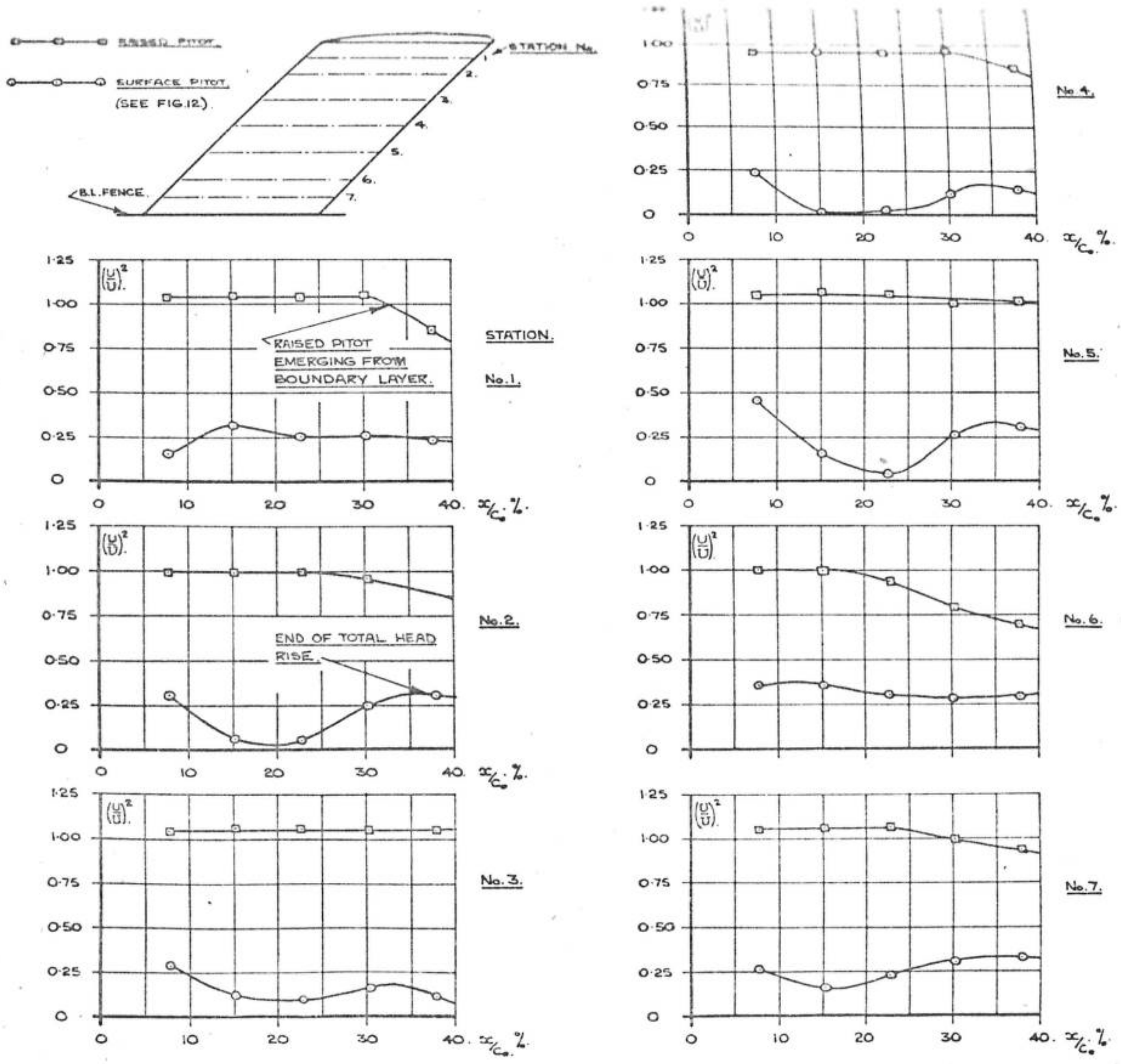

FIG. 34. TOTAL HEAD DISTRIBUTIONS: SPECIMEN RESULTS FROM TRANSITION INDICATOR READINGS.
$\alpha = 0^\circ$. $R_e = 0.88 \times 10^6$/FT.

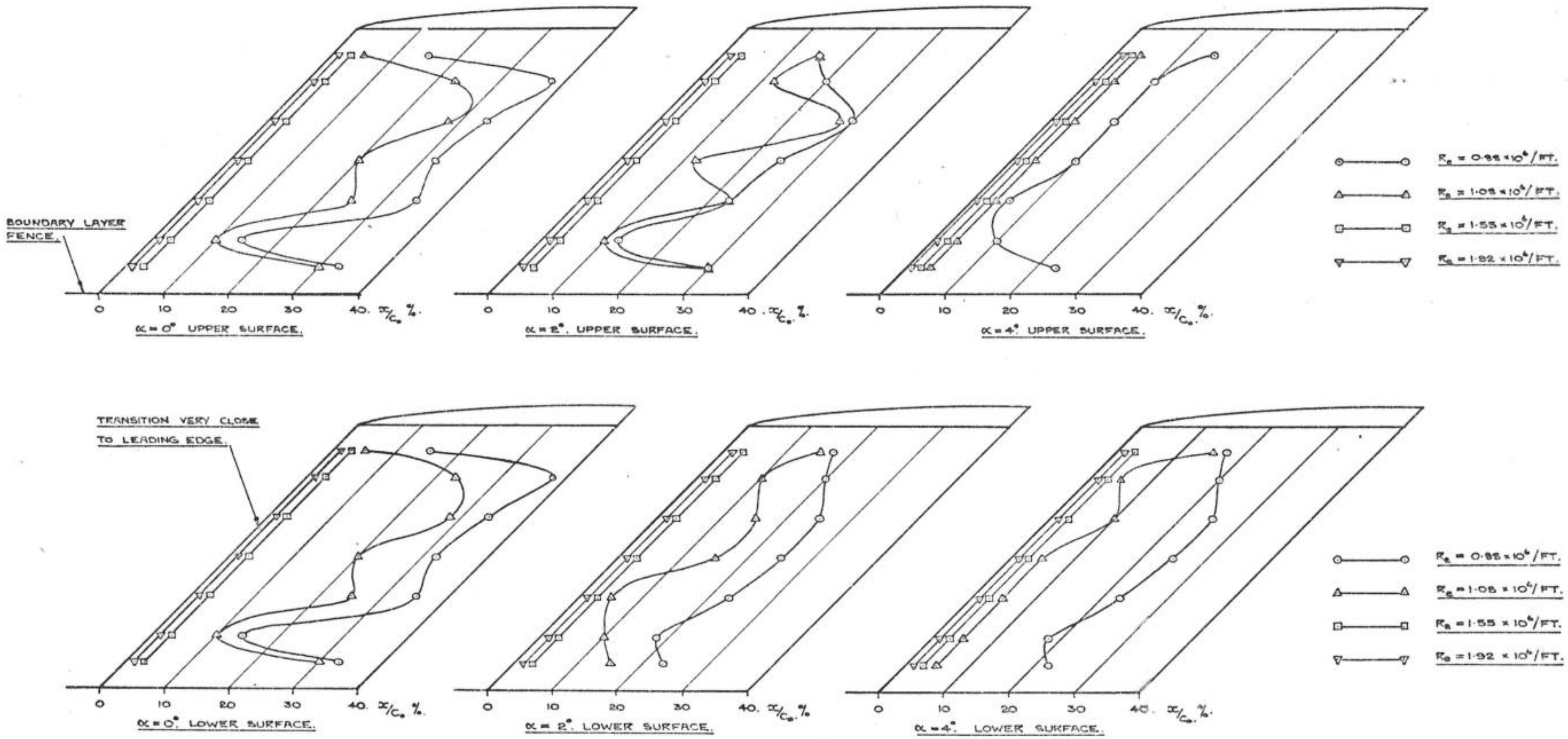

TRANSITION VERY CLOSE TO LEADING EDGE AT ALL REYNOLDS NUMBERS FOR $\alpha \geq 6°$, BOTH UPPER & LOWER SURFACES.

FIG.35. THE POSITION OF BOUNDARY LAYER TRANSITION.